Evolutionary dynamics of *Candida albicans* in the presence and absence of antifungal drug fluconazole

By

Wele Gedara Aruni Sandamali Sumanarathne

A thesis submitted to the Faculty of Graduate Studies of The University of Manitoba in partial fulfilment of the requirements of the degree of

MASTER OF SCIENCE

Department of Microbiology
University of Manitoba
Winnipeg

ABSTRACT

Candida albicans, the most prevalent human fungal pathogen, demonstrates remarkable adaptability and genome plasticity, enabling it to thrive in diverse environments within the human body. This pathogen unequivocally serves as a common commensal member of the human microbiota and poses as an opportunistic pathogen capable of causing infections under specific conditions. The *C. albicans* genome can undergo significant alterations, including single nucleotide polymorphisms, insertions, deletions, and chromosomal aneuploidy, particularly under environmental stresses such as exposure to azole drugs like fluconazole.

This thesis examines crucial aspects of microbial competition and the evolutionary dynamics of *C. albicans* under drug stress, particularly fluconazole. Competitive fitness, a fundamental concept in evolutionary biology, measures organisms' ability to survive, reproduce, and compete for resources. Traditional methods for assessing microbial competitive fitness are labour-intensive and involve manual colony counting. Chapter 2 introduces a high-throughput, automated method that employs fluorescent microscopy and machine learning to measure head-to-head competition between microbial populations quantitatively. This innovative approach significantly enhances the accuracy and reproducibility of fitness assessments.

Fluconazole is a widely used antifungal agent that has been shown to induce resistance in *C. albicans* through repeated use. Previous studies on fluconazole tolerance and resistance have largely focused on high population sizes where selection pressure is prominent. This thesis pioneers examining mutation accumulation and evolutionary responses of *C. albicans* at low population sizes, where genetic drift plays a more substantial role. In Chapter 3, I have evolved replicate lines of *C. albicans* through mutation accumulation experiments in both the presence and absence of fluconazole, followed by comprehensive phenotypic and genotypic analyses. The results indicate that *C. albicans* lines evolved without fluconazole showed no significant changes in fitness compared to ancestral lines. In contrast, lines exposed to fluconazole showed a significant, dose-dependent increase in drug tolerance, competitive fitness, and the prevalence of aneuploid chromosomes. These findings highlight the dual role of fluconazole in inducing and selecting advantageous mutations, driving rapid adaptation in *C. albicans*. This study underscores the profound impact of antifungal treatment on the evolutionary trajectories of pathogenic fungi and provides insights into the mechanisms underlying drug resistance.

ACKNOWLEDGEMENTS

I'm incredibly grateful to everyone who supported and guided me through the completion of my Master's thesis. This journey has been amazing, and I feel so lucky to have had the support of many remarkable individuals.

I would like to start by giving a big thank you to my supervisor, Dr. Aleeza Gerstein. Your guidance, support, and encouragement have been absolutely invaluable to my research. Your insightful feedback, vast knowledge, and patience have not only helped shape this thesis but also boosted my academic journey. I am also profoundly grateful to the members of my MSc committee, Dr Matthew Bakker and Dr Colin Garroway. Your expertise, constructive criticisms, and suggestions have significantly contributed to the improvement and refinement of my research. I could not have asked for a better committee. Also, I want to thank Dr Teresa O'Meara and Dr Andrea Hodgins-Davis from the University of Michigan, USA, for providing me with strains for my research.

I want to give a massive shoutout to my amazing lab mates at the Microstats lab: Javier, Parul, Abdul-Rahman, and Yana. You guys have created such a fantastic and supportive environment in the lab. Our chats, helping each other out, and our awesome discussions have made my time in the lab super fun and intellectually enriching. I'm incredibly thankful for your willingness to share your knowledge, offer help, and provide moral support whenever I've needed it.

I would also like to give a big thank you to all my friends for their enthusiastic support and encouragement, and especially for being the family away from home. Your friendship has provided a much-needed balance between work and life, offering moments of laughter and respite that have kept me grounded and motivated. I am grateful for all the 12.00 am calls, Miss You texts, random reels, occasional comfort food, all the teasing and all the love.

Most importantly, I want to give a big shoutout to my amazing family for always having my back. Mom and Dad, your belief in me and your endless support have been my rock throughout this journey. Thank you for all the sacrifices you've made and for always being my strength. And to Thilanka, thanks a ton for all the love and caring. Thank you for letting me spread my wings.

I am profoundly grateful to the Sri Lankan taxpayers and the free education system. Without their contributions, the opportunities for higher education that I have been privileged to receive would not be possible.

Finally, a big thank you to all the amazing souls I met along the way.

DEDICATION

This thesis is dedicated to my amazing parents for always being there for me and to the free education system in Sri Lanka for making this journey possible.

TABLE OF CONTENTS

LIST OF FIGURES

LIST OF TABLES

LIST OF ABBREVIATIONS

WHO	World Health Organization
LOH	Loss of heterozygosity
MA	Mutation accumulation
YPD	Yeast extract peptone dextrose
FLC	Fluconazole
GFP	Green fluorescent protein
PBS	Phosphate buffered saline
NLS	Nonlinear least squares
CI	Confidence intervals
MIC	Minimum inhibitory concentration
RAD	Radius of the zone of inhibition
FoG	Fraction of growth
GOH	Gain of heterozygosity
ANOVA	Analysis of variance
DDA	Disk diffusion assay
OD	Optical density

Chapter 1 : INTRODUCTION

Each year, more than 150 million severe cases of human fungal infections occur worldwide, resulting in approximately 1.6 million deaths (Kainz et al. 2020; Oladele et al. 2020). *Candida albicans* is the most prevalent human fungal pathogen among the causative fungal pathogens. *C. albicans* serves a dual role as both a common commensal organism within the healthy human microbiota (Liu 2002) and an opportunistic pathogen (Mixão and Gabaldón 2020). In 2022, the World Health Organization (WHO) categorised 19 fungal pathogens into three primary threat levels: critical, high, and medium. *Candida albicans* was designated as one of the four critical priority pathogens because of their substantial impact on global health and its notorious antifungal resistance (Parums 2022).

1.1 Understanding *Candida* species

1.1.1 The genus Candida

Of all the human fungal pathogens, the members of the genus *Candida* are the most frequently isolated from fungal infections in humans (Silva et al. 2012). Genus *Candida* belongs to the order Saccharomycetales, which contains ascomycete yeasts (Suh et al. 2006) and has more than 150 heterogeneous species (Calderone and Clancy 2011). Apart from *C. glabrata* and *C. krusei*, all the *Candida* species belong to the UTG clade, and within the clade, haploids (*C. guilliermondii, D. hansenii* and *C. lusitaniae*) and diploids (*C. albicans, C. dubliniensis, C. tropicalis, C. parapsilosis and L. elongisporus*) are separated into two distinct subclades (Butler et al. 2009). The clade is distinguished by translating CTG codons into serine instead of leucine (Santos and Tuite 1995), a translation which occurred ~170 million years ago (Massey et al. 2003). In recent reclassifications, changes have been made within the order Saccharomycetales, especially by renaming *C. glabrata* as *Nakaseomyces glabrata* (Kidd, Abdolrasouli, and Hagen 2023; San Juan Galán, Poliquin, and Gerstein 2023), which is more closely related to *Saccharomyces cerevisiae* than to the other *Candida* species (Fitzpatrick et al. 2006). *S. cerevisiae* belongs to a group that has undergone whole genome duplication (WGD) (Figure 1.1).

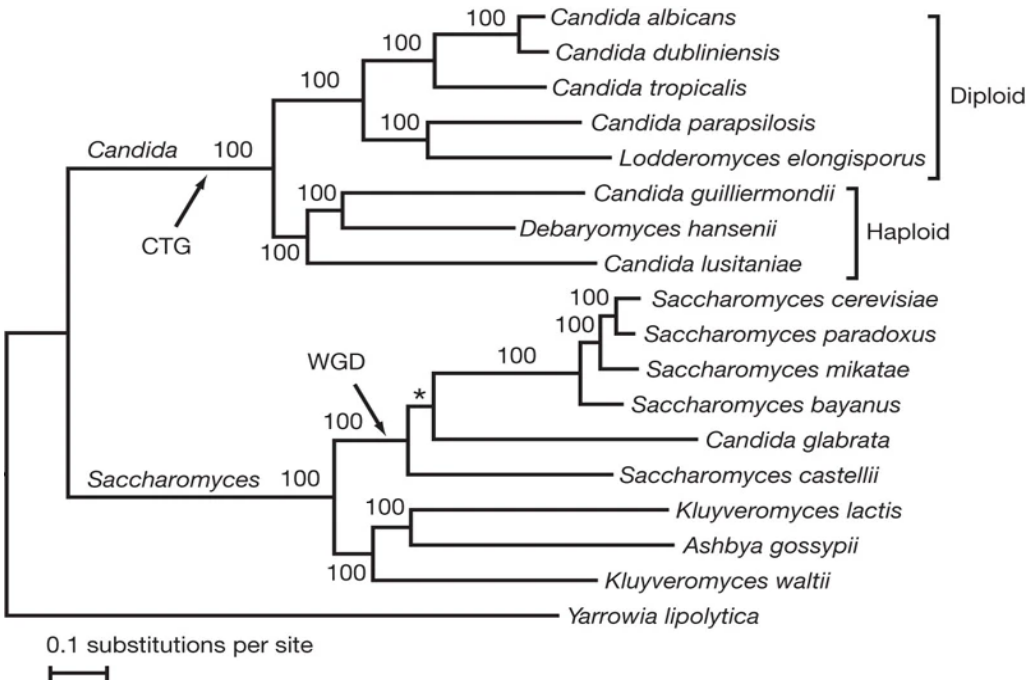

Figure 1.1: Phylogeny of Candida clade determined by using both coding and peptide nucleotide sequences. Haploids and diploids are arranged into two distinct sub-clades. The figure was obtained from (Butler et al. 2009)

1.1.2 Candida albicans

C. albicans is a typical heterozygous diploid whose genome comprises eight chromosomes (Olaiya and Sogin 1979; Riggsby et al. 1982). *C. albicans* genome is 14.3 MB, and 0.5 % of the genome consists of heterozygous positions (~70000 positions) (Braun et al. 2005; Muzzey et al. 2013; Jones et al. 2004). *C. albicans* maintain genome plasticity mainly via small-scale mutations such as single nucleotide polymorphism (SNPs), small insertions and deletions, and copy number variations in genes and chromosomes (Ene et al. 2018). In addition, large-scale chromosomal mutations such as variations in ploidy (i.e., an alteration in the number of complete sets of homologous chromosomes in a cell away from the diploid baseline) (Gerstein and Sharp 2021; Hickman et al. 2013), chromosomal aneuploidy (a change in the number of one or more chromosomes) (Selmecki, Bergmann, and Berman 2005) and loss of heterozygosity (LOH) (Forche et al. 2011), both as small-tract LOH (resulting from gene conversion or double crossovers) and large-tract LOH (resulting from single crossover event or break-induced replications) is also frequently observed in stressful conditions. *C. albicans* is largely asexual and known for the absence of meiosis (Alby and Bennett 2010). However, it participates in a unique, highly modified sexual cycle, the parasexual cycle for sexual

reproduction (Bennett and Johnson 2003; Forche et al. 2008). Although *C. albicans* lacks meiosis, the parasexual cycle allows the organism to expand its genetic and phenotypic diversity through recombination events and chromosomal relocation (Bennett and Johnson 2003; Forche et al. 2008). Analysis of clinical isolates revealed that the *C. albicans* population is predominantly clonal; hence, the importance of the parasexual cycle is not very clear (Liang and Bennett 2019; Ropars et al. 2018).

1.1.3 Commensal and pathogenic nature of C. albicans

Opportunistic fungal pathogens account for the majority of systemic fungal infections. Interestingly, these fungal pathogens are often present in the human microbiota without causing infection (Haoping Liu 2002). As a commensal, *C. albicans* can be found in diverse sites within the human body, including the oral cavity, gastrointestinal tract, and urogenital tract and on the skin (Fidel 1999; Kumamoto 2011; Limon, Skalski, and Underhill 2017). The presence of *C. albicans* is widespread across diverse environmental conditions, showcasing its ability to thrive in varying temperatures, pH levels, and nutrient availability. Studies by Brown et al. (2014), Ene et al. (2014), and Vylkova et al. (2011) have highlighted *C. albicans*' adaptable metabolism, which enables them to utilise a wide range of carbon and nitrogen sources. This suggests that *C. albicans* is highly adept at swiftly adjusting to and thriving in different environmental settings.

The exceptional adaptability of *C. albicans* is a key factor in its successful role as a formidable pathogen (Nicholls et al. 2011). The intricate interplay among the host immune system, human microbiota, and *C. albicans* population is crucial in maintaining the commensal state of this opportunistic pathogen (Niemiec et al. 2021). However, any disruption in this balance, brought about by compromised immunity, extensive use of broad-spectrum antimicrobials, pregnancy, or underlying conditions such as malignancy and diabetes, can lead to *C. albicans* causing various types of infections, ranging from superficial to systemic (Talapko et al. 2021; Pappas et al. 2018; Fidel 1999). A number of virulence factors are attributed to the pathogenic nature of *C. albicans* including stress response mechanisms (Mba and Nweze 2020), metabolic versatility (Pellon et al. 2022), phenotypic plasticity (Soll 2002) and biofilm formation (Salama and Gerstein 2022).

1.2 Antifungal treatments and their mechanisms

1.2.1 Overview of antifungal drugs

Treatment for *Candida* infections involves the use of four primary drug classes: azoles, polyenes, echinocandins, and antimetabolites. The drug activity, toxicity profiles, formulations, and drug interactions vary significantly across different drug classes. Nystatin, the first approved antifungal agent, is a polyene, representing the first antifungal drug class to be available in the clinical setting. Amphotericin B deoxycholate and its lipid formulations are widely used polyenes for treating systemic fungal infections. Fungal cell membranes contain ergosterol, the principal sterol in fungal cell walls, and polyenes can bind to ergosterol, altering the membrane permeability and ultimately resulting in cell death (Lakhani, Patil, and Majumdar 2019). 5-Fluorocyosine is an antimetabolite which has the ability to disrupt the integrity of fungal cell walls. Typically, this antifungal agent is coupled with amphotericin B to treat systemic infections (Ami, Lewis, and Kontoyiannis 2008). Alozes are the most widely used antifungal drug class (fluconazole, voriconazole and posaconazole). These synthetic agents inhibit the enzyme lanosterol 14 α-demethylase, which is crucial for the ergosterol biosynthesis pathway (Draskau and Svingen 2022). Echinocandins (caspofungin, anidulafungin and micafungin) are a novel antifungal class which comprises semi-synthetic lipopeptides that can inhibit the biosynthesis of β-1,3-D-glucan, a major structural component in fungal cell wall (Szymański et al. 2022).

1.2.2 Fluconazole

Fluconazole was discovered in the early 90s by a research program seeking a broad-spectrum antifungal agent (Richardson et al. 1990). This is the most common first-line antifungal treatment available in clinical settings (Goa and Barradell 1995). Fluconazole is a first-generation triazole with a five-membered ring comprising two carbon atoms and three nitrogen atoms $C_2H_3N_3$. Fluconazole inhibits the lanosterol 14α-demethylase, an enzyme encoded by *ERG11*, by binding to the heme iron. This blocks the active site of the enzyme, preventing the dimethylation of lanosterol. Demethylation of lanosterol is a crucial step in ergosterol biosynthesis, an important component in the fungal cell walls. Reduction in ergosterol alters the structure and function of the cell membrane and increases the membrane permeability (Yang et al. 2018).

1.3 Mechanisms of resistance and tolerance to fluconazole

Despite low resistance rates (< 1%), there is a > 30% chance of therapeutic failure against fluconazole-susceptible *C. albicans* isolates (Pfaller et al. 2019; Levinson et al. 2021). Fluconazole is a fungistatic drug in which the fungal cells can survive and grow slowly, retrieving new traits such as fluconazole tolerance and resistance (Lu et al. 2021). Resistance is the heritable reduction in sensitivity of a fungal population to an antifungal drug whereas drug-susceptible fungal strain can exhibit tolerance when a subpopulation of cells is capable of slow growth at fungistatic drug concentrations above the minimum inhibitory level, despite inhibiting fungal growth (Fisher et al. 2022). There are various methods to acquire drug resistance in *Candida*. Inhibition of the drug binding to the active site by changing the amino acids is a common resistance mechanism, alteration of R467K and G464S are the most common (Casalinuovo, Di Francesco, and Garaci 2004). *ERG11* overexpression is another mechanism of resistance, contributing to the resistance by increasing the target abundance (White 1997; Perea Sofia et al. 2001; Franz et al. 1998). Entire chromosomal duplication or formation of an isochromosome with duplication of the left arm of chromosome 5 leads to *ERG11* amplification (Selmecki, Forche, and Berman 2006). Chromosomal abnormalities such as LOH, CNV and chromosomal aneuploidy play a major role in fluconazole resistance and tolerance. Research conducted with clinical isolates showed that LOH is common in locations with resistance-related genes such as *ERG11, TAC1* (a transcription factor that activates *CDR1* and *CDR2* expression, which encode ABC transporters) and *MRR1,* starting as heterozygous and becoming homozygous via LOH (Coste et al. 2007). The left arm of chromosome 5 contains *ERG11* and *TAC1*; therefore for formation of isochromosome i(5L) increases the copy number (Selmecki, Forche, and Berman 2006). Moreover, it was found that azole exposure causes abnormal cell divisions via a tetraploid intermediate, leading to the formation of aneuploidy (Harrison et al. 2014). Salama and Gerstein (2020) examined clinical isolates of *Candida* and observed that those resistant to fluconazole also exhibited increased tolerance to the drug. Additionally, in a separate in vitro evolution study involving 20 *C. albicans* isolates, it was found that tolerance and resistance emerged as distinct traits. While some isolates developed resistance, many showed an increase in tolerance (Gerstein and Berman 2020). Yang et al. (2023) found a strong correlation between fluconazole tolerance and the presence of aneuploid chromosomes.

1.5 Competitive fitness

Competitive fitness is an essential concept in evolutionary biology that defines an organism's ability to survive, reproduce, and compete for resources within its environment. It is a complex trait influenced by the organism's genetics, specific environment, and interactions with other organisms (Ehrlén, 2003; Miller & Compagnoni, 2022), famously associated with Charles Darwin and his notion of "survival of the fittest" (Darwin, 1859). The growth rate measurements of monocultures are widely used in microbial studies as a high throughput indicator of fitness (Chevin 2010; Gallet et al. 2012). However, the most accurate and widely accepted method for determining competitive fitness is using pair-wise mixed cultures by either plating and counting or using flow cytometry. One prominent example of the importance of fitness measurement is the long-term evolution experiment (LTEE) with *Escherichia coli* conducted by Wiser & Lenski (2015). In this assay, a reference strain, often marked with a neutral genetic marker, is competed against an experimental strain. Lenski et al. (1991) used two different types of *E. coli* cells, one with the ability to grow on Arabinose-containing media (Ara+) and the other lacking the ability (Ara-). This arabinose-utilizing gene is selectively neutral in the DM25 medium, which they have used in the study. They used a special media for the plating, Tetrazolium Arabinose Agar, which produces red and white colonies by Ara+ and Ara- genotypes, respectively (Wiser and Lenski 2015). Aliquots are taken at the beginning and end of the competition period, and the relative frequencies of the two strains are determined by counting the number of colonies belonging to each strain after plating them (Lenski 2023). The relative fitness (w) is determined by taking the ratio of realised Malthusian parameters relative to that of the other strain during the considered period (Lenski et al. 1991; Wiser, Ribeck, and Lenski 2013). The second method to count cells is to use fluorescently marked cells with flow cytometry (Kao and Sherlock 2008; DeLuna et al. 2008). Here, competing cells are marked with fluorescing markers and pass through the flow cytometer, and the instrument can measure the fluorescent intensity, making it possible to distinguish between different cell types.

1.5.1 Necessity of developing a high throughput competitive fitness assay

Growth curves do not provide an accurate estimation for fitness despite having high throughput or lacking the need for the marked cells. The data collection is based on optical density measurements during the growth curve assay. While growth rates are calculated from the exponential phase of the growth curve, they do not fully represent the overall dynamics of all

growth phases (Hall et al. 2014). Recent research has highlighted discrepancies between cell density measurements and cell counts in *Saccharomyces* due to variations in cell size (Pinto et al. 2024), indicating that density measurements from growth curves might not accurately correspond with cell counts, potentially leading to erroneous fitness assessments. Existing protocols for competitive fitness determination with pair-wise cultures typically involve plating and colony counting or the use of fluorescently labelled cells with flow cytometry. The plating and colony counting method proposed by Lenski et al. (1991) is renowned, but the process is entirely manual and labour-intensive. The high amount of bench work involved, such as plate preparation, plating, and colony counting, limits the high-throughput nature of the assay, and the majority of the work needs to be done in a sterile environment. Although the flow cytometry-based methods are less laborious than plating and colony counting, this method uses fluorescent intensity as a proxy for cell count (Kao and Sherlock 2008; DeLuna et al. 2008). Moreover, a flow cytometer cannot take in all the samples at once, the operator has to load the samples one by one, limiting the high throughout nature of the assay. Given the increasing complexity and scale of microbial studies, there is a pressing need for high throughput methodologies that can provide precise and reproducible fitness measurements.

1.4 Mutation accumulation experiments

Given that *C. albicans* can accommodate diverse locations in the human body, the population size of *C. albicans* varies according to the environmental conditions of each niche. Therefore, studying the behaviour of *C. albicans* in vitro when the effective population size is low is more biologically relevant. Mutation accumulation (MA) studies are typically employed to study phenotypic and genotypic changes when the effective population size is small (Zeyl and DeVisser 2001). In MA experiments, replicate lines that share a common ancestor are subjected to repeated population bottlenecks (Andersson and Hughes 1996; Lenski et al. 1991). In microbes, this is done by repeatedly streaking single colonies which arise from a single cell. The repeated streaking of single random colonies enables the MA lines to have a small effective population size (N_e). Theoretically, this small N_e is too small for selection to occur on new mutations within these populations. As a result, most new mutations (except those extremely deleterious) have a theoretical fixation probability approximately equal to beneficial mutations (Sharp et al. 2018). Sharp et al. (2018) carried out a series of MA experiments with haploid and diploid lines of *Saccharomyces cerevisiae* derived from a common ancestor. After bottlenecking 220 lines per day for 100 days, it was determined that diploids are more

susceptible to large-scale mutations with detrimental fitness effects, while haploids are more prone to single-nucleotide mutations (Sharp et al. 2018). Lynch et al. (2008) bottlenecked 32 lines of haploid *S. cerevisiae* derived from a single clonal parent for 200 cycles (3-4 days per cycle) and found that the cells become nearly diploid within a few hundred generations and ~0.1 % of the mutations have a fitness effect under laboratory conditions (Lynch et al. 2008). Nishant et al. (2010) bottlenecked *S. cerevisiae* to observe the stability of the genome and found that the yeast diploid genome is remarkably stable in mitosis and miosis since they did not observe any indels or ploidy changes (Nishant et al. 2010).

In this thesis, I aimed to investigate the effect of fluconazole on *C. albicans* when the effective population size is low. I first developed a high throughput, mostly automated method to measure competitive fitness (Chapter 2). In Chapter 3, I evolved *C. albicans* lines under mutation accumulation experimental conditions with and without fluconazole in the media and compared them phenotypically and genotypically to the ancestral cells in terms of competitive fitness, drug responses, growth rates, genome size and presence of aneuploid chromosomes. Based on my research, it is evident that the lines that evolved without fluconazole in the media under a low effective population size did not gain any fitness advantages over ancestral cells. Conversely, the lines that evolved with fluconazole exhibited increased tolerance, competitive fitness, and genome size and a rise in aneuploid chromosomes.

1.5 Hypotheses

1. *Candida albicans* lines evolved under low effective population size in the presence of the antifungal drug fluconazole, a putative mutagen, will exhibit higher rates of aneuploidy than lines evolved in rich medium.

2. *C. albicans* lines evolved under low effective population size in the presence and absence of fluconazole will have similar competitive fitness as the ancestral lines.

Chapter 2 : Developing a novel high-throughput method to quantify competitive fitness using fluorescent microscopic imaging

2.1 Abstract

Competitive fitness is a fundamental concept in evolutionary biology that captures the ability of organisms to survive, reproduce, and compete for resources in their environment. Competitive fitness is assessed in the lab by growing two or more competitors together and measuring the frequency of each in the population at multiple time points. Traditional microbial competitive fitness assays are labour-intensive and involve plating and counting the colonies. Here, we propose a high throughput and efficient way to quantitatively measure the head-to-head competition between two microbial populations using fluorescent microscopic imaging and machine-learning-enabled image analysis. This high-throughput, primarily automated process gives accurate and reproducible results for competitive fitness. Here, I describe the entire process, from sample preparation through microscopy, and provide instructions and scripts for the image analysis, fitness calculations, and data visualisations.

2.2 Introduction

The concept of fitness, often associated with Charles Darwin, is captured in the famous phrase "survival of the fittest" (Darwin 1859). Competitive fitness is a vital concept in evolutionary biology, referring to an organism's ability to survive, reproduce, and compete for resources in its environment. Fitness is a complex factor influenced by an organism's genetics, the specifics of the environment it is in, and its interactions with other organisms in the environment (Ehrlén 2003; Miller and Compagnoni 2022). Competitive fitness is often measured using assays where multiple strains or species that are marked in some way to differentiate them are grown together under controlled conditions. These experiments typically use plating or flow cytometry to measure changes in the relative frequencies or population sizes of the competing organisms over time. The selection coefficient is then calculated to quantify one strain's relative advantage or disadvantage over another (Wiser, Ribeck, and Lenski 2013; Lenski et al. 1991). Competitive fitness assays are more labour-intensive than other phenotypic assays, such as growth curves and drug susceptibility testing (Ram et al. 2019). As a result, it is common to use other fitness indicators, like growth rate or optical density (a proxy for population size), which may or may not be well correlated with true competitive fitness (Chevin 2010; Crow 2017; Li et al. 2018).

Understanding competitive fitness is crucial for explaining evolutionary dynamics and population changes. It provides insights into how advantageous traits are selected and spread through populations, ultimately shaping the evolutionary trajectory of populations and species. The concept of competitive fitness is widely applied in various fields, including microbiology (Dimas Martins and Gjini 2020) and ecology and conservation biology (Samuel et al. 2023), to study phenomena such as antibiotic resistance (Andersson et al. 2020), invasive species dynamics (Kaushik et al. 2022), and the impact of environmental changes on biodiversity (Li et al. 2019). Several factors influence competitive fitness in microbes, including stress response mechanisms (Mba and Nweze 2020), metabolic versatility (Pellon et al. 2022) and phenotypic plasticity (Soll 2002).

Most competitive fitness assays of microbes are based on the protocols that Lenski et al. (1991) popularised to measure the relative fitness of bacterial strains. Relative fitness is a comparative measure of fitness that describes how well a genotype or phenotype performs compared to other genotypes or phenotypes in the population (Orr 2009). It has been notably employed to quantify how fitness has changed over time during the long-term evolution experiment (LTEE) with *Escherichia coli* (Wiser and Lenski 2015). In this study, a reference

strain competes against an experimental strain, with the relative frequencies of the two strains determined by counting the number of colonies belonging to each after plating them (Lenski 2023). The relative fitness (w) is determined by calculating the ratio of realised Malthusian parameters of the two strains during the period (Lenski et al. 1991; Wiser et al. 2013). However, it has been recommended that when one strain or both decrease during the considered period (i.e., when a drug is in the media), the selection rate (r), the difference between the realised Malthusian parameters of two strains, should be used instead of w (Travisano and Lenski 1996). The approach introduced by Lenski et al. (1991) is simple and straightforward but relies entirely on manual procedures. This entails significant hands-on bench work, including the preparation of agar plates and the manual counting of colonies. This makes it very cumbersome when the goal is to assay a large number of samples.

The second method to count cells is to use fluorescently marked cells with flow cytometry (Kao and Sherlock 2008; DeLuna et al. 2008). Although it is easier to use flow cytometry than counting colonies on the agar plates, it is not a direct or definitive method to estimate the number of cells in a sample. Gerstein et al. (2011), used fluorescently labelled strains coupled with flow cytometry. The competitive fitness (m) was estimated using the equation

$$\text{NonFlour} = p_0 e^{mT} / 1 - p_0 + p_0 e^{mT}$$

where NonFluor is the fraction of non-fluorescing cells, and T is the generation of competition. The nonlinear least squares (NLS) function from the R programming language is used to find the best fitting parameter estimates for p_0, which is the initial fraction of non-fluorescing cells at the start of the competition, and m (Gerstein et al. 2011). They used the NLS function of R for the calculations. Similar to plating and counting, dealing with a large number of samples is difficult due to the manual process of sample preparation and taking readings with flow cytometry.

Here, we used fluorescent time-lapse microscopy to mimic the plating method and count the number of cells of different types directly. However, fluorescence microscopy coupled with automated image analysis is able to count a much larger number of cells of each type and hence enable the measurement of many samples simultaneously. The Evos FL Auto 2 (Thermo Scientific, cat. no. AMAFD2000) microscope used in this study is an inverted microscope equipped with the ability to capture fluorescing cells. Once the operator sets the parameters such as light, exposure, and focus, the imaging process is automated except for mounting the specimens (Fallarero 2017). Automated image analysis is critical to elevate the speed and reproducibility of the image analysis results. There are numerous analysis tools

available for automated image analysis. One such tool is Orbit Image Analysis, an open-source software application with a machine-learning algorithm (Stritt, Stalder, and Vezzali 2020). This cutting-edge software is designed for easy training to accurately detect and measure various cell types within a single image (Escobar Díaz Guerrero et al. 2022). This algorithm can also handle bulk data; therefore, the user can provide a large number of data files to the software and get an assembled output file, which can be directly used in any other statistical software, such as RStudio, if further analysis is required.

In this protocol, we employ a method that is largely automated and high-throughput, with minimal bench work and instrument handling time. This makes it suitable for large studies where the goal is to quantify the competitive fitness from a large number of samples simultaneously. We use *Candida albicans* as a model organism to showcase this method. *C. albicans* is a human fungal pathogen measuring between 5-6 μm in size (Cottier and Hall 2019). With higher-powered lenses, other fluorescent microscopes would work for even smaller organisms. We use fluorescent microscopic imaging coupled with a machine learning algorithm trained to count fluorescing and non-fluorescing cells near-simultaneously across a large number of images, permitting high replication. We include protocols for all steps, from growing cells initially through to R scripts used for data analysis.

We provide a general protocol for assessing the competitive fitness of fungal species. Minor modifications to the timing of the data collection should be made to suit any population type and environmental condition desired. Protocol 1 describes the sample preparation from freezer stock to a processed plate ready for imaging. Protocol 2 explains the fluorescent microscopic imaging process, from loading the plate to setting up an automated protocol in the microscope. Counting the cells with Orbit Image Analysis Software is explained in protocol 3, along with training the model to get the final counts by bulk analysis. Protocol 4 describes a method of renaming the files using RStudio. Finally, protocol 5 describes the data analysis and visualisation with RStudio. Overall, this novel and highly automated approach facilitates a high-throughput quantification of competitive fitness in yeast, which can be performed without prior knowledge of the technical aspects. We demonstrate the method on two sets of *C. albicans* isolates. One set is anticipated to have very similar competitive fitness to the marked strain, while the other set has evolved in the antifungal drug fluconazole and is expected to have much higher fitness.

2.3 Protocol 1: Sample preparation

The sample preparation protocol explains the culturing and plate processing of yeast isolates for fluorescent microscopic imaging. Here, I have used 6 lines of *C. albicans* that evolved at low population size in the rich medium yeast extract peptone dextrose ("YPD") and 6 lines that evolved in YPD supplemented with 16 µg/mL fluconazole ("YPD+FLC"). These lines competed in the medium they were evolved in against an ancestral reference isolate that was engineered to produce a green fluorescent protein (GFP). We competed ancestral and evolved lines in the medium they evolved in (i.e., YPD or YPD+FLC, as appropriate). It was anticipated that the YPD lines would have similar fitness to the ancestor, whereas the YPD+FLC lines would have much higher fitness. The initial experimental component is done in sterile 96-well culture boxes, which facilitates the use of multichannel pipettes and enables us to process a large number of samples efficiently. Ten biological replicate competitions were carried out for each evolved line. The number of cells of each type is counted and transferred into a fresh medium every 24 h. Since a greater number of transfers will give more consistent data (Wiser, Ribeck, and Lenski 2013), the YPD competitions were carried out for five days (5 transfers). A pilot experiment in YPD+FLC determined that few ancestral cells remained after two transfers in YPD+FLC, which puts the upper limit on the length of the experiment.

Materials

YPD liquid media (Recipe 1)

Strains of interest (this has been tested for 12 replicates of SC5314; *Candida albicans* reference strain with 10 biological replicates each)

0.01 M phosphate-buffered saline/ PBS (Recipe 2)

Stock solutions of drugs of interest (this has been tested with 16 µg/mL fluconazole in YPD) (Recipe 3)

96-well culture boxes (Corning®, cat. no. AXYP2MLSQC)

96-well flatbottom microplates with lids (Corning®, cat. no. CLS3370)

30°C incubator with shaker

Centrifuge

Sterile pipette tips (Rainin, cat. no. 30389299)

Aliquotting pipet controller (VistaLab, cat. no. 2000-0005)

200-µL multichannel pipettor (Pipet-Lite Multi Pipette L12-200XLS+; Rainin, cat. no. 17013810)

Breath-easy membranes (Electron Microscopic Sciences, cat. no. 70536-10)

1. Inoculate 10 µL of fluorescing ancestral strain ("ancestor") and each evolved strain (will be referred to as "competitors" throughout) separately from freezer stock into 1 mL of YPD in a 2 mL sterile 96-well culture box.
2. Cover the culture box with a breath-easy membrane and incubate at 30 °C for 24 h with shaking.
3. After the incubation, mix the wells thoroughly with a multichannel pipettor and inoculate 100 µL from the ancestor and each competitor separately into 900 µL of YPD in a 2 mL sterile culture box.

   If the experiment involves a drug, after the incubation, mix the wells thoroughly with a multichannel pipettor and inoculate 200 µL of the ancestor and competitor separately into 800 µL of YPD supplemented with the drug (In this experiment, I have used YPD supplemented with 16 µg/ mL fluconazole), to acclimatise the cells to the drug.
4. Cover the culture box with a breath-easy membrane and incubate at 30 °C for 24 h with shaking.
5. After 24 h, thoroughly mix the wells by pipetting up and down with a multichannel pipettor. Then, dilute the ancestor and competitors separately by adding 50 µL from each to 950 µL of 0.01 M PBS in a 2 mL culture box.

   Depending on the number of strains, you might need more than one well (1 mL) of ancestor. You will need 100 uL of the ancestor for each competitor. So, either dilute the ancestor into multiple wells at this step or use a larger vessel, such as a test tube, maintaining the same 1:19 ratio of ancestor culture to PBS.
6. Thoroughly mix the wells with a multichannel pipettor. Add 100 µL from the diluted ancestor and each diluted competitor to 800 µL of YPD in a 2 mL culture box to initiate the competition experiment.

   If the experiment involves a drug, thoroughly mix the wells with a multichannel pipettor. Add 100 µL of each diluted evolved strain to 800 µL of YPD supplemented with the drug (In this experiment, I have used YPD supplemented with 16 µg/ mL fluconazole) in a 2 mL culture box and add 100 µL of the diluted ancestral strain.
7. Thoroughly mix the wells, then take 100 µL from each mixture and add to a 96-well microtiter plate. Add 200 µL of 0.01 M PBS to each well.
8. Cover the 96-well culture box (which has 900 µL remaining) with a breath-easy membrane and incubate at 30 °C for 24 h with shaking

9. Centrifuge the 96-well microtiter plate at 2000 g for 5 mins at room temperature to pellet the ancestral and competitor cells.
10. Discard the supernatant, then resuspend the pellets in 300 µL of 0.01 M PBS and centrifuge the plate again at 2000 g for 5 mins at room temperature.
11. Repeat the wash step 10 to remove the culture medium completely and resuspend the final pellet in 100 µL of 0.01 M PBS.

    If the culture media causes autofluorescence (such as YPD), thorough cleaning is necessary to remove any media traces. Different base media may necessitate additional (or require fewer) wash steps.

Note: If you later find that the cell images are too dense and cells overlap, the final volume of PBS could be adjusted based on the cell concentration in the well.

12. Cover the plate with a lid for microscopic image analysis.
13. After 24 h incubation of the 96-well culture box, thoroughly mix the wells and transfer 100 µL of culture into 900 µL 0.01M PBS in a 2 mL culture box.

    Depending on the specifics of your experiment and how quickly your cells grow, the incubation could be extended beyond 24 h.

14. Thoroughly mix the wells with a multichannel pipettor. Add 100 µL of each diluted well to 900 µL of YPD in a 2 mL culture box.

    If the experiment involves a drug, skip step 13. After 24 h incubation, repeat the steps 7, 9 to 12 to obtain the cells for imaging.

15. Repeat steps from 7, 9, to 12 to obtain the cells for imaging.
16. Repeat steps 8, 13 and 14 as often as required for the data collection.

    When the actual competition starts, you can decide the number of transfers besed on the presence of ancestral cells after incubations. I did five transfers in YPD and found out more number of transfers will give more consistent data. However, most of the ancestral cells did not survive after two transfers with the drug.

2.4 Protocol 2: Visualising GFP and non-GFP cells in the same media using an EVOS microscope

Images will be captured from the microplate from step 11 in Protocol 1. Images should always be taken on the initial day of the competition experiment (Day 1). Images should also be taken after each 24 h incubation phase. The total number of days will depend on the specifics of your experiment. We set the EVOS microscope to capture images from six different regions in each well at each time point. If the cells are homogeneous throughout the well, six images are enough to represent the whole well. However, if different parts of the wells contain different cell densities, increase the number of images.

Materials

Processed 96-well plate with a lid from Protocol 1, step 11

EVOS FL Auto 2 (Thermo Scientific, cat. no. AMAFD2000)

Computer with at least 4 GB RAM

EVOS FL Auto 2 Imaging System software

1. Turn on the machine
2. Place the 96-well plate prepared according to the sample preparation section (protocol 1; step 11) on the holder stage. Remove the outermost cover of the incubation chamber to allow light to pass through.
3. Open the Invitrogen EVOS FL Auto 2 Imaging system software.
4. Go to the **Capture** tab (Figure 2.1A) and select **Vessel**. Go to the **Well Plates** tab and select **Well Plate (OSI) | AMEP-VH028** for the **Holder** and the type of plate you are using for the **Plate**. Click **Done** to finish setting up the plate (Figure 2.1B).

   If the plate that you are using is not already added to the plate list, you might need to perform a calibration and add it to the imaging software prior to the imaging. The calibration option is stated under the ***Settings*** *tab.*
5. On the well plate image, manually select a well with a sample and choose 20X as the focus (Figure 2.1C).
6. Select GFP and Trans (Bright-field) as the light source (make sure both sources are ticked - Ticks indicate the selected channels) (Figure 2.1D).
7. To get the image, the **Mode** should be **Actual,** and the Camera should be **Mono** (the selected option will be punched) in the Brightness and camera settings under the wheels beside the light bulb icon (Figure 2.1E).

8. Select the current light source (Bright-field) where the blue outline around the box indicates the current light source, and turn on the light (the option will become blue when selected).
9. To get a well-focused image, adjust the light, exposure, gain, course, and fine focus in this order (Figure 2.1F).

   Light, exposure and gain should kept at a level where the image is illuminated enough, yet you can discriminate cells. Go from minimum to gradually increase each to get a well-focused image.
10. Go to the other light source (GFP) and repeat step 9.

    Optional: can use autofocus without focusing on the course and fine focus scroll bars.
11. Select **Capture Channels** to get the final image (Figure 2.1G).
12. In the visualising area, there should be a merged image with GFP and non-GFP cells (Figure 2.1H).
13. If the image is satisfactory, go to the **Automate** tab (Figure 2.1I).

    Both fluorescent and non-fluorescent cells should be visible in the visualisation area and the cells should be well separated from each other.
14. Go to the Automate tab and **Edit** each option individually to create an automation protocol. Most of the options should be filled automatically at this point, except for **Image Save Settings** and **Scan Area**.
15. Go to **Scan Area** and change the Scan Area (the wells containing the cells) and number of images needed per well (Figure 2.2A).

    I captured six images per well (3 % of the well). If the images look very different from each other, you might need to capture more images per well to represent the whole well.
16. Go to **Image Saving Settings** and select the desired location for the output images to be saved. By ticking/ unticking the options (Raw images, Merged images) (Figure 2.2B), you can add or remove other options.
17. To save the current protocol, click **Save** and save the protocol with an appropriate name (Figure 2.2C).

    *You can load a previously saved protocol using the **Load** option (Figure 2.2D).*
18. Once all parameters have been reviewed, select **Run** to start imaging (Figure 2.2E). Press **Done** after completing the run to finish the protocol.

    All the images will be saved in the given location.

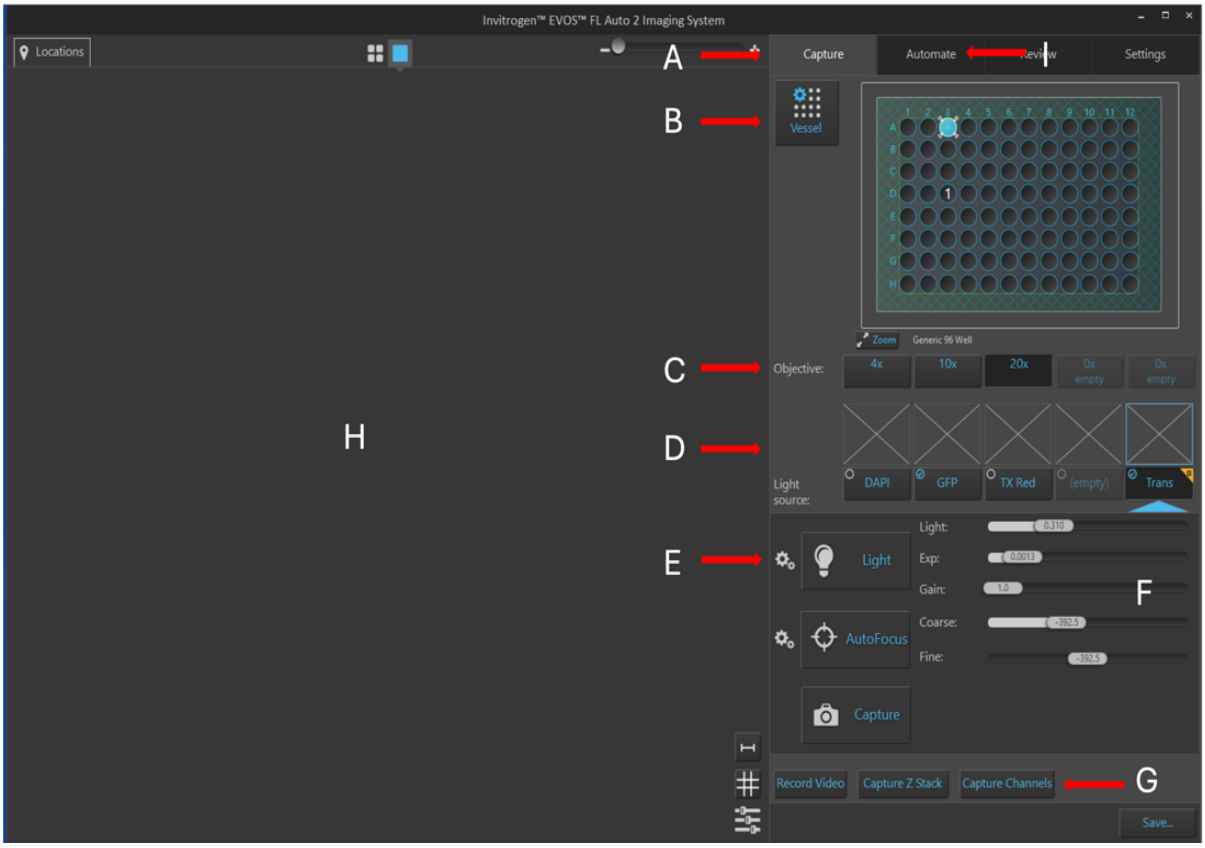

Figure 2.1: Options to adjust the parameters on the interface of the Invitrogen EVOS FL Auto 2 Imaging system. A) Go to the Capture tab. B) Go to Vessel. Select Well Plate (OSI) | AMEP-VH028 for the Holder and click Done to finish setting up the plate. C) On the well plate image, manually select a well with a sample and select 20X as the focus (in here, the well A3 is selected). D) Select GFP and Trans (Bright field) as the light source. E) The Mode should be set to Actual, and the Camera should be set to Mono in the Brightness and camera settings. F) Adjust the light, exposure, gain (minimum is recommended), course and fine focus. G) Select Capture Channels to get the final image. H) A merged image with GFP and non-GFP cells should be in the visualising area. I) If the image is satisfactory, go to the Automate tab and review each option individually to create an automation protocol.

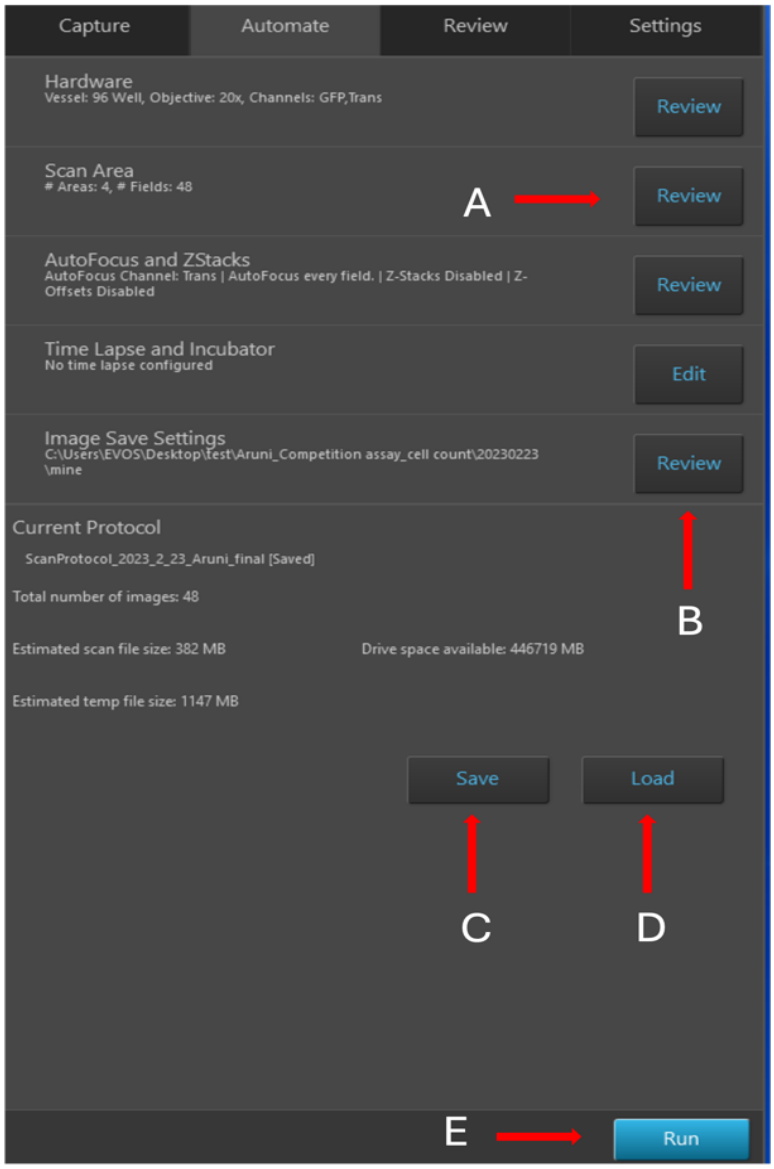

Figure 2.2: Automate tab of the Invitrogen EVOS FL Auto 2 Imaging system. A) Go to Scan Area and change the Scan Area and number of images needed per well. B) Go to Image Saving Settings and select the desired location for the output images to be saved. Add or remove other options as required by ticking/ unticking the options (Raw images, Merged images). C) To save the current protocol, click Save and save the protocol with an appropriate name. D) Can load a saved protocol using the Load option. E) If all the parameters are reviewed and up to the requirements, select Run to start imaging.

2.5 Protocol 3: Count fluorescing (ancestor) and non-fluorescing (competitor) cells with Orbit Image Analysis

The number of images generated from fluorescent microscopic imaging will vary depending on the size of the experiment and the number of replicates. Orbit Image Analysis software is a free, open-source image analysis tool that can easily be trained to count cells from a large number of images (Stritt, Stalder, and Vezzali 2020). Moreover, it can detect and count cells from relatively dense images as long as the cells are not overlapping. After the image processing, Orbit provides a data file that contains the fluorescing and non-fluorescing cell counts, which is required for the downstream data analysis.

Materials

A computer with 8GB (or above) RAM

Orbit Image Analysis Software (Version 3.64 or higher)

Images from Evos output

1. The first time you use it, download the software as appropriate for your OS from https://www.orbit.bio/download/.
2. Unzip the downloaded file and install Orbit onto your computer.
3. To configure, open Orbit by double-clicking on the icon (some Windows OS will not open the software right away, so you may need to use the Run as administrator command).
4. A pop-up window will ask whether you want to configure the Omero server; press **No** (Figure 2.3A).
5. Another pop-up window will notify you that the image provider is unavailable; press **Continue** (Figure 2.3B).
6. Select a few images from the Evos output to train the algorithm. One image is sufficient if all the images contain all the cell types; if you have different cell types, ensure they are all represented in your training set. Go to **Open Image** under the Image tab and select **Open Image from File System** (Figure 2.3C).
7. Select one (or a few) images from the pop-up window, **Open File(s)**.

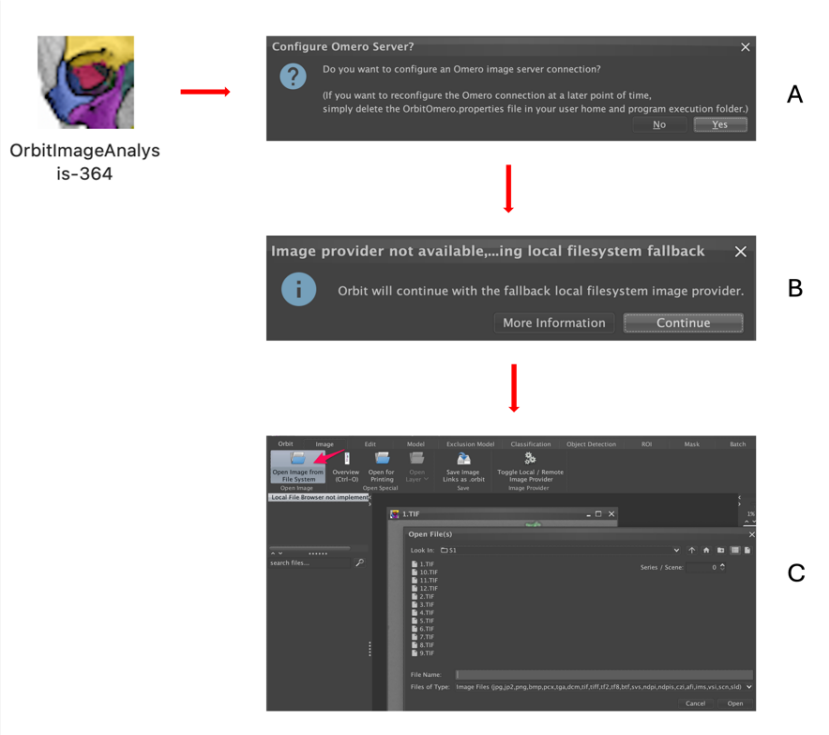

Figure 2.3: Configuring Orbit Image Analysis Software. A) A pop-up window will ask whether you want to configure the Omero server; press No. B) Another pop-up window will notify you that the image provider is unavailable; press Continue. C) To import images to the software, go to Open Image under the Image tab and select Open Image from File System

8. The first step is to identify the foreground (all of the objects in the images, including stained and unstained cells, and ensuring representation of cells of all sizes) and background (the space in between cells).
    a. Go to **Setup Classes** under the **Object Classification** section under the **Object Detection** tab (Figure 2.4A).
    b. Reset current training data? → **Yes**
    c. Then, go to the Setup Classes section under the **Object Detection** tab (Figure 2.4B).
    d. Reset current training data? → **Yes**
    e. To define the foreground and background, go to the drop-down class menu on the top left corner (Figure 2.4C).
    f. Select **Background**.
    g. Zoom in the image until the objects are large enough to be able to mark their margins.

h. Go to the Classification tab → Select **Polygon**

i. Use a polygon to demarcate areas of the background. Ideally, some margins should be drawn very close to, though not touching, the cells (Figure 2.4D). Mark at least three different areas on the image.

j. Next, select the **Foreground** class from the drop-down class menu. Use a polygon to demarcate cells. Ideally, the margins should be drawn very close to the cells. Mark at least five different cells from fluorescing and non-fluorescing each on the image.

k. To train the model, choose **Train Objects** under the **Object Detection** tab (Figure 2.4E).

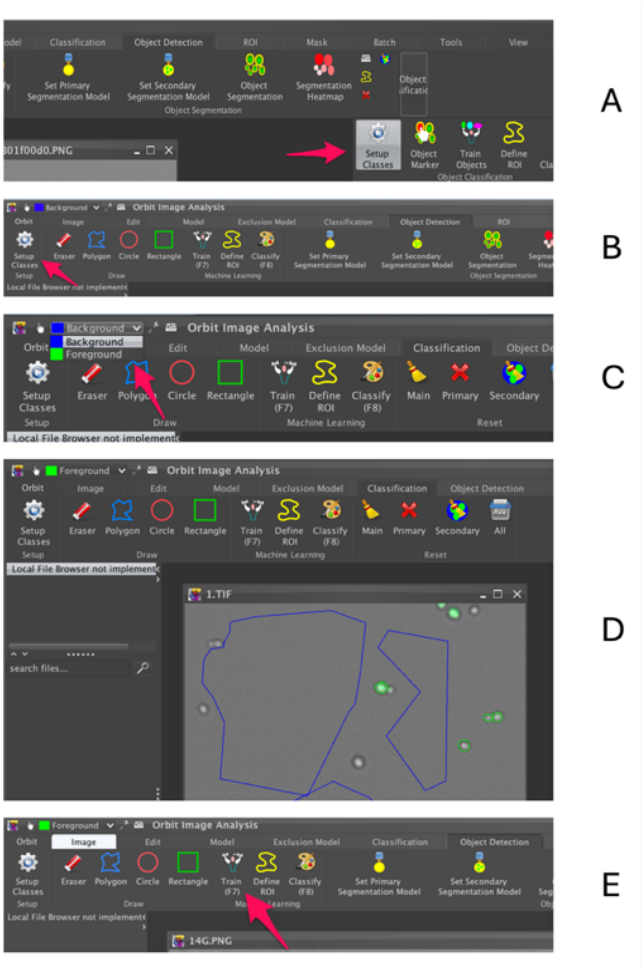

Figure 2.4: Identifying the foreground and background of an image using Orbit software. A) Go to Setup Classes under the Object Classification section under the Object Detection tab. B) Then go to the Setup Classes under the Setup section under the Object Detection tab. C) To define foreground and background, go to the drop-down class menu on the top left corner. D) Using the cursor, mark the margins around the objects. E) To train the model, select Train Objects under the Object Detection tab.

l. Click Set **Primary Segmentation Model** in the Object Detection tab (Figure 2.5A).

m. Segmentation Model Set → **Yes**

n. Select **Object Segmentation** in the Object Detection tab (Figure 2.5B).

o. Detected objects (foreground) will be marked with a yellow margin (Figure 2.5C).

p. **Object Count** will give the number of objects detected in the image (foreground) (Figure 2.5D).

If the margins do not appropriately discriminate the objects and some of the cells appear without yellow margins around, go to Features (F3) under the ***Object Segmentation*** *section under the* ***Object Detection*** *tab and adjust the parameters accordingly.*

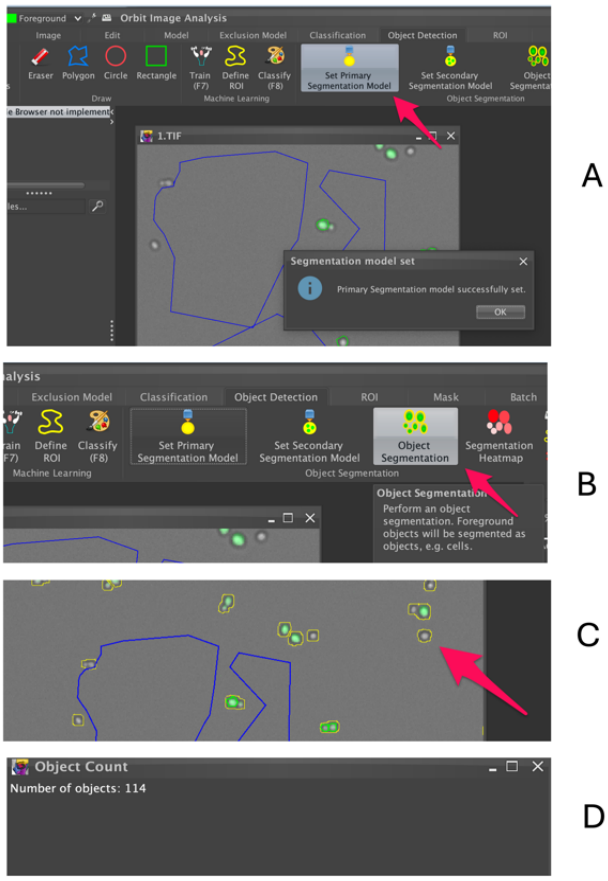

Figure 2.5: Setting up an Object segmentation model in Orbit Image Analysis software. A) Click Set Primary Segmentation Model in the Object Detection tab. B) Select Object Segmentation in the Object Detection tab. C) Detected objects (foreground) will be marked a yellow margin. D) Object Count will give the number of objects detected in the image (foreground).

9. The second step is to define the fluorescing and non-fluorescing cells from the detected foreground.
    a. Go to the **Setup Classes** under the **Object Detection tab**'s **Object Classification section** (Figure 2.6A).
    b. Reset current training data? → **Yes**
    c. Go to the **Classes (F2)** option under the **Configure Model section** under the **Model** tab and change classes accordingly → **OK** (Figure 2.6B)

       *Change Stained Objects to **Fluorescing cells** (this will be the ancestor cell count) and Non-Stained Objects to **Non-fluorescing cells** (this will be the cell count of competitors) using the **rename class** option.*

       *Remove Other Objects using the **remove class** option.*
    d. Select one type of class from the drop-down class menu (e.g. Fluorescing cells).
    e. Go to **Object Marker** under the **Object Classification** section under the **Object Detection** tab.
    f. Click at least five cells of the fluorescing/ancestor class inside the yellow margin (should appear after step 8o).

       After selecting, they will have another margin according to the respective colour (e.g., green), inside the initial yellow margin. If there is variation in fluorescence intensity, cell size, or cell shape, make sure you select cells that fully capture the variation.
    g. Select the other class type from the drop-down Class menu (e.g. Non-fluorescing cells).
    h. Go to **Object Marker** under the **Object Classification** section under the **Object Detection** tab (Figure 2.6C).
    i. Click within the yellow margin (should appear after step 8o) of at least five cells of the non-fluorescing/competitor class (they will have another margin according to the respective colour/ blue).

       If there are variations in cell size or shape, make sure you select cells that capture the variation.
    j. To train the model, go to **Train Objects** under the **Object Classification** section under the **Object Detection** tab (Figure 2.6D).
10. To get the number of cells in each individual class, go to **Object Classification** under the **Object Classification** section under the **Object Detection** tab (Figure 2.6E).

a. The C**ell Classification Result** Window will give the individual counts of all the classes (Figure 2.6F).

b. Cells will be highlighted with their respective colours if the model is appropriately trained. Conduct a visual inspection to ensure that what you see has been accurately captured. If you are unsatisfied, return to step 9d-j and re-define the cell classes.

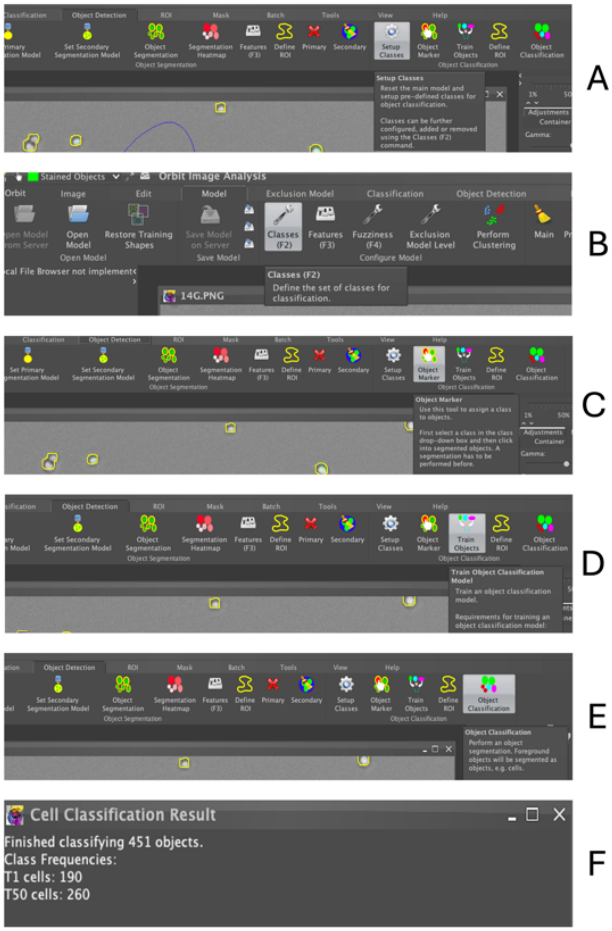

Figure 2.6: Defining fluorescing and non-fluorescing cells in the Orbit Image Analysis software. A) To define the stained and unstained objects from the detected foreground, go to the Setup Classes under the Object Classification section under the Object Detection tab. B) Go to the Classes (F2) option under the Configure Model section under the Model tab and change classes accordingly. C) Go to Object Marker under the Object Classification section under the Object Detection tab. D) To train the model, go to Train Objects under the Object Classification section under the Object Detection tab. E) To get the number of individual classes, go to Object Classification under the Object Classification section under the Object Detection tab. F) The Cell Classification Result Window will give the individual counts of all the classes.

11. Go to the **Batch** tab for bulk analysis (Figure 2.7A).
12. Select **Local Execution** under **Batch Execute** under the **Batch tab** (Figure 2.7B).
13. From the pop-up window, select all the image files that need to be analysed.
    a. Click on the first file and then choose the rest with the shift + arrow keys (or CTR+A). Click **Open** to complete the selection (Figure 2.7C).
14. Select **Yes** when the **Starting Batch Mode** window appears (Figure 2.7D).

    This step can take a considerable amount of time, depending on the number of images you have. During the exporting process, a Batch export notice will appear on the right side (Figure 2.7E).
15. After the analysis, a **Cell Classification** window will appear, giving a list of cell counts (Figure 2.7F).
    a. Select the whole list using CTR+A and copy the list with CTR+C
    b. It can be copied onto a spreadsheet and used in the data analysis

    We use separate sheets within the same Excel file to collect cell count data from different days. The sheets are saved sequentially so that the first one is Day 1

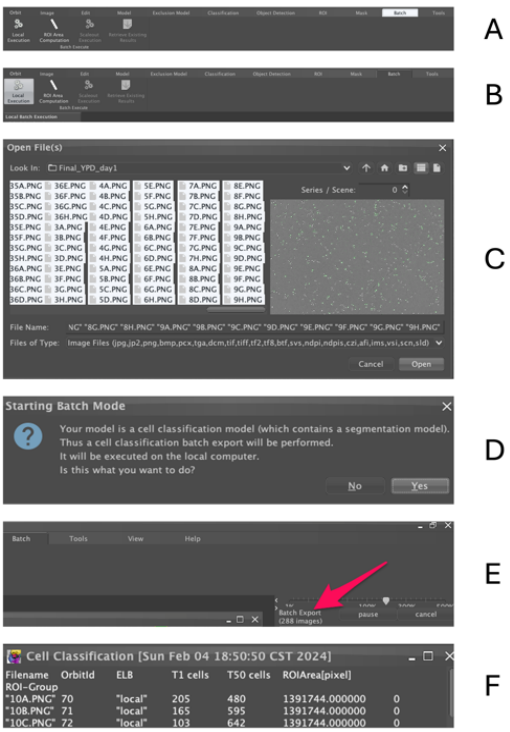

Figure 2.7: Perform Bulk analysis in Orbit Image Analysis software. A) To do the bulk analysis, go to the Batch tab. B) Select Local Execution under Batch Execute under the Batch tab. C) Select the 1st file and choose the rest with the Shift + arrow keys. Click Open to complete the selection. D) Select Yes when the Starting Batch Mode window appears. E) It will take time, depending on your number of images. There will be a Batch export notice on the right side while the exporting happens. F) After the analysis, a Cell Classification window will appear, listing cell counts.

data, the second is Day 2, etc. To use the scripts we will provide below without changing the filename, name your Excel file "Cell_counts.xlsx".

16. To save the current model, go to the **Save as** option under the **Save Model** section under the **Model** tab (Figure 2.8A).
    a. A **Save** window will appear.
    b. Change the **File Name** and **Save In** location accordingly → **Save** (Figure 2.8B).

    It is easy to save the model and use it every time, rather than training the model for each run. However, you need to make sure that the saved model can identify the cells on the images of the current batch by repeating steps 8n and 10. If the results match with what you see in the picture, you can proceed to step 11-15.

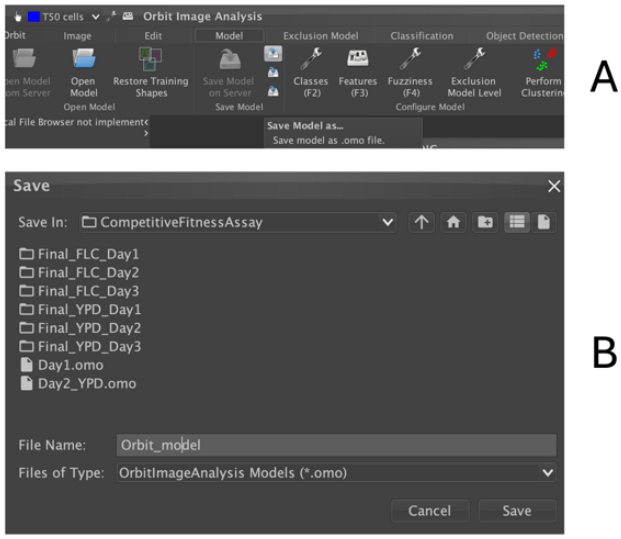

Figure 2.8: Saving a Model in Orbit Image Analysis software. A) To save the current model, go to the Save as option under the Save Model section under the Model tab. B) Change the File Name and Save In location accordingly.

2.6 Protocol 4: Renaming the images

Renaming the images or counts in the data table can be laborious and time-intensive. It is also susceptible to errors and typos, which can extend the time required for the downstream analysis. The following method is not required but is an easy method to rename the counts in the data table using R.

Materials

Excel files with cell counts (Orbit output)

Excel files with actual image names

A computer with at least 4GB RAM

R and RStudio software

2.6.1 [If necessary] Install R and RStudio

1. To download R software, go to https://www.r-project.org and download the relevant version for the OS. Then, install the software using the default settings.
2. To download RStudio, visit https://www.rstudio.com/products/rstudio/download/ and download the relevant OS version. Then, install the software using the default settings.

2.6.2 Set up a new R project

1. Open RStudio. Go to **Create Project** and select **New Project.**
2. Go to **Create New Project** and provide your desired name for the project in the **Directory name** and choose the location where the data files are → **Create Project.**
3. Create a folder called **Input_files in** the given project location.
4. Move the Cell_counts.xlsx file and the Image_names.xlsx files into the Input_files folder.
5. In RStudio, go to **New File → R Script**

   This will open an untitled blank script where you can type your commands

2.6.3 Creating an Excel file with actual image names

1. **Create** a copy of the Excel file that contains the Orbit output (Cell_counts.xlsx) and name it **Image_names.xlsx**.

   You can name these files however you want. If you import the Excel file into R, remember not to use spaces or hyphens between words. Use underscores instead.

2. Delete the columns in all sheets with data except the **Filename** column.
3. Create a new column named **Real_name**, adjacent to the Filename column and fill it with the actual names of the images corresponding to the names in the Filename column.

   Here, the Real_name implies the combination of the replicate number and the actual name of the isolate that those images belong to, separated by an underscore (e.g., Rep1_1). All six images belong to the same isolate, and the same replicate will have the same name.
4. When you import both the Orbit output file and the image names file into R, R can easily cross-check the Filename column and replace it with the Real_name column if there are matching Filename columns in both files.

2.6.4 Exporting data sheets to R

For this data analysis section, I have only included data from ten biological replicates of six lines of *C. albicans* grown in YPD for two days. As above, the data should all be collected in a single Excel worksheet, with cell counts from each day on different sheets sequentially, starting with the Day 1 data on sheet 1.

1. Import the **Cell_counts.xlsx** Excel file tab by tab

   # Import the first sheet (Day 1 data) from the Cell_counts.xlsx file located in the Data_in folder and store it as the YPD_D1 data frame.

```
YPD_D1 <- readxl::read_xlsx ("Data_in/Cell_counts.xlsx",
    sheet = 1)


YPD_D2 <- readxl::read_xlsx ("Data_in/Cell_counts.xlsx",
    sheet = 2) #second day of data
```

   Repeat the second line of code, changing the "DX" part as appropriate to include additional days of data, depending on your experiment.

   To run each line of code, put your cursor anywhere on that line and press **run**.

2. The Image_names.xlsx file should similarly be imported sheet by sheet (increase the number of days, as required)

   # Importing the files with image names

```
YPD_D1_imagenames <- readxl::read_xlsx
```

```
    ("Data_in/Image_names.xlsx", sheet = 1)

YPD_D2_imagenames <- readxl::read_xlsx
    ("Data_in/Image_names.xlsx", sheet = 2)
```

2.6.5 Removing unwanted columns and merging the data frames

1. The only essential columns in the YPD_D1 and YPD_D2 data frames are the Filename and two cell counts columns (Fluor and NonFluor). Therefore, we need to select those columns from the data frame. For that, we need to install the **tidyverse** package (Wickham et al. 2019) and load the package into R.

   ```
   install.packages("tidyverse")
   library(tidyverse)
   ```

   # This will overwrite the YPD_D1 and YPD_2 data frames to keep just the selected columns. Do this for the data frame from each day all .

   ```
   YPD_D1 <- YPD_D1 %>% select(Filename, Fluor, NonFluor)
   YPD_D2 <- YPD_D2 %>% select(Filename, Fluor, NonFluor)
   ```

2. Merge the data frames from Cell_counts.xlsx (YPD_D1) and Image_names.xlsx (YPD_D1_imagenames) to create a single file that contains with real image names. Do this for the data collected from all days.

   # Meriging the data frames

   ```
   YPD_D1_merged <- data.frame(YPD_D1, YPD_D1_imagenames)
   YPD_D2_merged <- data.frame(YPD_D2, YPD_D2_imagenames)
   ```

2.7 Protocol 5: Calculating competitive fitness using R

2.7.1 Clean and rearrange the data

2.7.1.1 Get the average cell count per well

Cell counts were acquired from 6 images per well (Protocol 4, Step 18). So, there will be six rows with counts for each well. They will all have the same name in the "Real_name" column. We first want to average across them for downstream analysis. Note that you can also add them together to get the total number rather than the average number of cells. The results should be similar.

```
# Getting averages across images
YPD_D1_avrg <- YPD_D1_merged %>%
  group_by(Real_name) %>%
  summarise(Avrg_T1_D1 = mean (Fluor, na.rm = T),
      Avrg_T50_D1 = mean (NonFluor, na.rm = T))

YPD_D2_avrg <- YPD_D2_merged %>%
  group_by(Real_name) %>%
  summarise(Avrg_T1_D2 = mean (Fluor, na.rm = T),
      Avrg_T50_D2 = mean (NonFluor, na.rm = T))
```

As above, if additional days of data were collected, copy the above code and change the DX number in all places.

2.7.1.2 Merging Day 1 and Day 2 data tables to get the full data frame

The next step is to merge across all days to get the complete data set for the experiment.

```
# Create a data frame called YPD_df by merging all the data frames mentioned in the
YPD_merged list into a single data frame based on the Real_name column.
YPD_merged <- list(YPD_D1_avrg, YPD_D2_avrg)

YPD_df <- Reduce(function(x, y) merge(x, y, by =
    "Real_name", all = TRUE), YPD_merged)
```

2.7.1.3 [Optional] Adding dilution factor to the data

If the images of Day 1 were taken without diluting the original media with the two competitors, we would not add any dilution factor for Day 1 data (in protocol 1, we did not do any dilution).

However, before getting the Day 2 images, we did a 1:100 dilution (Protocol 1; Steps 13 and 14). Therefore, multiply all Day 2 counts by the 100, the dilution factor.

```
# Set the dilution factor. Change as appropriate if it is different than 1:100
dilutionfac2 <- 100/1 # dilution factor for day 2

# Add two new columns that take into account the dilution factor and then select the required columns to keep
YPD_dil <- YPD_df %>%
    mutate(Avrg_Fluor_D2_dil     =     Avrg_Fluor_D2     *
dilutionfac2) %>%
    mutate(Avrg_NonFluor_D2_dil   =   Avrg_NonFluor_D2   *
dilutionfac2) %>%
    select(Real_name, Avrg_Fluor_D1, Avrg_Fluor_D2_dil,
Avrg_NonFluor_Day1, Avrg_NonFluor_D2_dil)
```

2.7.2 Code for calculating r using the Malthusian parameter of each competitor

The code was generated according to an equation proposed by Travisano and Lenski (1996). The selection rate (r) was calculated as a proxy to competitive fitness by taking the differences in Malthusian parameters of two competitors. Here, we calculate r separately for each replicate and combine them at the end.

2.7.2.1 Getting the ratio between the cell count on Day1 and Day2 for Fluor and NonFluor

We use the YPD_dil data frame from the 2.7.1.3 section.

```
# Add two new columns, Fluor_D2_D1 and NonFluor_D2_D1, by dividing Avrg_Fluor_D2_dil by Avrg_Fluor_D1 and Avrg_NonFluor_D2_dil by Avrg_NonFluor_D1
# Select Real_name, Fluor_D2_D1 and NonFluor_D2_D1 to create a new data frame named YPD_D2_D1

YPD_D2_D1 <- YPD_dil %>%
   mutate(Fluor_D2_D1 = Avrg_Fluor_D2_dil / Avrg_Fluor_D1)
%>%
 mutate(NonFluor_D2_D1 =
```

```
            Avrg_NonFluor_D2_dil/Avrg_NonFluor_D1) %>%
  select(Real_name, Fluor_D2_D1, NonFluor_D2_D1)
```

2.7.2.2 Calculating the Malthusian parameter for each competitor

Applying natural logarithms for the above ratio will give the Malthusian parameter for each competitor

```
# Transform the Fluor_D2_D1 and NonFluor_D2_D1 columns into their natural logarithms.
YPD_ln <- YPD_D2_D1 %>%
    mutate_at(vars(Fluor_D2_D1, NonFluor_D2_D1), log)
```

2.7.2.3 Code for calculating the competitive fitness (r)

Getting the difference between the Malthusian parameters of the competitors will give you the value for r.

```
# Create a new column, r, by subtracting Fluor from NonFluor
# Select the columns Real_name and r
YPD_r <- YPD_ln %>%
    mutate(r = NonFluor_D2_D1 - Fluor_D2_D1) %>%
    select(Real_name, r)

# Get the mean of r
YPD_r_mean <- YPD_r %>%
    summarize(mean = mean(r, na.rm = TRUE))
```

The number of columns/ data points in the final data frame will depend on the size of the experiment. More days and replicates will add extra columns. You can manipulate the same code to calculate r for all the days/ replicates accordingly.

2.7.2.4 Plotting r with package ggplot2 in R

The code below uses the **ggplot2** package in R. Axis labels and aesthetics can be changed according to user preferences. Before plotting the data, separate the Real_name column into two columns, Line_name and Replicate.

```
# Split the "Real_name" column to add more details
YPD_r_detailed <- YPD_r %>%
```

```
    separate(Real_name, into = c("Replicate",
    "Line_name"), sep = "_", remove = FALSE)

# Plot the data
# Change the parameters of the mapping function to alter the appearance of the data points.
# The labs function allows you to change the axis labels to your preference.
# The theme function is responsible for the overall appearance of the graph, e.g., the position of the axis texts and titles)
YPD_r_plot <- ggplot(data = YPD_r_detailed, mapping =
   aes(x = Line_name, y = r)) +
    geom_jitter(width = 0.1, height = 0, alpha = 0.6,
        size=1, shape = 1, stroke = 1) +
    scale_y_continuous(breaks = seq (-3, 3, by = 1),
        limits = c (-3, 3)) +
    scale_x_discrete() +
    labs(x = "C. albicans line (YPD_10reps)",
       y = "Competitive fitness (r)") +
    theme_classic() +
    theme(axis.text.x = element_text (hjust = 0.5,
        face = "bold"), axis.text.y = element_text(face =
        "bold"),axis.title.x = element_text(hjust = 0.5,
        face = "bold"), axis.title.y = element_text
        (hjust = 0.9, vjust = 1, face = "bold")) +
    geom_hline(aes(yintercept = mean), color =
        "darkblue", linetype = "dashed", linewidth = 0.3)
```

2.7.3 Nonlinear least squares (NLS) model

We use R to perform a nonlinear least square fitting on the data set, which will estimate the best-fitting parameters for p_0 and m for each competitor to a nonlinear model. This will give results that are approximately similar to the method described in section 2.7.2. In the NLS method, all data from replicates is combined into a single data frame for model fitting.

2.7.3.1 Create a single data frame that contains information from all experiment days and replicates

We need to rearrange the data for the next analysis step. The easiest way to do this is to export the data frame as a .csv file, save it to your computer, and edit it in Excel. However, it is also possible to do this in RStudio.

We use the YPD_dil data frame from the 2.7.1.3 section.

```
# Exporting the data frame as a .csv file
write.csv(YPD_dil, file = "Data_out/YPD_dil.csv",
    row.names = FALSE)
```

We must create a spreadsheet with Strain, Replicate, day, Fluor, NonFlour and fracNonFluor columns (Strain is the line number of each unique competitor). These exact column names must be used for the NLS model in the next step to work (unless you change the parameter names in the model). If you have more than one exported .csv file from R, combine them in a way that fits into this layout so that we can use a single .csv file for the NLS analysis. Save the spreadsheet as YPD_fracNonFlour.csv in the Data_out folder. Values in the fracNonFluor column are calculated by getting the fraction of T50 cells in each occurrence (e.g., fracNonFluor = NonFluor/ [Fluor+NonFluor]) (Figure 2.9).

	A	B	C	D	E	F	G
1	Strain	Replicate	day	Fluor	NonFluor	fracNonFluor	
2	1	1	0	19	13.5	0.41538462	
3	2	1	0	20.3333333	17	0.45535714	
4	3	1	0	22.8333333	21.5	0.48496241	
5	4	1	0	24.3333333	18.6666667	0.43410853	
6	5	1	0	21.5	24.3333333	0.53090909	
7	6	1	0	22.3333333	27.6666667	0.55333333	

Figure 2.9: Spreadsheet created for NLS fitting

2.7.3.2 Loading the spreadsheet into R studio

We need to import the .csv file back into R. To load a .csv file, we us load the **here** package to the R Studio.

```
library(here)

# Importing the data frame back to R
YPD <- read_csv(here("Data_out", "YPD_fracNonFlour.csv"))
```

2.7.3.3 Declaring the functions for NLS fitting

We need to store the NLS model as a function called "eqn".

```
# The object eqn is specified as a function that will calculate the values based on "p0",
"mmm", and "day" parameters using the formula described in the introduction.
# "mmm" represents the competitive fitness
eqn <- function(p0,mmm,day){
    ((p0*exp(mmm*day))/(1-p0+p0*exp(mmm*day)))
    }

# Create empty vectors for "p0", "mmm", and "names"
p0<-c()
mmm<-c()
names<-c()

YPD_nls <- function(dataset){
    nls(fracNonFluor~eqn(p0,mmm,day), data=dataset,
        start=list(p0=0.4, mmm=0.1))
    }
```

"start = list(p0 = 0.4, mmm = 0.1)" provides the initial values for the parameters to start the process. If you find issues with model fit you can try and change these parameters depending on your expectations for the initial ratio of non-fluorescing and fluorescing cells (p0) and the competitive fitness of non-fluorescing cells (mmm).

2.7.3.4 Creating subsets for each strain

In this example, we have six strains (one for each unique competitor); adjust as necessary.

```
# Create one data frame for each strain.
YPD_1 <- subset(YPD, Strain == 1)
YPD_2 <- subset(YPD, Strain == 2)
YPD_3 <- subset(YPD, Strain == 3)
YPD_4 <- subset(YPD, Strain == 4)
YPD_5 <- subset(YPD, Strain == 5)
YPD_6 <- subset(YPD, Strain == 6)
```

2.7.3.5 Fitting the NLS model

After creating the subsets, we fit the NLS model to the data from each strain.

```
# Fitting the NLS model
YPD_1_par <- compFit_nls(YPD_1)
YPD_2_par <- compFit_nls(YPD_2)
YPD_3_par <- compFit_nls(YPD_3)
YPD_4_par <- compFit_nls(YPD_4)
YPD_5_par <- compFit_nls(YPD_5)
YPD_6_par <- compFit_nls(YPD_6)
```

2.7.3.6 Calculating the Confidence Intervals (CI) in non-linear regression

We use the **confint2** function in the **nlstools** package (Baty et al. 2015) to calculate 95% confidence intervals for the parameter estimates.

1. Calculate the CI

```
install.packages("nlstools2")
library(nlstools)

# Calculating the CI
confint1 <- confint2(YPD_1_par)
confint2 <- confint2(YPD_2_par)
confint3 <- confint2(YPD_3_par)
confint4 <- confint2(YPD_4_par)
confint5 <- confint2(YPD_5_par)
confint6 <- confint2(YPD_6_par)
```

2. Initialize an empty data frame

We only need the confidence values related to m from the above matrixes. Therefore, we need to extract those and create a new data frame. The necessary values will be located in the last row of each matrix.

```
# Create an empty data frame named CI with three columns: Strain (a character column
with Strain names), CI2.5 (a double column to store the lower bound of 2.5% CI), and
```

CI97.5 (a double column to store the upper bound of 97.5% CI). This table will store the CI for each strain.

```
CI <- data.frame (strain=character(), CI2.5=double(),
    CI97.5=double())
```

3. Create a list of CI

 # Create a list named confints containing the names of six CI matrixes created above. Each of these objects contains the CI data for different strains.

```
confints <- list(confint1, confint2, confint3, confint4,
    confint5, confint6)
```

4. Loop through the list and combine CI into one data table

After the loop completes, the CI data frame will contain six rows, each corresponding to a different strain, with their respective 2.5% and 97.5% confidence intervals.

 # The loop iterates over a list of confidence intervals, appending a new row to the data frame CI in each iteration, where each row contains the current index and the last value of the corresponding confidence interval list. If you have a different number of samples than in the example, update the 6 in the for loop as appropriate to your study.

```
for(i in 1:6){
    CI <- rbind(CI, c(i, tail(confints[[i]], n=1)))
    }
```

5. Change the column names of the CI data frame to what we want.

```
colnames(CI) <- c("Strain", "CI2.5", "CI97.5")
```

2.7.3.7 Plotting the data using the ggplot2 package in R

We need to extract CI values to create a new dataset. Since it is the second coefficient, we must specify that in the code.

 # Extract second coefficient values (mmm) from each fitted model and corresponding Strain name to create a new data frame named df.

```
df <- data.frame(Strain = 1:6, m = c(coef(YPD_1_par)[2],
    coef(YPD_2_par)[2], coef(YPD_3_par)[2],
```

```
    coef(YPD_4_par)[2], coef(YPD_5_par)[2],
    coef(YPD_6_par)[2]))

# Convert the Strain variable to a factor for plotting purposes.
df$Strain <- as.factor(df$Strain)
```

Axis labels and aesthetics can be changed according to preferences.

```
library(tidyverse)

# By changing the parameters of the "mapping" function, you can change the appearance of the data points.
# "labs" function allows you to change the axis labels to your preference.
# "theme" function is responsible for the overall appearance of the graph (e.g. position of the axis texts and titles)
YPD_comfit_plot <-
    ggplot() +
    geom_sina(data = df, mapping = aes(x = Strain, y = m,
        colour = Strain), width = 0.1, height = 0, alpha =
        0.6, size=3, shape = 1, stroke = 1) +
    geom_jitter() +
    geom_errorbar(data = CI , aes(x = Strain, ymin =
        CI2.5, ymax = CI97.5), width = 0.1, position =
        position_dodge(0.9), color = "black", size = 0.3)+
    scale_y_continuous (breaks = seq (-3, 3, by = 1),
        limits = c (-3, 3)) +
    scale_colour_manual(values = c("#38040E","#800E13",
        "#880E4F","#E66169", "#996A6A", "#B89896")) +
    scale_x_discrete() +
    labs(x = "C. albicans line (YPD_10reps)",
        y = "Competitive fitness (m)") +
    theme_classic() +
    theme(axis.text.x = element_text (hjust = 0.5, face =
        "bold"), axis.text.y = element_text(face =
```

```
    "bold"), axis.title.x = element_text (hjust = 0.5,
    face = "bold"), axis.title.y = element_text(hjust
    = 0.9, vjust = 1, face = "bold")) +
geom_hline(aes(yintercept = 0), color = "darkblue",
    linetype = "dashed", linewidth = 0.3)
```

2.8 Reagents and solutions

2.8.1 YPD liquid medium (Recipe 1) – for 750 mL

Mix 15 g Bacto Peptone (Gibco, cat. no. DF0118-17-0), 7.5 g Yeast Extract (Gibco, cat. no. 288610), 120 mg adenine hemisulfate (Thermo Fisher Scientific, cat. no. A1696409), 60 mg uridine (Sigma-Aldrich, cat. no. U3750) and 712.5 ml dH2O in a 1 L media bottle. Autoclave the media. Add 37.5 ml of 40% glucose stock (see recipe 4), 750 µL of 1000× ampicillin stock (see recipe 5) and 750 µL of 1000× chloramphenicol stock (see recipe 6) when ready to use.

2.8.2 Phosphate-buffered saline - 0.01M (Recipe 2) – for 400 mL

Dissolve two PBS tablets (BioReagents, cat. no. BP308100) in 400 ml of dH2O in a 500 mL reagent bottle. Autoclave the solution.

2.8.3 Fluconazole - 20 mg/ mL (Recipe 3) – for 10 mL

Dissolve 200 mg of Fluconazole (Sigma, cat. no. F8929) in 10 mL of Dimethylsulfoxide (Fisher Chemical, cat. no. D139-1). Filter sterilise and divide the solution into 1 mL aliquots. The solution can be stored for up to 1 year at -20 °C.

2.8.4 Glucose - 40% (Recipe 4) – for 37.5 mL

Dissolve 15 g of dextrose (Fisher Chemical, cat. no. D16500) using a magnetic stirrer in 20 mL of dH2O. Bring volume up to 37.5 ml using dH_2O. Autoclave

2.8.5 Ampicillin stock - 1000× (Recipe 5) – for 7.5 mL

Dissolve 750 µg of ampicillin sodium salt (Fisher BioReagents, cat. no. BP176025) in 7.5 mL of autoclaved dH_2O. Filter, sterilise, and divide the solution into 750 µL aliquots. The solution can be stored for up to 1 year at 4°C.

2.8.6 Chloramphenicol stock - 1000× (Recipe 6) – for 7.5 mL

Dissolve 187.5 mg of chloramphenicol (Fisher BioReagents, cat. no. BP904-100) in 7.5 mL of 95% ethanol (Greenfield Global, cat. no. P025EA95). Divide into 750 µL aliquots. It can be stored for up to 1 year at 4°C.

2.9 Troubleshooting

2.9.1 Sample preparation

As indicated in the sample preparation protocol, all the steps until step 7 should be performed in a biosafety cabinet under sterile conditions, and all the reagents and other materials should be sterile. After step 8, the sample preparation can be carried out on the bench top, and the reagents used are not required to be strictly sterile. Including a blank well with media (without culture inoculum) ensures the media is not contaminated in each 24h incubation step. The experiment should be repeated if this blank well is turbid after incubating. After 24h of incubation, each well should have a visible cell pellet at the bottom, and the liquid portion should be slightly turbid (this can vary depending on the environment). If the media is clear, the incubation time should be increased. Ensuring all the multichannel tips draw in the same sample volume is necessary to eliminate the biases and volume differences. Also, it is advisable to dispense the ancestral line to the mixture (at step 6) from the same diluted sample using single rather than multichannel pipetting.

2.9.2 Protocol for visualising GFP and non-GFP cells in the same media using EVOS microscope

Ensuring that the cells in the cell visualising area (Figure 2H) do not overlap is essential. The image can be crowded with cells, but further dilution is needed if the cells overlap. If there are not enough cells, the plate can be centrifuged again, and the resulting cell pellet can be resuspended in a smaller amount of 0.01 M PBS to increase the cell concentration. To detect the GFP properly in the downstream analyses, all the traces of auto-fluorescence in the growth medium must be removed from the solution. If the background of the images contains green areas or dots, another cleaning round should be included before taking the photos. The number of pictures per well can be adjusted depending on the requirements and positioning of the cells. There is, however, a tradeoff, as the time to complete imaging a plate increases as the number of photographs taken per well increases.

2.9.3 Protocol for counting the cells with Orbit Image Analysing Software

After training the algorithm in Orbit once, it can be saved and loaded for future use. However, running it through one image before processing all the photos is advisable to ensure it can detect the cells correctly. Depending on the number of pictures per batch, the time it takes to process can vary. Also, Orbit can drastically slow down computer performance if other

programs are also running in the background. The Orbit Image Analysis handbook can be found at https://www.orbit.bio/wp-content/uploads/sites/2/2016/08/OrbitHandbook.pdf

2.9.4 Protocol for renaming the images and data analysis using R Studio

Before loading the data into R Studio, the text within the data files should be free from spaces and invalid characters (i.e. #, @, %). All of the required R packages must be installed on first use (using install.packages()). They need to be loaded into the R Studio workspace every time before running the code using the library() function. The commands in the data visualisation section can be altered depending on the requirements and aesthetics.

2.10 Results

2.10.1 Competitive fitness of YPD-evolved mutation accumulation lines

For the first competitive fitness assay, we picked six strains (i.e., six competitors) that evolved at a low effective population size in YPD for 50 transfers. For each ancestor × competitor pair, we conducted ten separate competitions (i.e., ten biological replicates) over five transfer days (i.e., a total of 96 h after initiation, with pictures taken on day 1 - hour 0, day 2, day 3, day 4 and day 5). We calculated r (section 2.7.2) and m (section 2.7.3), and we obtained similar results from both measurements for competitive fitness (Figure 2.10). The competitive fitness of all six lines has remained approximately similar, and compared to the ancestral line, the fitness of the evolved lines was very similar to ancestral lines.

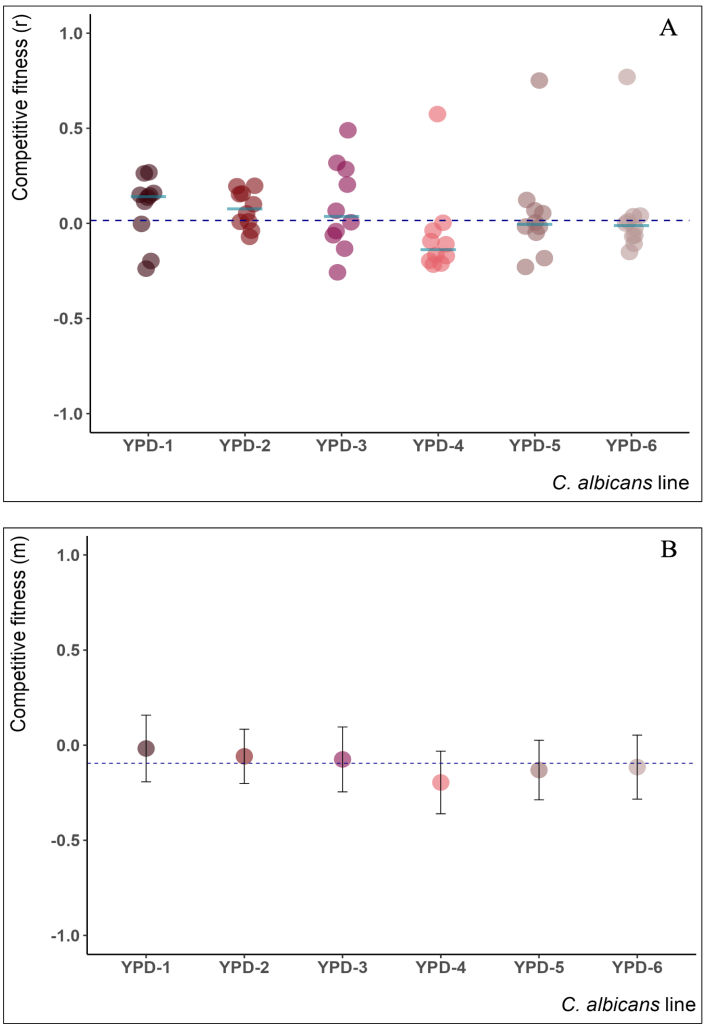

Figure 2.10: Competitive fitness of YPD-T50 lines. The median value of competitive fitness in each plot is represented by a dark blue horizontal dashed line. A) Competitive fitness calculated using Malthusian parameter (r). Each circle represent one biological replicate (10 per line). Teal blue horizontal bars indicate the median of each *C. albicans* line. B) Competitive fitness calculation with NLS model fitting (m). Black vertical bars indicate the 95 % confidence interval of the data calculated using confint2 function of nlstools package in R.

2.10.2 Competitive fitness of FLC-evolved mutation accumulation lines

For the third competitive fitness assay, we picked six strains (i.e., six competitors) that evolved in YPD+FLC for 50 transfers. For each ancestor × competitor pair, we conducted ten separate competitions (i.e., ten biological replicates) over two days (i.e., a total of 24 h after initiation, with pictures taken on day 1 - hour 0 and day 2). The evolved lines all have a nearly three-fold increase in competitive fitness compared to the ancestral line (Figure 2.11). Compared to the other experiments, the evolved lines have considerable variation in competitive fitness. This is likely due to different beneficial mutations that were acquired during the evolution to FLC.

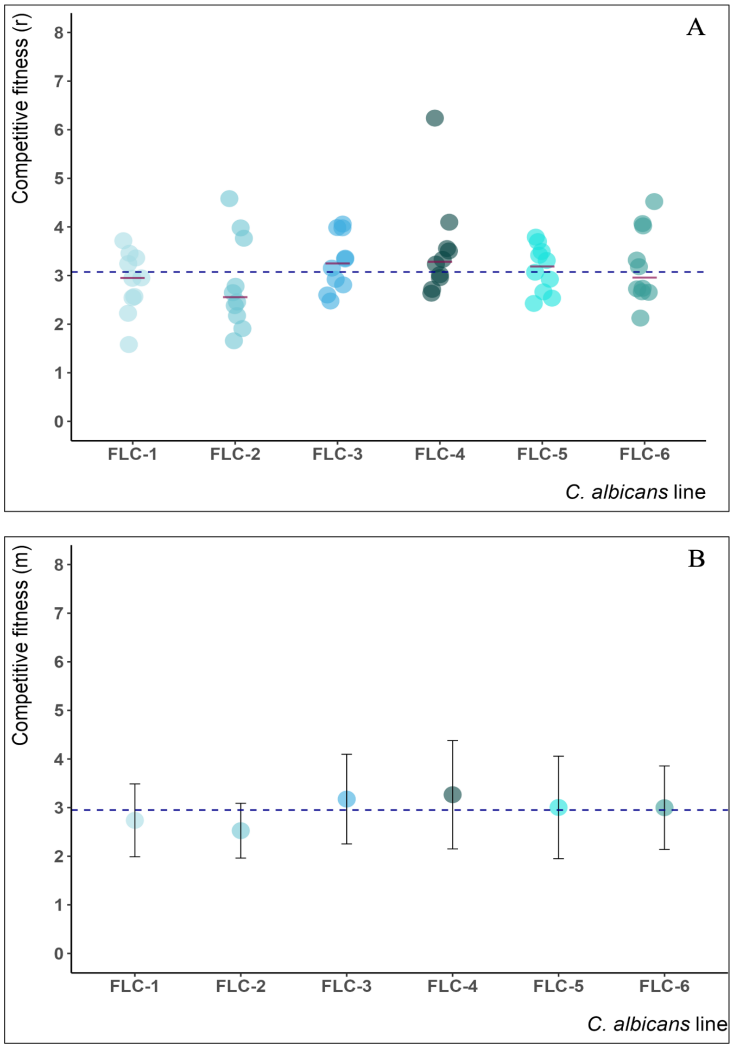

Figure 2.11: Competitive fitness of YPD-T50 lines. The median value of competitive fitness in each plot is represented by a dark blue horizontal dashed line. A) Competitive fitness calculated using Malthusian parameters (r). Each circle represent one biological replicate (10 per line). Maroon horizontal bars indicate the median of each *C. albicans* line. B) Competitive fitness calculation with NLS model fitting (m). Black vertical bars indicate the 95 % confidence interval of the data calculated using confint2 function of nlstools package in R.

2.10.3 Change in the precision of competitive fitness with the number of biological replicates

Both YPD and FLC competitive fitness assays were conducted with ten bio-replicates each. To test how the precision of the calculated competitive fitness values changed with the number of bio-replicates, we conducted a bootstrap analysis where we compared the results obtained from ten, eight, five and three replicates. We did not observe any notable changes in fitness values according to the number of replicates; however, precision decreased with a lower number of replicates, as expected, as the confidence interval clearly increased with a reduced replicate size (Figure 2.12).

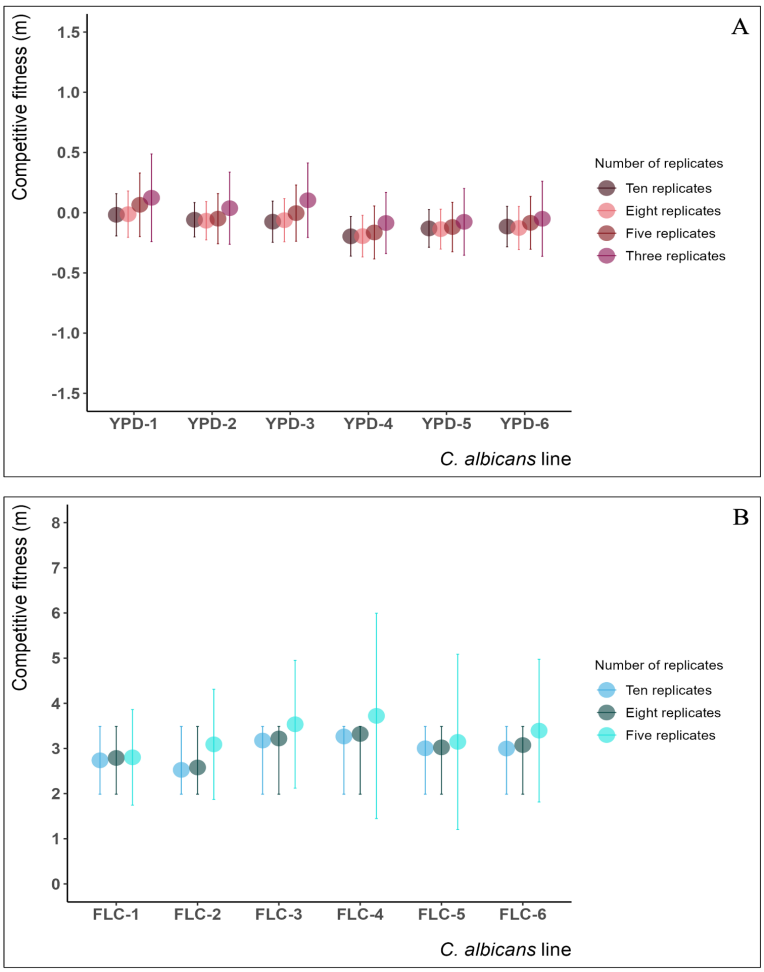

Figure 2.12: Change in the precision of competitive fitness with the number of biological replicates. Vertical bars in respective colours indicate the 95 % confidence interval of the data calculated using confint2 function of nlstools package in R. A) Competitive fitness calculation with NLS model fitting using ten, eight, five and three biological replicates of YPD assay. B) Competitive fitness calculation with NLS model fitting using ten, eight and five biological replicates of FLC assay.

Chapter 3 : Assessing the replicate lines of *C. albicans* in the presence and absence of fluconazole to determine the nature of the mutations acquired when the effective population size is small

3.1 Abstract

Candida albicans, the most prevalent human fungal pathogen, is a common commensal member of the healthy human microbiota. It is also an opportunistic pathogen. *C. albicans* populate various sites within the human body, with population sizes differing significantly due to varying environmental conditions. Although the evolutionary trajectories of *C. albicans* have been widely explored, all previous studies have been done in experimental evolutionary settings at very high population sizes, where selection is prominent. Fluconazole, a triazole antifungal agent, is a putative mutagen used in clinical settings to treat *C. albicans* infections. Recent studies suggest that *C. albicans* can develop resistance to fluconazole due to frequent use. Most of the studies related to fluconazole resistance and tolerance were only done at very high population sizes, yet they might not always be biologically relevant. The impact of fluconazole concentration on *C. albicans* resistance and tolerance when the effective population size is small has yet to be thoroughly explored. This will be the pioneer evolutionary study done at a low population size in *C. albicans.* We have evolved *C. albicans* lines with and without fluconazole in the media and compared the evolved lines and ancestral lines phenotypically and genotypically to determine the effect of fluconazole on *C. albicans.* The lines that evolved without fluconazole were similar to ancestral lines in growth rates, genome size, drug responses, and competitive fitness, However, the lines that evolved with fluconazole exhibited a significant and rapid increase in fluconazole tolerance and competitive fitness compared to the ancestral lines, and showed a dose-dependent increase in fluconazole tolerance and genome size, along with a higher presence of aneuploid chromosomes. Similarly, the competitive fitness of the evolved lines also increased with the fluconazole concentration when the environmental conditions were similar to those in which they had evolved. These findings strongly emphasise the significant impact of fluconazole on the evolution of *C. albicans*, propelling rapid adaptations that enhance drug tolerance and competitive fitness.

3.2 Introduction

More than 150 million severe cases of human fungal infections arise globally every year (Kainz et al. 2020), with a mortality rate of ~1.6 million people (Oladele et al. 2020). *Candida albicans*, the most prevalent human fungal pathogen, is both a common commensal member of the healthy human microbiota (Haoping Liu 2002) and an opportunistic pathogen (Mixão and Gabaldón 2020). *C. albicans* can grow in diverse environments in the human body in both commensal and pathogenic states, such as the oral cavity, gastrointestinal tract, and urogenital tract, on the skin and in the blood (Fidel 1999). *C. albicans* can potentially cause a diverse range of infections, from superficial infections to systemic diseases (Talapko et al. 2021). The sites it is found at differ significantly in terms of temperature, pH, nutrient availability, and other environmental factors; *C. albicans* can thus tolerate a broad range of environmental conditions and has a versatile metabolism on a wide range of carbon and nitrogen sources (Brown et al. 2014; Ene et al. 2014; Vylkova et al. 2011). The large niche breadth of *C. albicans* suggests it can rapidly acclimate or adapt.

The diploid genome of *C. albicans* comprises eight chromosomes and is known to be heterozygous (Olaiya and Sogin 1979; Butler et al. 2009). Like most microbes, the *C. albicans* genome exhibits genome plasticity via single nucleotide polymorphism (SNPs), small insertions and deletions, and copy number variations in genes and chromosomes (Ene et al. 2018). In addition, variations in ploidy are common in both natural isolate sets of *C. albicans* and emerge rapidly among *in vitro* evolution experiment replicates, resulting in increases and decreases in ploidy (Gerstein and Sharp 2021; Hickman et al. 2013). Chromosomal aneuploidy has also been seen to arise frequently (Selmecki, Bergmann, and Berman 2005). In addition to changes in ploidy and aneuploidy, loss of heterozygosity (LOH) is also frequently observed in stressful conditions, both as small-tract LOH and large-tract LOH (Forche et al. 2011).

Previous studies have found that different environmental stresses, such as temperature, pH, oxidative, and drug stress, can induce genomic variations in *C. albicans* (Harrison et al. 2014; Forche et al. 2011). *C. albicans* is particularly prone to spontaneous genomic changes under drug stress. Agyare-Tabbi et al. (2024) found that antifungal agents such as fluconazole and caspofungin can cause DNA double-strand breaks in *C. albicans* (Agyare-Tabbi et al. 2024). Fluconazole is the most common first-line antifungal treatment (Goa and Barradell 1995). Despite low intrinsic resistance rates (< 1%), there is a > 30% chance of therapeutic failure against fluconazole-susceptible *C. albicans* isolates (Pfaller et al. 2019; Levinson et al. 2021). Fluconazole is a fungistatic drug in which the fungal cells can survive and grow slowly

(Lu et al. 2021). Tolerance is the ability of a subpopulation of cells within a drug-susceptible fungal strain to grow slowly at above-MIC concentrations of fungistatic drugs that inhibit fungal growth (Fisher et al. 2022). Unlike antifungal resistance arising from genomic mutations, tolerance mostly depends on the organism's stress responses, and mutations can contribute to tolerance by altering pathways that regulate stress responses, cell wall integrity and metabolic state (Berman and Krysan 2020). Salama and Gerstein (2020) screened clinical *Candida* isolates and found that fluconazole-resistant isolates have a tendency to be more tolerant of the drug as well. Moreover, another *in vitro* evolution experiment in fluconazole with 20 isolates of *C. albicans* showed that tolerance and resistance developed individually, and isolates evolved resistance, while many increased in tolerance (Gerstein and Berman 2020). The concept of tolerance is somewhat understudied in *C. albicans*, and the mechanisms responsible for drug tolerance still need to be better understood (Druseikis, Mottola, and Berman 2023). The persistence of tolerant phenotypes hints at the idea of a connection between drug tolerance and clinical treatment failures in current days (Rosenberg et al. 2018).

Fluconazole and other azole drugs increase the aneuploidy rate in *C. albicans* by inducing abnormal cell divisions, and nearly 50 % of fluconazole-resistant isolates are aneuploids (Harrison et al. 2014). It is also well-established that some aneuploidies are beneficial in the presence of fluconazole; therefore, fluconazole may cause and select for aneuploidy (Ford et al. 2015). Selmecki et al. (2006) found that complete aneuploidy, as well as segmental aneuploidy (isochromosome composed of the two left arms of chromosome 5), can confer azole resistance in *C. albicans* (Selmecki et al. 2006). Yang et al. (2023) found a strong correlation between fluconazole tolerance and the presence of aneuploid chromosomes. Aneuploidy can result in the amplification of *ERG11* and *TAC1*, well-characterized genes responsible for fluconazole resistance, located in chromosome 5 of the *C. albicans* genome can confer fluconazole resistance (Selmecki, Forche, and Berman 2006).

C. albicans genome is 14.3 MB, and 0.5 % of the genome consists of heterozygous positions (~70000 positions) (Braun et al. 2005; Muzzey et al. 2013; Jones et al. 2004). These heterozygous regions can easily undergo LOH under stressful conditions (Diogo et al. 2009; Forche et al. 2011; Rosenberg 2011; Hirakawa et al. 2015). Ene et al. (2018) found that mutation rates were considerably higher in the telomeric regions, repeat regions and genes responsible for encoding glycosylphosphatidylinositol-linked cell wall proteins (Ene et al. 2018). In the process of microevolution, short-tract LOH frequencies are effectively balanced out by *de novo* gain of heterozygosity (GOH) rates, thereby ensuring the stability of heterozygous levels in the genome. Long-tract LOH events are notably rare and have the

potential to profoundly impact crucial genes, resulting in significant phenotypic changes. Consequently, such events are subject to strong selective pressure (Ene et al. 2018). Forche et al. (2011) proposed the idea of "stress-induced LOH", referring to the increased rates of LOH in *C. albicans* under different stress conditions such as antifungal drugs.

Most of the studies described above have been done in an experimental evolution setting, where the experiments were carried out under a high effective population size, and selection is efficient at enabling beneficial mutations to rise to high frequency (Cowen et al. 2000). Since *C. albicans* is capable of colonising various sites in the human body, and the population sizes differ in each of these sites, studying the evolutionary dynamics of high population sizes alone may not always be biologically relevant. Mutation accumulation (MA) studies are typically employed to study phenotypic and genotypic changes when the effective population size is small (Zeyl and DeVisser 2001). In experiments, replicate lines with a common ancestor undergo repeated population bottlenecks by streaking single colonies from a single cell. This results in a small effective population size (N_e), which theoretically limits the selection of new mutations (Sharp et al. 2018). Sharp et al. (2018) conducted experiments on haploid and diploid *S. cerevisiae* lines, finding that diploids are more susceptible to large-scale mutations with detrimental effects, while haploids are more prone to single-nucleotide mutations. Nishant et al. (2010) observed that the yeast diploid genome is stable in mitosis and meiosis, with no observed indels or ploidy changes. Lynch et al. (2008) studied haploid *S. cerevisiae* and found that the cells became nearly diploid within a few hundred generations with around 0.1% mutations having a fitness effect.

Here, we have conducted the pioneer set mutation accumulation experiments with *C. albicans* under different fluconazole concentrations to assess the effect of drug stress when the effective population size is low. We found that lines evolved on rich media have no fitness benefit over ancestral lines regarding growth rate, competitive fitness or tolerance and resistance to fluconazole. In contrast, lines that evolved in fluconazole exhibited a substantial increase in fluconazole tolerance and competitive fitness in a dose-dependent manner, along with an increase in genome size and the presence of aneuploid chromosomes. These findings emphasise the profound impact of fluconazole on the evolution of *C. albicans*, driving rapid adaptations that enhance drug tolerance and competitive fitness, highlighting the importance of understanding drug resistance mechanisms in pathogenic fungi.

3.3 Results

3.3.1 competitive fitness

Evolved and ancestral lines of both MA experiments were subjected to a competitive fitness assay under their evolved drug concentrations. YPD-T_{50} lines had similar competitive fitness as T_1 lines, with a mean fitness of -0.06. When FLC16-T_{50} competed against T_1 in FLC16, their competitive fitness increased three-fold compared to T_1 lines, with a mean fitness of 3.09. All the other FLC-evolved lines (concentrations between 0 µg /mL and 16 µg /mL) show a significant increase in competitive fitness compared to the ancestral lines when they grow in an environment similar to the one they have evolved (Figure 3.1). The results show a dose-dependent increase in competitive fitness in evolved lines, suggesting that the competitive fitness increases improve significantly with higher drug concentrations (ANOVA; $F_{5, 114} = 311.6$, $p < 0.0001$). All the drug classes are significantly different from each other (Supplementary Table 1), except for FLC4 and FLC8 (Tukey's HSD; *diff* = -0.041, $p = 0.999$).

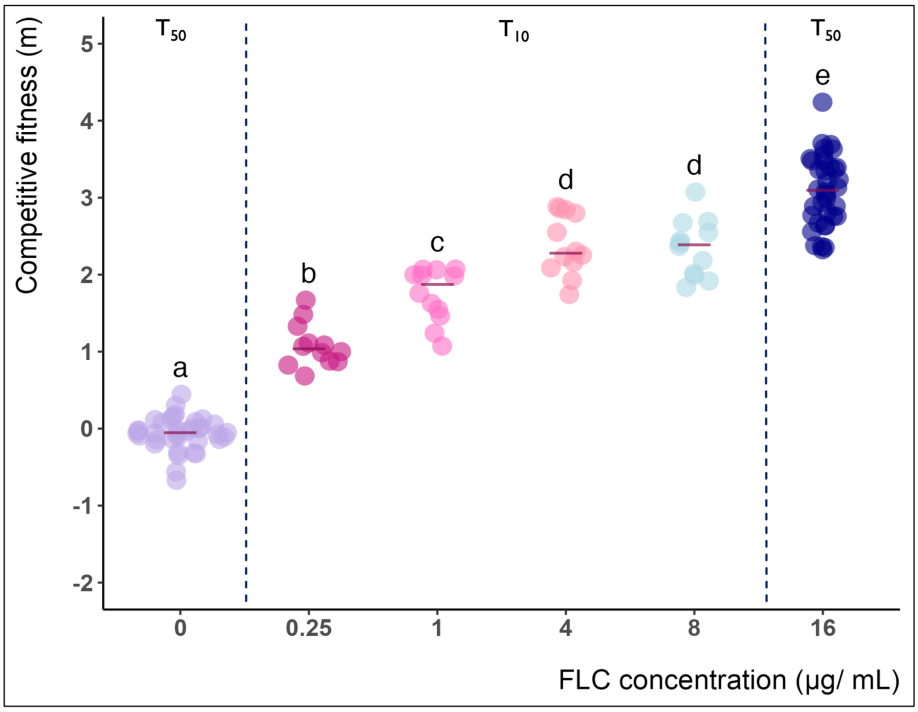

Figure 3.1: Comparison of competitive fitness (m) measurements of the evolved lines (YPD-T_{50} /36 lines, FLC0.25-T_{10} /12 lines, FLC1-T_{10} /12 lines, FLC4-T_{10} /12 lines, FLC8-T_{10} /12 lines, and FLC16-T_{50} /36 lines) compared to T_1 lines when they compete in a media that is similar to the one they have evolved. Each circle represents four biological replicates. Maroon horizontal bars represent the median of each concentration category. Tukey HSD test results show the mean values for different concentrations using a 95% family-wise confidence level. Different letters above the data points indicate significant differences between groups ($p < 0.05$). Groups sharing the same letter are not significantly different from each other.

3.3.2 Tolerance and Resistance

According to the DDA results, the resistance of T_1 and YPD-T_{50} are similar to each other. Although the resistance of FLC16-T_{50} is slightly higher than the former two, it is not significant (ANOVA; $F_{2, 105} = 1.103$, $p = 0.336$, Figure 3.2A). In contrast, tolerance values were highly significant (ANOVA; $F_{2. 105} = 1834$, $p < 0.0001$). There was no significant difference in tolerance between T_1 and YPD-T_{50} (Tukey's HSD; *diff* = 0.021, $p = 0.108$). However, the tolerance of FLC16-T_{50} is significantly higher than that of T_1 (Tukey's HSD; *diff* = 0.561, $p < 0.0001$, Figure 3.2B).

According to the results of DDA done with evolved lines from all MAs, the resistance exhibits a significant but slight increase among evolved lines (ANOVA; $F_{6, 77} = 2.667$, $p = 0.021$). However, post hoc analysis using Tukey's HSD test revealed that only the resistance of T_1 and FLC0.25-T_{10} lines differed significantly (Tukey's HSD; *diff* = 2.958, $p = 0.046$). There was no clear trend in the magnitude of change among different concentrations (Figure 3.3A). All the FLC-evolved lines (concentrations between 0.25 µg /mL and 16 µg /mL) show a significant increase in tolerance (ANOVA; $F_{6, 77} = 78.27$, $p < 0.0001$). Similar to competitive fitness results, the tolerance results show a dose-dependent increase in evolved lines, suggesting that the tolerance improves significantly with higher drug concentrations (Figure 3.3B). Post-hoc analysis using Tukey's HSD test showed that some categories were significantly different from others, although these differences were not consistent across all pairwise comparisons (Supplementary Table 2). Interestingly, both resistance (Tukey's HSD; *diff* = -1.458, $p = 0.741$) and tolerance (Tukey's HSD; *diff* = 0.002, $p = 0.999$) data of FLC16-T_{10} and FLC16-T_{50} are not significantly different implying that the tolerance emerges in earlier stages of MA experiments with exposure to fluconazole. Similarly, both resistance (Tukey's HSD; *diff* = 0.291, $p = 0.999$) and tolerance (Tukey's HSD; *diff* = 0.007, $p = 0.999$) data of T_1 and FLC0.25-T_{50} are not significantly different implying that the tolerance will not emerge when the drug level is very low.

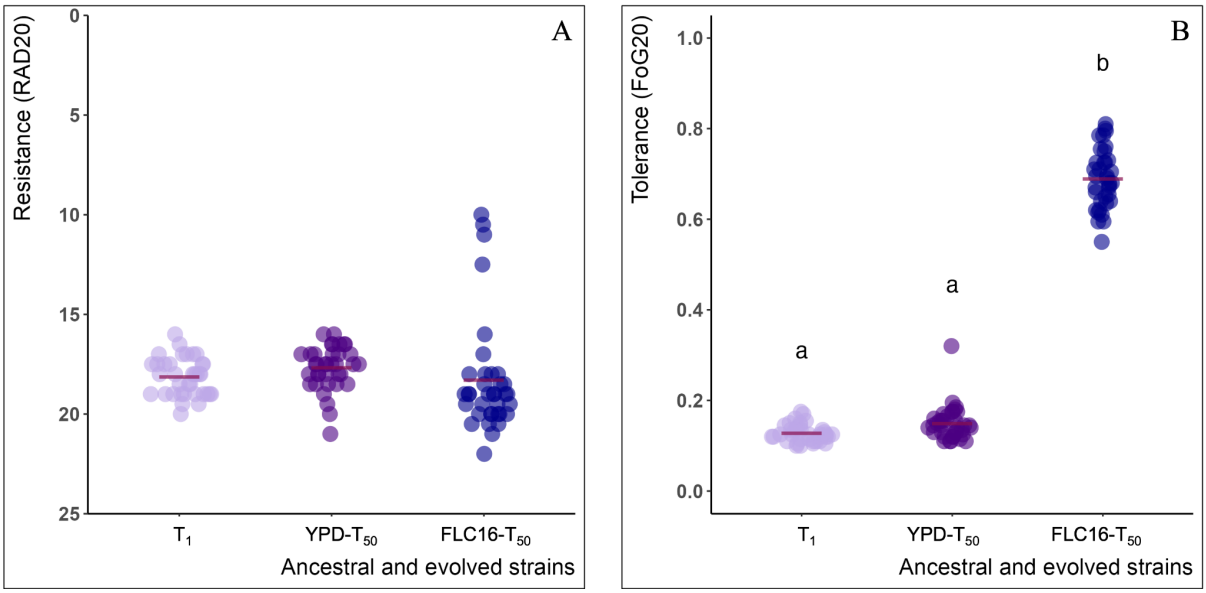

Figure 3.2: Comparison of resistance and tolerance of T_1 lines, YPD-T_{50} lines and FLC16-T_{50} lines from YPD-MA and FLC16-MA. Each circle represents the mean tolerance/ resistance value of two technical replicates. Maroon horizontal bars represent the median of each category. A) Resistance plot where resistance is measured as RAD20 from the DDA results. B) Tolerance plot where tolerance is measured as FoG20 from the DDA results. Different letters above the data points indicate significant differences between groups ($p < 0.05$). Groups sharing the same letter are not significantly different from each other.

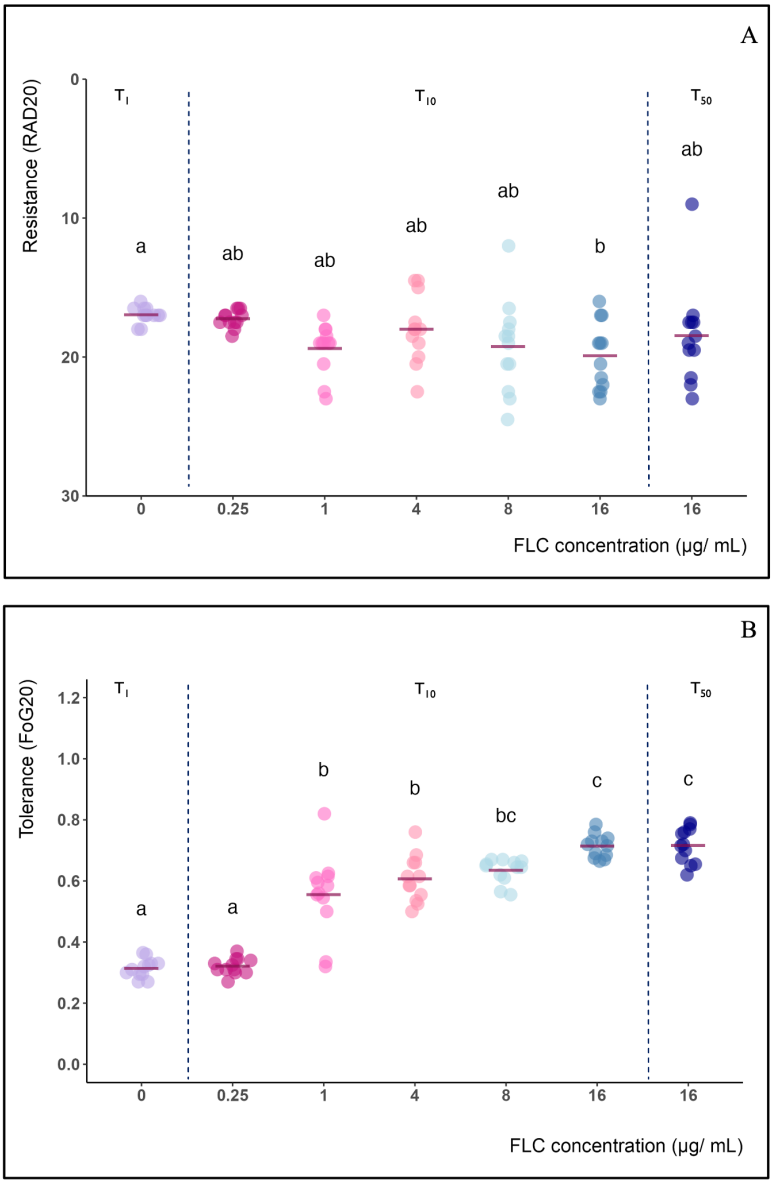

Figure 3.3: Comparison of resistance and tolerance of T_1 lines, FLC-T_{10} lines and FLC16-T_{50} lines from FLC-MA. Each circle represents the mean resistance / tolerance value of two technical replicates. Maroon horizontal bars represent the median of each category. Different letters above the data points indicate significant differences between groups ($p < 0.05$). Groups sharing the same letter are not significantly different from each other. A) Resistance plot where resistance is measured as RAD20 from the DDA results. B) Tolerance plot where tolerance is measured as FoG20 from the DDA results.

3.3.3 Measuring the genome size to detect the presence of aneuploids

According to the flow cytometry analysis, the genome size (the size of unreplicated DNA in the Gap1 phase/ G1 means) was similar between the T_1 and YPD-T_{50} lines. However, the G1 means of FLC16-T_{50} lines were slightly higher than that of T_1 with six definitive polyploids (Figure 3.4). Fluorescence values were used as a proxy for genome size. The genome size (G1 means) of T_{10} lines was higher than that of T_1, except for FLC0.25-T_{10} lines. The genome size and the number of large-size genome changes increased in a dose-dependent manner, which is in line with the tolerance results. Interestingly, the results of FLC16-T_{10} were remarkably similar to those of FLC16-T_{50} lines, with all FLC16-T_{10} polyploids present in FLC16-T_{50} as well (Figure 3.5).

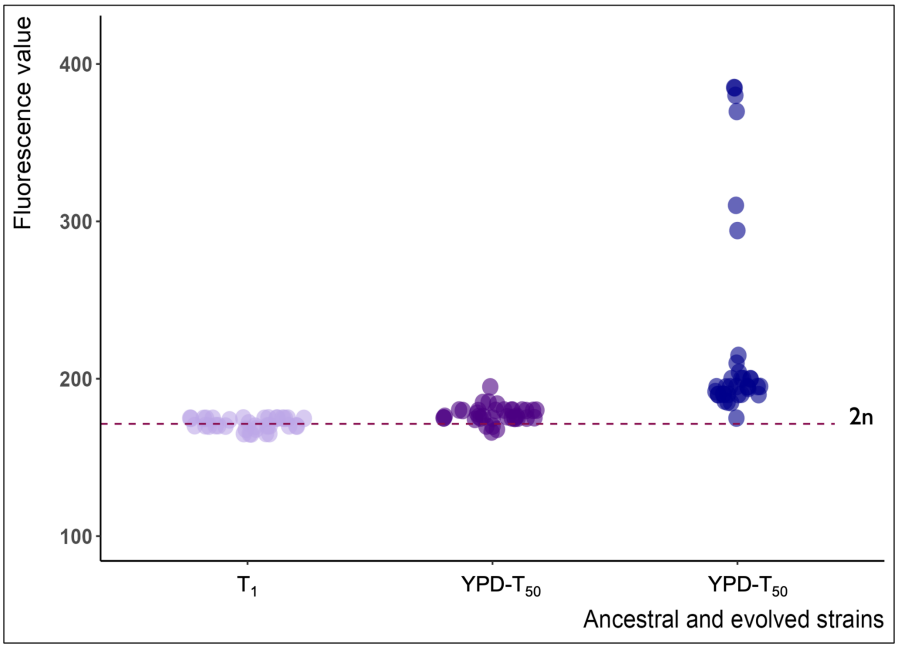

Figure 3.4: Genome size of ancestral and evolved *C. albicans* lines determined using flow cytometry. The maroon horizontal dashed line indicates the midpoint of the G1 mean of T_1 (diploid genome). Fluorescence values were used as a proxy for genome size. Each circle represents a single biological replicate (36 per category).

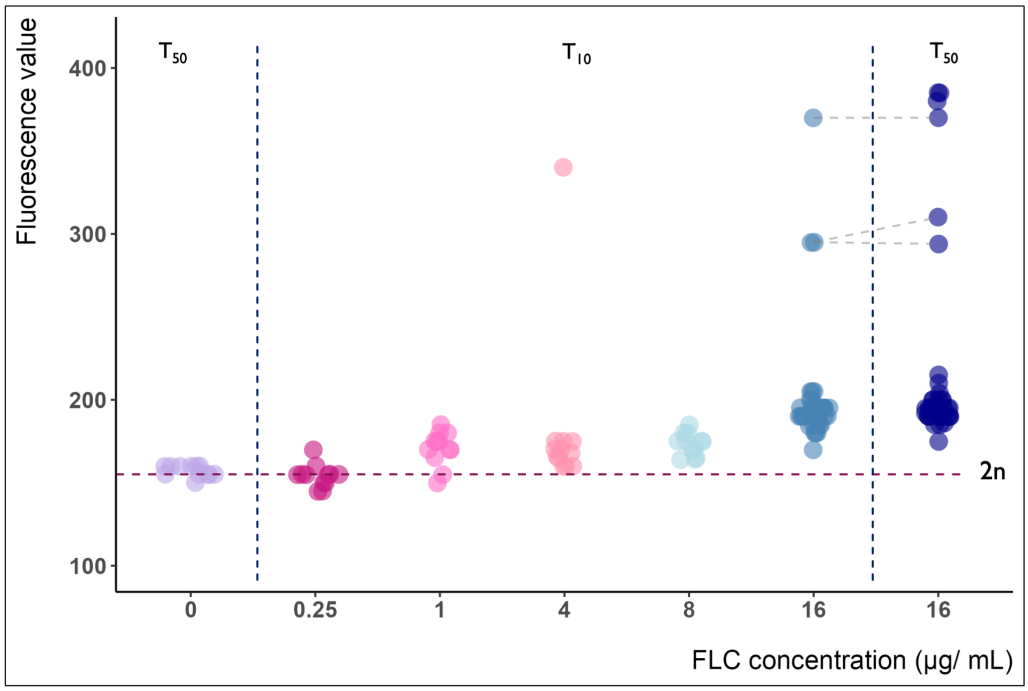

Figure 3.5: Genome size comparison of lines from all MA experiments. The maroon horizontal dashed line indicates the midpoint of the G1 mean of T_1 (diploid genome). Fluorescence values were used as a proxy for genome size. Each circle represents a single biological replicate (12 per category).

3.3.4 Detection of aneuploid chromosomes with Y-map using whole genome sequences

T_1 (3 lines), YPD-T_{50} (36 lines), FLC0.25-T_{10} (12 lines) and FLC1-T_{10} (12 lines) were whole genome sequenced and analysed with the Y_{MAP} tool to detect aneuploid chromosomes. Aneuploidy was not detected among T_1, YPD-T_{50} and FLC0.25-T_{10} (except for chromosome 5 of FLC0.25-T_{1-6}), which was consistent with the flow cytometry data, and the chromosomal maps were similar (Figure 3.6). In contrast, aneuploidy was detected in all FLC1-T_{10} lines, particularly in chromosome R (Figure 3.7). Interestingly, of all 12 sequences from FLC1-T_{10} lines, FLC1-$T_{10\text{-}10}$ had two complete aneuploid chromosomes (chromosome 6 and chromosome R), while FLC1-$T_{10\text{-}8}$ and FLC1-$T_{10\text{-}9}$ had none. However, FLC1- $T_{10\text{-}9}$ had partial aneuploidy in the right arm of chromosomes 5 and 7. All the other lines had complete aneuploidy in chromosome R. These results tally with the tolerance values of FLC1-T_{10} lines. Of all 12 lines, FLC1-$T_{10\text{-}10}$ had the highest tolerance, while FLC1-$T_{10\text{-}8}$ and FLC1-T_9 had the lowest (Figure 3.8).

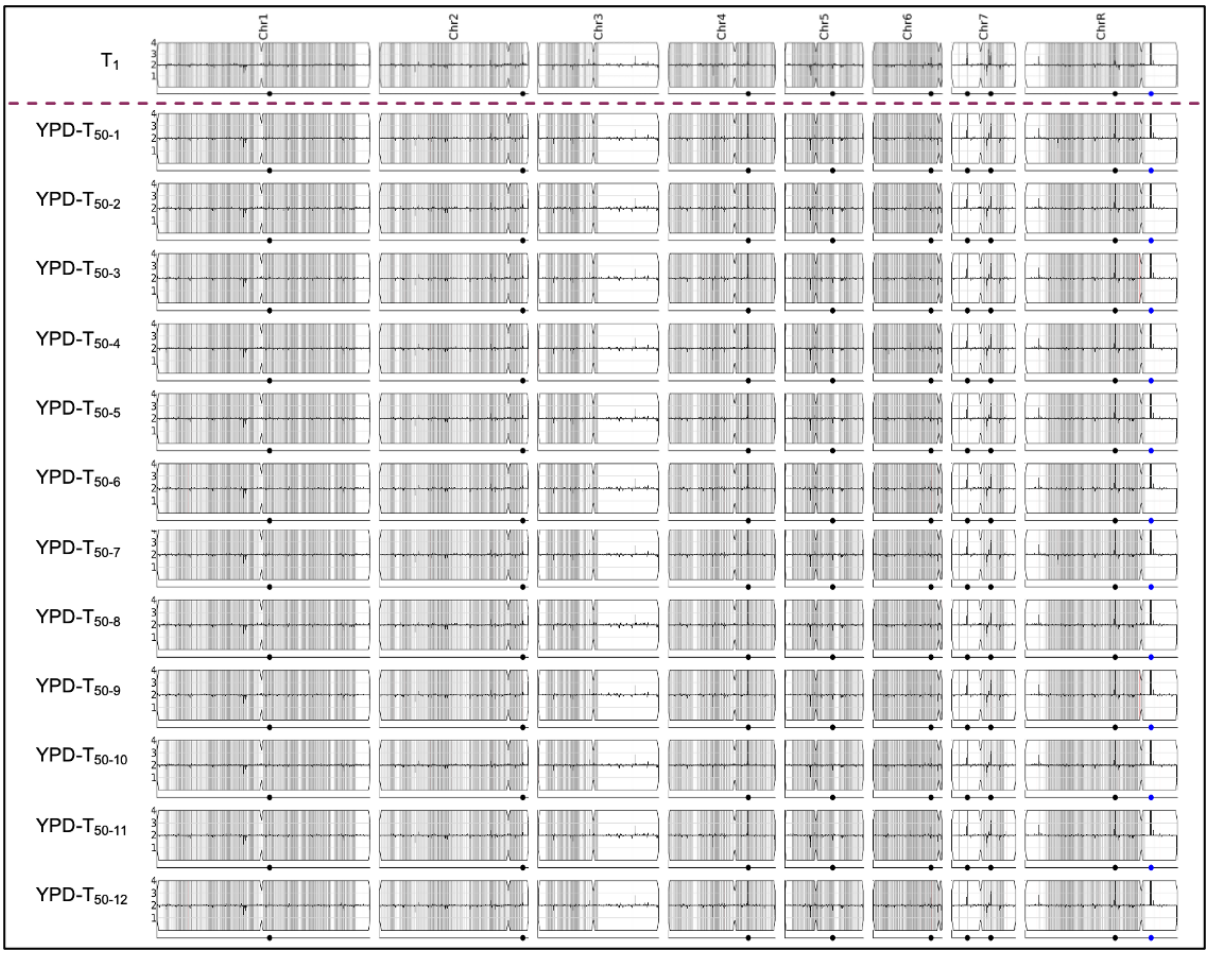

Figure 3.6: Chromosome maps of ancestral and evolved *C. albicans* lines of YPD-MA. No aneuploids were present among the evolved lines, and all the chromosomal maps were identical. Only 12 chromosomal maps out of 36 were displayed in the figure as a representative of all YPD-MA evolved lines. White and grey areas are homozygous and heterozygous regions, respectively.

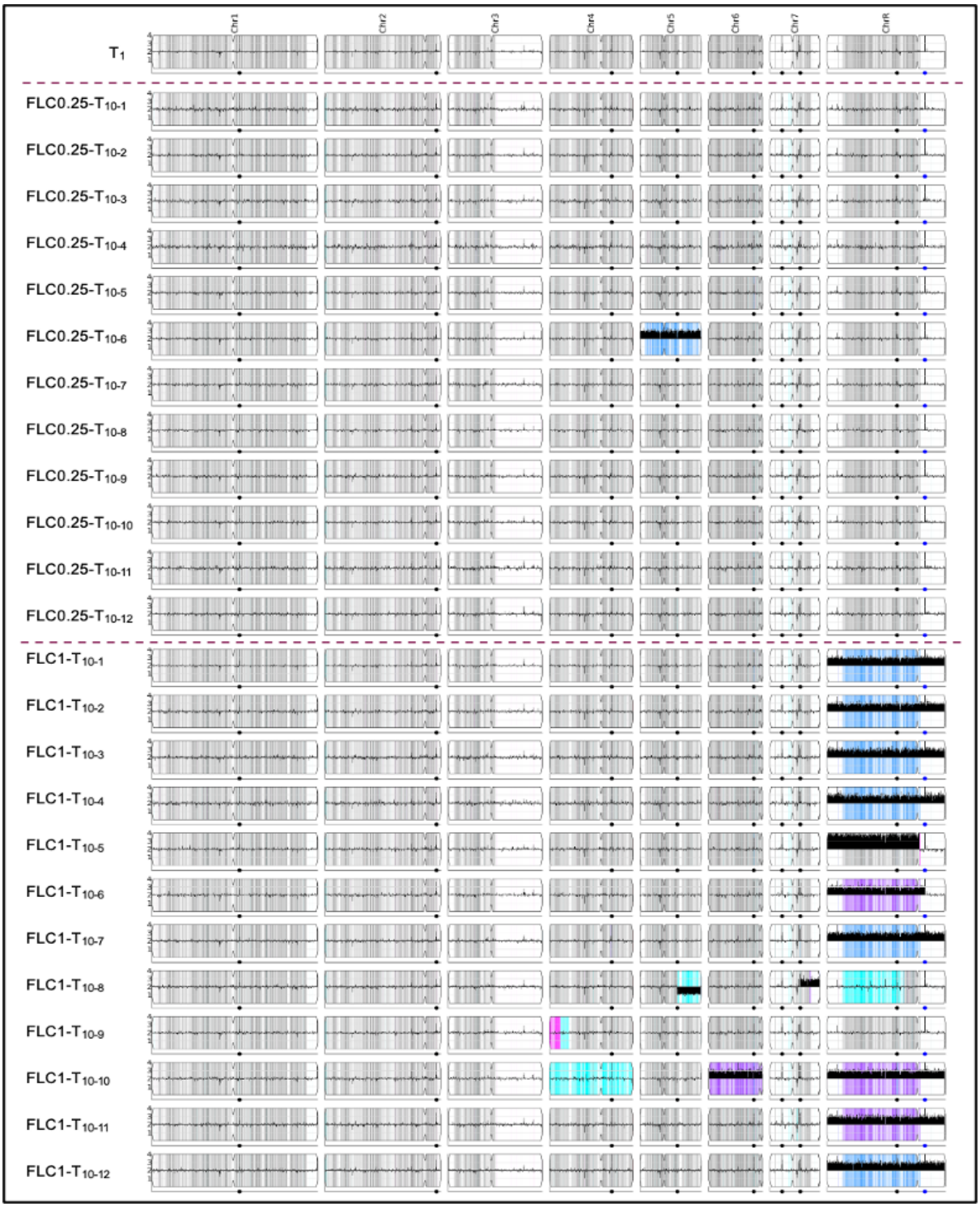

Figure 3.7: Chromosome maps of ancestral and evolved *C. albicans* lines of FLC0.25 and FLC1-MA experiments. Thick black-coloured vertical bars indicate the presence of aneuploid chromosomes. Colours represent various newly formed LOH regions; however, when combined with aneuploid regions, the coloured regions represent homozygosity due to aneuploidy.

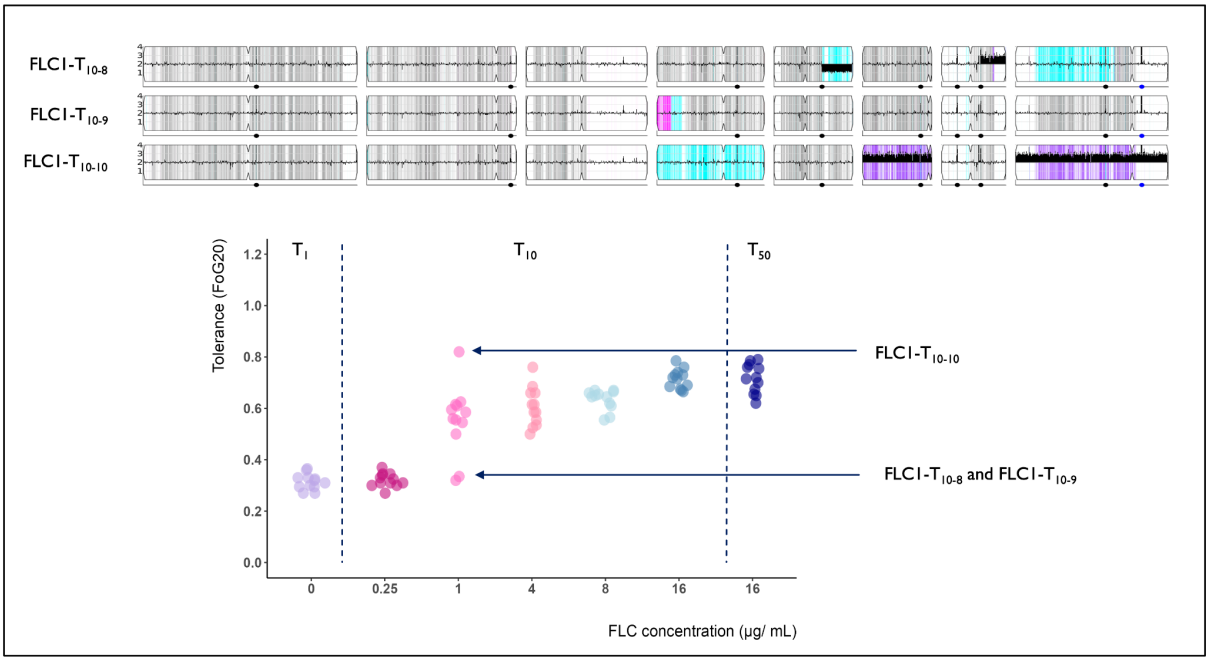

Figure 3.8: Comparison between the presence of aneuploid chromosomes and tolerance to fluconazole in *C. albicans*. Of all 12 lines, FLC1-$T_{10\text{-}10}$ had the highest tolerance with two aneuploid chromosomes, while FLC1-$T_{10\text{-}8}$ and FLC1-$T_{10\text{-}9}$ had the lowest with no aneuploid chromosomes.

3.3.5 Differences in growth rates

Growth curve experiments were carried out using the evolved (T_{50}) and ancestral lines (T_1) from both YPD-MA and FLC16-MA experiments to test whether the growth rate changed after evolution. As expected for an MA experiment done in a rich medium, growth rates were very similar between T_1 and YPD-T_{50} lines when grown YPD media (Welch Two Sample t-test; $t_{61.347} = -0.014$, $p = 0.959$, Figure 3.9A). The growth rate of FLC16-T_{50} was slightly higher than that of T_1 strains grown in FLC16 (Welch Two Sample t-test; $t_{60.336} = -3.009$, $p = 0.003$, Figure 3.9B).

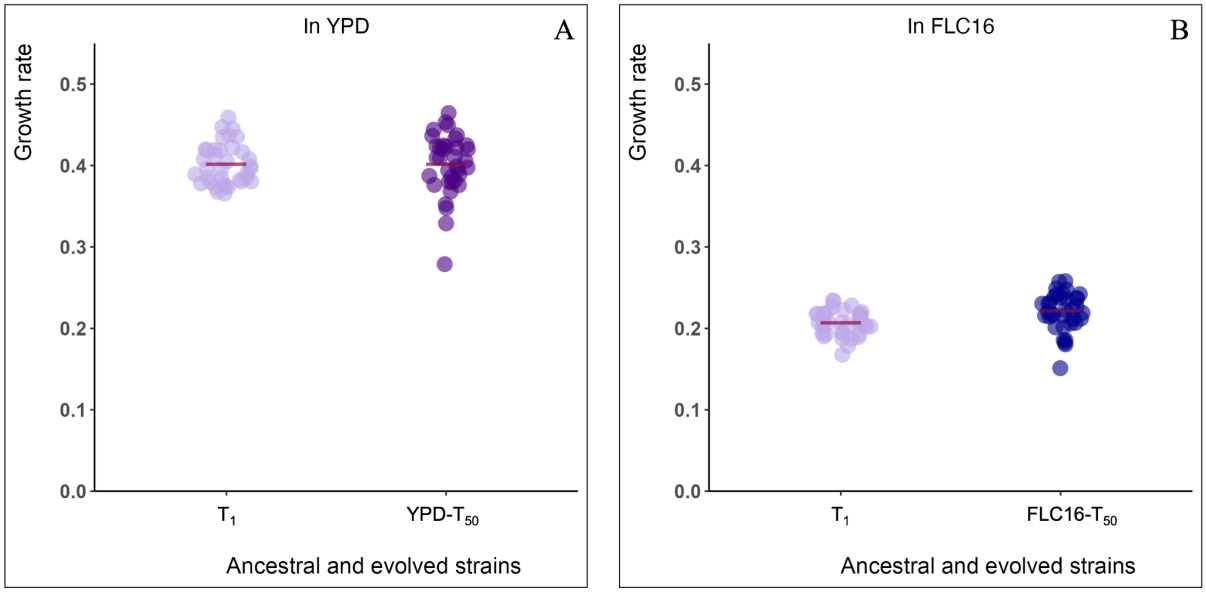

Figure 3.9: Growth rate of ancestral and evolved *C. albicans* lines. The maroon horizontal bars indicate the mean growth rate. Each dot represents one biological replicate (36 per T1 and T50). A) Growth rate comparison between T_1 and YPD-T_{50}. B) Growth rate comparison between T_1 and FLC16-T_{50} in FLC 16 µg /mL media.

3.4 Discussion

In relatively large populations, natural selection cannot effectively curb the accumulation of spontaneous mutations, even when the effects of single mutations are neutral or only moderately deleterious (Korona 1999). Mutation accumulation experiments are specifically designed to observe the accumulation of spontaneous mutations in the absence of natural selection. These experiments involve passing organisms through multiple generations while deliberately minimising selective pressures, often by bottlenecking populations to a few individuals per generation (Andersson and Hughes 1996; Lenski et al. 1991). This method allows researchers to accurately observe the baseline mutation rates and the distribution of mutational effects. Previous MA studies with yeast suggest that yeast can be effectively frozen and revived, allowing samples from each population to be cryopreserved at regular intervals (Zeyl and DeVisser 2001), making them highly suitable for MA studies (Korona 1999; Haoxuan Liu and Zhang 2021). Subsequently, these samples can be competitively tested against their ancestors to obtain accurate and consistent estimates of fitness. In this study, I bottlenecked the SC5314 ancestral strain (reference strain for *C.albicans*) in seven separate MA experiments with different fluconazole concentrations (0, 0.25, 1, 4, 8, and 16 µg/ mL fluconazole in YPD) to obtain evolved lines (FLC0.25-T_{10}, FLC1-T_{10}, FLC4-T_{10}, FLC8-T_{10} and FLC16- T_{50}) and I compared them with ancestral (T_1) lines to assess competitive fitness, drug responses, genome size and presence of aneuploid chromosomes.

Competitive fitness assays measure the fitness of two competitors by having them compete against each other in the same environment (Lenski et al. 1991; Wiser, Ribeck, and Lenski 2013). Lines evolved in YPD without any drug stress (YPD-T_{50}) showed similar competitive fitness as ancestral lines. This similarity in competitive fitness strongly suggests that the majority of the accumulated mutations over the generations are neutral or nearly neutral without affecting the competitive fitness of the evolved lines. This is in line with the expectations of MA studies, indicating that minimal selective pressure allows random mutations to persist (Fijarczyk et al. 2021; Baer, Miyamoto, and Denver 2007). The use of bottlenecking has clearly reduced the influence of natural selection (Sharp et al. 2018; Haoxuan Liu and Zhang 2021), facilitating the fixation of mutations without significant fitness consequences. However, genomic analysis of the accumulated mutations is essential to confirm their neutral nature (Keightley et al. 2014). Lines evolved in fluconazole (all concentrations) increased in competitive fitness compared to the ancestral lines when they competed at the evolutionary drug level. It was evident that the competitive fitness of the evolved lines increased with the drug concentration. This suggests that the fluconazole clearly exerted a

selective pressure, leading to the selection of mutation that enhanced the competitive fitness under the experimental conditions. Fluconazole is the most common first-line antifungal treatment for *Candida* infections (Goa and Barradell 1995), and fluconazole inhibits the synthesis of ergosterol in yeast (Odds, Brown, and Gow 2003). Any mutation that can confer tolerance and resistance towards fluconazole can provide a significant fitness advantage (Cowen et al. 2000). There are common azole resistance mechanisms in *C. albicans*, such as inhibiting the binding of the drug by changing the amino acids in the drug target (Morio et al. 2010; Casalinuovo, Di Francesco, and Garaci 2004), increased drug efflux (Sofia et al. 2001) and overexpression of *ERG11* (White 1997; Franz et al. 1998). Moreover, chromosome abnormalities such as loss of heterozygosity and chromosomal aneuploidy can lead to azole resistance and tolerance as well (Coste et al. 2007; Selmecki, Forche, and Berman 2006; Yang et al. 2023). One or more above-mentioned alterations can be responsible for the elevated competitive fitness in evolved lines. Precise genome analysis of evolved lines is needed to pinpoint the specific mutations responsible (Keightley et al. 2014).

Agar-based susceptibility testing methods have gained widespread popularity because of the straightforwardness and reproducibility of results (Negri et al. 2009). Tolerance and resistance are assessed based on the RAD20 (average radius corresponds to 20% growth inhibition) and FoG20 (fraction of growth within zone of inhibition corresponds to RAD20) readings obtained from disk diffusion assays (Salama and Gerstein 2022). Corresponding to the competitive fitness results, fluconazole tolerance and resistance of lines evolved without fluconazole were similar to ancestral lines. The findings strongly support the neutral theory of molecular evolution in the absence of selective pressure, indicating that many spontaneous mutations do not substantially affect fitness (Kimura 1979; Ohta 1992), particularly tolerance and resistance to fluconazole. These results were in line with anticipated results from MA experiments, capturing the neutral mutations (Zeyl and DeVisser 2001). These evolved lines have failed to evolve resistance or tolerance, even though the fungi can rapidly develop resistance and tolerance to a drug, even without prolonged exposure to a particular drug (Cowen and Lindquist 2005), using mechanisms like cross-resistance and cross-tolerance (White, Marr, and Bowden 1998). The lines that evolved with fluconazole in the media (FLC16-T_{50}) exhibited a slight increase in fluconazole resistance, consistent with fluconazole resistance profiling, which indicates low fluconazole resistance rates among *C. albicans* (Pfaller et al. 2019). In stark contrast, the same lines demonstrated a substantial increase in fluconazole tolerance compared to the ancestral lines. Moreover, tolerance to fluconazole increased with the fluconazole concentration with which the lines have evolved. FLC16-T_{10}

and FLC16-T_{50} lines unequivocally demonstrated similar behaviour in relation to tolerance and resistance, conclusively suggesting that tolerance emerges significantly earlier in the MA lines under fluconazole levels exceeding the MIC. Delarze et al. (2020) found that tolerance to the drug enables better survival in *C. albicans* at higher drug levels by examining the deletion mutants of tolerance-related genes in *C. albicans* (Delarze et al. 2020). Moreover, tolerant phenotypes appear more frequently in the above-MIC fluconazole levels, and resistance appears slower (Yang et al. 2023). The SC5341 reference strain, which is used as the ancestral lines, is susceptible to fluconazole (Li et al. 2019); therefore, exposure to fluconazole during the MA experiment selected for mutations that are beneficial for the survival and growth of *C. albicans* in the presence of fluconazole (Ford et al. 2015). Fluconazole and other azole drugs can induce abnormal cell divisions in *C. albicans* and promote the occurrence of chromosome abnormalities, which can lead to fluconazole tolerance and resistance (Harrison et al. 2014; Selmecki, Forche, and Berman 2006; Forche et al. 2009).

Flow cytometry is a powerful technique for determining the genome size of various organisms, including fungi. This technique involves using fluorescent dyes that bind to DNA, and depending on the intensity of the fluorescent signal, the genome size can be determined (Chang, Khanal Lamichhane, and Kwon-Chung 2018; Haase and Reed 2002). Corresponding to tolerance results, lines evolved in YPD and below-MIC fluconazole levels have similar genome sizes to ancestral lines, and the genome size increased in a dose-dependent manner with the fluconazole concentration that they have evolved in. The flow cytometry results perfectly correlate with the results obtained from whole genome analysis with Y_{MAP} (Abbey et al. 2014), indicating the increase in genome size is due to the presence of aneuploid chromosomes. Harrison et al. (2014) definitively demonstrated that exposure of *C. albicans* cells to fluconazole and other azole drugs can significantly increase the aneuploidy rate by inducing abnormal cell divisions. This was confirmed through meticulous flow cytometry analysis and found that fluconazole induces the formation of tetraploid intermediates in *C. albicans* which precede the development of aneuploid cells. The researchers observed a direct correlation between ploidy and cell size (Chang, Khanal Lamichhane, and Kwon-Chung 2018; Hickman et al. 2013) in fluconazole-exposed cells, noting that increased ploidy was associated with larger cell size (Harrison et al. 2014).

Interestingly, the comparison between tolerance and Y_{MAP} data shows a noteworthy connection between fluconazole tolerance and ploidy changes in *C. albicans*. This specifically correlates with aneuploidy in chromosome R. Other than chromosome R, some other chromosomes also acquired complete or partial aneuploidy, giving them varying degrees of

tolerance. Yang et al. (2023) suggest that individual cells use chromosomal instability as their primary adaptation mechanism, resulting in non-identical combinations of aneuploid chromosomes for growth advantages in different fluconazole concentrations. Moreover, loss of aneuploidy is related to loss of fluconazole tolerance in *C. albicans* (Yang et al. 2023). It is also well-known that some aneuploidies are beneficial in the presence of fluconazole; therefore, fluconazole may cause and select for aneuploidy (Ford et al. 2015). Selmecki et al. (2006) found that complete aneuploidy, as well as segmental aneuploidy (isochromosome composed of the two left arms of chromosome 5), can confer azole resistance in *C. albicans*. Although aneuploidies are considered detrimental under most conditions, increasing virulence and resistance to fluconazole have been observed with an extra chromosome 3 or chromosome 4 in *C. albicans* (Forche et al. 2009).

Growth rate measurements are frequently used as a proxy for fitness in microbes (Chevin 2010; Gallet et al. 2012). The growth rates are calculated using the slope of the exponential phase of the growth curve (Hall et al. 2014). Although the relative fitness is determined by accounting for all growth phases during competitive experiments (Crow 2017; Lenski et al. 1991), exponential growth rates do not capture the complete dynamics of growth curves (Wahl and Zhu 2015). A recent study discovered that cell density measurements and cell counts can differ in *Saccharomyces* due to variations in cell sizes (Pinto et al. 2024). This suggests that density measurements of *C. albicans* may not align with cell counts, potentially leading to inaccurate fitness values. Growth rates of lines evolved in fluconazole were similar to that of ancestral lines despite having a superior competitive fitness. Yang et al. (2023) screened 133 clinical isolates to investigate the impact of fluconazole in terms of tolerance, resistance and growth parameters and found that growth rates of *C. albicans* were lower in supra-MIC levels (2-128 μg/ mL*)* than sub-MIC levels, yet independent from the drug concentration. Moreover, similar growth properties were observed in the supra-MIC levels despite the fluconazole concentration (Yang et al. 2023). Although it is laborious and time-consuming, competitive fitness experiments can provide an accurate competitive fitness estimation compared to growth curves (Ram et al. 2019).

We found that the lines that evolved without drug stress acted as expected for MA populations without showing any drastic fitness changes compared to ancestral lines. However, lines evolved under drug stress have developed noteworthy fitness benefits, allowing them to acquire beneficial traits such as higher tolerance and competitive fitness than the ancestral lines. Lines evolved in supra-MIC fluconazole levels behave as lines evolved in experimental evolution (EE), where the effective population size is high, and selection dominates (Cowen et

al. 2000). We also found that fluconazole has a profound effect on *C. albicans*, allowing them to select for chromosomal changes such as aneuploidy, resulting in enhanced tolerance and competitive fitness, even if the effective population size is very low. Although the effect of selection cannot be completely eliminated from MA experiments (Kibota and Lynch 1996; Trindade, Perfeito, and Gordo 2010), Wahl and Agashe (2022) demonstrated the effect of selection can bias the results from typical MA protocols and proposed a mathematical correction to overcome biases in positive selection in MA experiments to get more accurate and reliable results when calculating mutation rates (Wahl and Agashe 2022).

3.5 Conclusion

Our research indicates that lines that evolved without exposure to drugs have not demonstrated any fitness advantages compared to the original lines. They are behaving as expected when the effective population size is low. Lines that evolved with fluconazole, regardless of evolving under a low effective population size, exhibit similar behaviour to lines that evolved through experimental evolution. The positive correlation between evolved fluconazole concentration, and tolerance, competitive fitness and aneuploid chromosomes is undeniably strong. We also found that the presence of aneuploid chromosomes (especially in chromosome R) can confer fluconazole tolerance in *C. albicans*. We found that fluconazole tolerance of *C. albicans* becomes higher with the presence of aneuploid chromosomes in the genome, suggesting a clear connection between tolerance and the presence of aneuploids.

3.6 Methods

3.6.1 Mutation Accumulation Experiments

Six mutation accumulation (MA) experiments were carried out: YPD (no drug, evolved on yeast extract peptone dextrose /YPD plates), FLC0.25, FLC1, FLC4, FLC8 and FLC16. To initiate the study, the freezer stock of SC5314 (the reference strain for *C. albicans*) was streaked on a 15 mL YPD plate, and the plate was incubated for 48 h at 30 ºC. After the incubation, 36 random colonies were selected and frozen as glycerol stocks (T_0 1-36).

For YPD-MA, each glycerol stock was streaked onto 36 fresh 15 mL YPD plates (T_1 1-36) using sterile toothpicks, and the plates were incubated statically for 48 h at 30 ºC. After the incubation, a random, medium-sized single colony was selected from each plate and streaked onto fresh 15 mL YPD plates (T_2 1-36) and incubated for 48 h at 30 ºC statically. All 36 lines were bottlenecked on 15 mL YPD plates for 50 transfers to obtain the evolved lines (T_{50} 1-36). All the T_1 and T_{50} lines were frozen in 50 % glycerol, along with every 10^{th} transfer in between.

I determined the baseline drug level for FLC16 by streaking T_1 lines from YPD-MA onto 15 mL YPD plates supplemented with different concentrations of fluconazole (0, 4, 8, 16, 32, 64, 128, and 254 µg/ mL). The baseline drug level was determined as the level of the drug where growth is visibly impaired, yet colonies with similar size as the ones selected in YPD-MA are present at 72 hours. After a 72-hour incubation period at 30 ºC, 16 µg/ mL was selected to use for the highest drug level on colony formation. The FLC16-MA experiment was conducted in the same manner as YPD for 50 transfers, except with a 72-hour incubation time between transfers, as colonies were too small to transfer after 48h.

The remaining four experiments were done in lower replication and for a shorter period of time. For each, glycerol stocks of T_1 1-12 were streaked onto 15 mL YPD plates supplemented with each drug concentration separately, and the plates were incubated for 48 h at 30 ºC statically. The 12 lines at each drug level were bottlenecked on 15 mL YPD plates with relevant drug concentrations for ten transfers to obtain evolved lines (T_{10} 1-12). All T_{10} lines were frozen in 50 % glycerol.

3.6.2 Competitive Fitness Assay

The competitive fitness of evolved lines was measured using the method described in Chapter 2. A fluorescently-labelled ancestral line was used as the competitor against the evolved lines. Briefly, 10 µL of frozen ancestral and evolved lines were inoculated into 1 mL of YPD in a

sterile 2 mL culture box, covered with a breath-easy membrane and incubated for 24 h at 30 ºC with shaking (380 rpm). After the incubation, 100 µL of the grow-up was subcultured into 900 µL of YPD in a sterile 2 mL culture box, covered with a breath-easy membrane and incubated for 24 h at 30 ºC with shaking (380 rpm). After 24h, 50 µL of the grow-up was added to 950 µL of 0.01 M PBS in a sterile 2 mL culture box. 100 µL was removed from each diluted evolved line and added to 800 µL of YPD in a sterile 2 mL culture box, followed by 100 µL of the ancestral line. 100 µL from the final mixture was added to a 96-well plate, and the culture box was covered with a breath-easy membrane and incubated for 24 h at 30 ºC with shaking (380 rpm). The cells in the 96-well plate were cleaned with several rounds of 0.01 M PBS. The plate was used to take images using fluorescent microscopic imaging. This was continued for five days to obtain all the required data for YPD. For FLC experiments, the protocol was carried out in the same way for two days, except for using YPD supplemented with relevant concentrations of fluconazole after the initial inoculation. Orbit Image Analysis software was trained to count the cells in the images, and the counts were used to calculate the competitive fitness of the evolved lines in R.

3.6.3 Measuring drug resistance and tolerance

We measured drug resistance and tolerance in disk diffusion assays (DDA) on ancestral (T_1) and evolved (T_{10} and T_{50}) lines from all MA experiments (i.e., T_{10} lines from all five FLC-MA experiments and T_{50} from YPD-MA and FLC16-MA experiments). The protocol was adapted from standard CLSI M44 guidelines for antifungal disk diffusion susceptibility testing (Sheehan et al. 2004). Briefly, 5 µL from glycerol stocks of T_1, T_{10} and T_{50} lines were inoculated into 500 µL of YPD in a sterile 2 mL culture box, covered with a breath-easy membrane and incubated for 48 h at 30 ºC with shaking (380 rpm). After the incubation, all the cultures were standardised to an optical density (OD_{600}) of 0.01 in 1 mL of 0.01 M PBS. To prepare the spread plates, 100 µL of standardised culture was added in duplicates to 15 mL YPD plates aligned with sterile beads. The beads were removed after shaking for 30 seconds and to ensure all the cultures were evenly distributed throughout the plate. After 20 minutes of plating, single disks containing 25 mg of fluconazole (6 mm, Fisher Scientific) were placed in the middle of the plate. The plates were incubated upside down statically for 48 h at 30 ºC. Individual photographs were taken on a lightbox after 48 hours, and the images were edited using ImageJ software (Schneider, Rasband, and Eliceiri 2012) according to the specifications in diskImageR vignette V2. Resistance and tolerance were calculated using the diskImageR package (Gerstein 2016).

3.6.4 Flow cytometry analysis

The genome size of ancestral and evolved lines through flow cytometry. Briefly, 5 µL from glycerol stocks of both T_1 and T_{50} lines were inoculated into 500 µL of YPD in a sterile 2 mL culture box, covered with a breath-easy membrane and incubated for 48 h at 30 ºC with shaking (380 rpm). After the incubation, 10 µL of the grow-up was subcultured into 500 µL of YPD and was incubated for 4-6 hours at 30 ºC with shaking (350 rpm). 200 µL of the cultures were transferred into a 96-well plate, and the plate was centrifuged at ×1000g (Acc:7 / Dcc:7) for 5 mins to remove the supernatant. The pellet was resuspended in 20 µL 50/ 50 TE (50 mM Tris pH8/ 50 mM EDTA) by vortexing, and 180 µL cold ethanol (95%) was added to each well, drop by drop. The plate was covered in aluminium foil and stored at -20 ºC overnight. The next day, the supernatant was removed by centrifuging, and the pellet was resuspended in 200 µL of 50/50 TE by vortexing. The supernatant was removed again by centrifuging, and 50 µL of 1 mg/mL RNase A was added to the wells. The plate was incubated at 37 ºC overnight. The next day, the supernatant was removed by centrifuging, and the pellet was resuspended in 50 µL of 1:100 Sytox:50/50 TE solution by vortexing. The plate was incubated overnight at room temperature in the dark. The next day, the supernatant was removed by centrifuging, and the pellet was resuspended in 200 µL of 50/50 TE by vortexing and transferred the solutions into centrifuge tubes containing 0.5 mL 50/50 TE. These final samples were run through the sorter, and the data were processed using the PloidyPeaks package (https://github.com/margothenry/PloidyPeaks) in R.

3.6.5 gDNA extraction

Genomic DNA was extracted from T_1 (3), YPD-T_{50} (36), FLC0.25-T_{10} (12) and FLC1-T_{10} (12) lines using standard phenol: chloroform protocol (Nobile and Mitchell 2009). The quality of DNA was assessed on Thermo 449 Scientific™ NanoDrop 2000, and the DNA was quantified with Qubit® 2.0 Fluorometer. Genomic DNA was sent for sequencing to SeqCoast Genomics (New Hampshire Ave., USA). Sample preparation at SeqCoast was done using an Illumina DNA prep tagmentation kit with unique dual indexes. Sequencing was carried out on the Illumina Nexteq2000 platform using a 300-cycle flow cell kit to generate 2×150bp paired reads. The DRAGEN v3.10.11 was employed to assess read quality, demultiplex and trim adapter sequences.

3.6.6 Whole genome sequence analysis using Y_{MAP}

A genome-wide LOH and copy number variant (CNV) analysis of paired-end reads were done using visual inspection from the web-based yeast analysis pipeline (Y_{MAP}) (Abbey et al. 2014). Paired-end reads obtained from whole genome sequencing were uploaded and analysed against the SC5314 A21-s02-557 m09-r10 reference genome. The default value was used as the ploidy (two/ diploid), and GC-content bias correction and chromosome-end bias correction were enabled for the analysis.

3.6.7 Growth curve experiments

Growth curve experiments were carried out using the evolved (T_{50}) and ancestral lines (T_1) from YPD-MA and FLC16-MA experiments. Briefly, 5 µL from glycerol stocks of all T_1 and T_{50} lines were inoculated into 500 µL of YPD in a sterile 2 mL culture box, covered with a breath-easy membrane and incubated for 48 h at 30 ºC with shaking (380 rpm). After the incubation, the cultures were standardised to an optical density (OD_{600}) of 0.01 in either 1 mL YPD or YPD + 16 µg/mL FLC. 200 µL of the standard culture was transferred into a 96-well plate and covered with a breath-easy membrane. The plate was incubated for 48 h at 30 ºC with orbital shaking in a plate reader, and the OD measurements were taken every 15 seconds. Four biological replicates were conducted for all ancestral and evolved lines. Tables containing the raw OD600 data generated from the growth curve experiments were exported to R, and maximal growth rates were calculated using custom R scripts.

DISCUSSION

Every year, there are over 150 million severe cases of human fungal infections worldwide (Kainz et al. 2020), leading to approximately 1.6 million deaths annually (Oladele et al. 2020). Despite being a commensal member of the healthy human microbiota, *Candida albicans* is considered the most prevalent human fungal pathogen. The most prescribed antifungal drug for *Candida* infections is fluconazole which is a putative mutagen (Goa and Barradell 1995). Fluconazole, as a fungistatic rather than a fungicidal, allows *Candida* to develop resistance and tolerance, complicating and limiting the effectiveness of drug treatments (Lu et al. 2021). However, understanding the mechanisms behind the emergence of fluconazole-resistant and tolerant strains is crucial to reducing the adverse effects of the drug, keeping it as a viable option to treat *Candida* infections. In this thesis, I present a high-throughput, highly automated method to quantify the competitive fitness of *C. albicans* in the presence and absence of fluconazole (Chapter 2). I have also phenotypically and genotypically explored the effect of varying fluconazole concentrations on *C. albicans* when the effective population size is low (Chapter 3).

Competitive fitness captures an organism's capacity to survive and thrive in a particular environment. Growth rates derived from optical density over time data from monoculture are often used as a proxy for competitive fitness in microbiology. The growth rate is easy to measure, has no strain marker requirements, and is typically done in 96 well plates. Although it is easy to do in high throughput, growth rates do not capture the complete dynamics of the microbial growth phases, as it predominantly represents the exponential phase, leaving out lag and stationary (Wahl and Zhu 2015), and differences in growth rate measured in a monoculture do not necessarily correlate well with growth in competition with others (as will almost always be the case outside of a test tube).

To obtain a precise estimation of fitness, competitive fitness assays with pairwise-mixed cultures are the undisputed gold standard. Most existing protocols related to competitive fitness estimation involve manual plating and colony counting, so relatively few samples can be processed at the same time (Wiser, Ribeck, and Lenski 2013; Lenski et al. 1991). Analysis of fluorescently labelled cells with flow cytometry is faster and less laborious than traditional plating and counting; however, the fluorescent signal is used as a proxy for cell counts rather than counting the actual cells. Moreover, depending on the set up, the machine operator may have to load the samples one by one, making it hard to process many samples in one go. There is thus a need for an easy, affordable, and high-throughput method to measure actual cells

rather than using proxies to calculate competitive fitness. To address this need, I developed a protocol based on fluorescent microscopic imaging coupled with a machine-learning algorithm to measure competitive fitness and Chapter 2 gives a detailed process from sample preparation to data visualisation, with all the necessary parameters and R codes. I have presented a generalised protocol, which will permit its use to address a wide range of biological questions. It can be easily employed to explore changes in competitive fitness under different environmental conditions and strain backgrounds in parallel, with a minimal amount of bench work. Moreover, the Orbit image analysis software can detect a wide range of cell types other than fluorescently labelled cells. Orbit can also distinguish between cell shapes and sizes, making it a versatile tool to work with different microbes, even without marked strains. This mostly automated method could replace the traditional time-consuming competitive fitness assays for fungal microbes. Future work will use this protocol to determine how currently-used fitness proxies (such as growth curve assays, optical density measurements, and drug response tests) correlate with competitive fitness.

I sought to investigate the behaviour of *C. albicans* strains that evolved with and without drug stress under low effective population size. Previous research on *C. albicans* has mainly focused on high population sizes, where selection plays a prominent role. However, given the varied population sizes of *C. albicans* in different locations in the human body, studies conducted under high population sizes may not always be biologically relevant. In Chapter 3, I discussed the phenotypic and genotypic data obtained from *C. albicans* lines evolved through several mutation accumulation (MA) experiments, making this as the pioneering MA study conducted in *C. albicans*.

I selected random, medium-sized, circular colonies in the YPD agar plates for the MA experiments. Colony size is the physical dimensions of a microbial colony and is typically measured by its diameter or area. The size is indicative of the growth rate of the microbial cells in the colony. There are a few factors that influence the colony size, growth rate, nutrient availability, environmental conditions and genetic factors. Calls with higher growth rates typically form large colonies in a given period of time, and rich media provide nutrients for the microbes to form large colonies. Environmental factors such as temperature, pH, drug stress and oxygen availability also affect the colony size. Moreover, mutations affecting metabolic pathways and stress responses can also lead to changes in colony size. In the case of aneuploidy, an abnormal number of chromosomes can disrupt normal cellular functions, which leads to changes in colony sizes. Cells with aneuploid chromosomes can exhibit genetic instability and can increase the rate of mutations in other genes (Sheltzer et al. 2011), which

can reduce the growth rates, resulting in smaller colonies. While aneuploid chromosomes generally result in reduced fitness, they can sometimes confer selective advantages under certain conditions (i.e. drug stress) (Harriso et al. 2014) and can lead to the formation of larger colonies. To avoid biases in the MA experiment, I selected medium-sized colonies throughout the experiment.

Based on the MA experiments done with other organisms, I anticipated finding that lines evolved in rich media would acquire predominantly neutral mutations that do not provide a fitness benefit over the ancestral lines (Fijarczyk et al. 2021; Baer, Miyamoto, and Denver 2007). I analysed the evolved and ancestral lines with respect to growth rate, tolerance and resistance to fluconazole, genome size, competitive fitness and presence of aneuploid chromosomes. As predicted, these lines did not display any fitness benefit over the ancestral lines, even after 50 bottlenecking events (~ 750 generations). This is consistent with the acquisition of neutral genetic variation. In the future, whole genome sequencing can be used alongside the phenotypic data. I expect the majority of mutations to be synonymous mutations, the mutations in the coding regions that do not change the amino acid sequence and the mutations to be in the introns and intergenic regions.

Given that fluconazole is a known mutagen, I hypothesised that there would be elevated mutation rates in the lines evolved in fluconazole, particularly in the rates of chromosomal aneuploidy, despite being evolved under a low effective population size. As predicted, the lines that evolved under FLC1 showed a drastic increase in chromosomal aneuploidy, particularly with aneuploidy in chromosome R. Notably, I observed a dose-dependent increase in competitive fitness in FLC-evolved lines, despite being evolved under low population size. The competitive fitness was calculated using the method I proposed in Chapter 2, and the results corroborate the other phenotypic assays, confirming the robustness of the proposed protocol. Moreover, I did not find a significant difference between the growth rates of FLC-evolved lines and ancestral lines. This implies that the growth rates are not reliable estimators for competitive fitness, implying the importance of the competitive fitness assay protocol I developed in Chapter 2. Consistent with the observed karyotypes from the whole genome sequencing data, I observed a clear increase in genome size in flow cytometry data from all FLC-evolved lines in a dose-dependent manner, indicating the presence of aneuploid chromosomes and/ or copy number variations (CNV) in all the evolved lines. Fluconazole has previously been shown to jeopardise the cell division in *C. albicans* and increase the rate of aneuploidy (Harrison et al., 2014), as well as induce LOH (Forche et al. 2011). Interestingly, I found that tolerance to fluconazole also increased in FLC-evolved lines in a dose-dependent manner, and the presence

and absence of aneuploid chromosomes correlated with changes in the level of tolerance to fluconazole. These results are similar to the findings of Yang et al. (2023), who evolved *C. albicans* at a high population size. They found that tolerant phenotypes appear more frequently under supra-MIC levels of fluconazole compared to sub-MIC levels.

Given that aneuploidy is often unstable, it was interesting to see the similarities in the genome size at the 10^{th} and 50^{th} transfer. Aneuploid chromosomes become euploid again when the stress is removed from the environment and the effective population size is high (Berman 2016). In *C. albicans*, aneuploidy can arise quickly, especially under stressful conditions; however, whenever the cost of aneuploidy outweighs the benefit, the chromosome usually becomes euploid (Kaplan and Li 2012). If the stress persists, the microbial populations can undergo genetic changes, and these transient aneuploids will become a more permanent feature of the genomes. In future, it will be interesting to conduct another set of experiments to examine the stability of the aneuploid chromosomes of my evolved lines.

When comparing the *in vitro* conditions of the MA experiment to those in the human body, there are many significant differences. *In vitro* conditions are often associated with highly controlled environmental conditions, and these conditions are kept constant throughout the experiment. However, the conditions in the human body are dynamic, and the microenvironments are very different from the *in vitro* conditions. In the laboratory settings, the stresses applied in the experiments are uniform and controlled, whereas in the in vitro settings, there is a natural selective pressure, and organisms can experience a variety of stresses. Moreover, cells are often cultured as clonal populations, leading to reduced genetic diversity compared to natural populations and the interactions between cells are limited compared to the complex cell-cell interactions in the *in vivo* conditions. While *in vitro* experiments provide fundamental insights into the evolutionary dynamics of *C. albicans*, simple and controlled environmental conditions in vitro settings can lead to potentially different dynamics than *in vivo* conditions.

In the future, whole genome sequence analysis of all FLC-evolved lines will be used to precisely determine the per base pair mutation rate alongside the rates of aneuploidy and LOH and to try and classify single base pair mutations as neutral, beneficial or deleterious. Furthermore, targeted genetic experiments (e.g. with CRISPR) can be used to establish a direct connection between the mutations and elevated tolerance in *C. albicans*. Moreover, the microfluidic MA approach will be applied instead of the traditional MA to examine the evolutionary dynamics of *C. albicans* when the population size is reduced to a single cell. Also, it will be interesting to explore the behaviour of evolved lines in competitive fitness assays

conducted in fluconazole concentrations other than those in which they have evolved to see how the mutations evolved in one drug level affect the competitive fitness when the lines are exposed to completely different drug levels.

CONCLUSION

I have developed a high-throughput, highly automated method for analysing competitive fitness in *C. albicans* isolates. This method can be easily tailored to investigate the competitive fitness of various other microbes. Moreover, with a pioneer mutation accumulation experiment, I have shown that *C. albicans* strains that have evolved under low effective population size without drug stress do not exhibit any fitness advantage. However, lines evolved with fluconazole stress increased in tolerance, competitive fitness and genome size, compared to the ancestral size. We also found that higher fluconazole concentrations favour the emergence of aneuploid chromosomes in evolved lines, particularly in chromosome R. It is evident that fluconazole tolerance in *C. albicans* is positively correlated with the presence of aneuploid chromosomes in the genome.

BIBLIOGRAPHY

Abbey, D. A., Jason Funt, Mor N. Lurie-Weinberger, Dawn A. Thompson, Aviv Regev, Chad L. Myers, and Judith Berman. 2014. "YMAP: A Pipeline for Visualization of Copy Number Variation and Loss of Heterozygosity in Eukaryotic Pathogens." *Genome Medicine* 6 (11): 100.

Agyare-Tabbi, M. R., Deeva Uthayakumar, Desiree Francis, Laetitia Maroc, Chris Grant, Peter McQueen, Garret Westmacott, et al. 2024. "A Role for the Putative Error-Prone Polymerase REV1 in DNA Damage and Antifungal Drug Resistance in *Candida albicans*." *bioRxiv*. https://doi.org/10.1101/2024.06.24.600412.

Alby, K., and Richard J. Bennett. 2010. "Sexual Reproduction in the *Candida* Clade: Cryptic Cycles, Diverse Mechanisms, and Alternative Functions." *Cellular and Molecular Life Sciences: CMLS* 67 (19): 3275–85.

Ami, R. B., R. E. Lewis, and D. P. Kontoyiannis. 2008. "Immunopharmacology of Modern Antifungals." *Clinical Infectious Diseases: An Official Publication of the Infectious Diseases Society of America* 47 (2): 226–35.

Andersson, D. I., Nathalie Q. Balaban, Fernando Baquero, Patrice Courvalin, Philippe Glaser, Uri Gophna, Roy Kishony, Søren Molin, and Tone Tønjum. 2020. "Antibiotic Resistance: Turning Evolutionary Principles into Clinical Reality." *FEMS Microbiology Reviews* 44 (2): 171–88.

Andersson, D. I., and D. Hughes. 1996. "Muller's Ratchet Decreases Fitness of a DNA-Based Microbe." *Proceedings of the National Academy of Sciences of the United States of America* 93 (2): 906–7.

Baer, C. F., Michael M. Miyamoto, and Dee R. Denver. 2007. "Mutation Rate Variation in Multicellular Eukaryotes: Causes and Consequences." *Nature Reviews. Genetics* 8 (8): 619–31.

Baty, F., Christian Ritz, Sandrine Charles, Martin Brutsche, Jean-Pierre Flandrois, and Marie-Laure Delignette-Muller. 2015. "A Toolbox for Nonlinear Regression in R: The Package Nlstools." *Journal of Statistical Software* 66 (August):1–21.

Bennett, R. J., and Alexander D. Johnson. 2003. "Completion of a Parasexual Cycle in *Candida albicans* by Induced Chromosome Loss in Tetraploid Strains." *The EMBO Journal* 22 (10): 2505–15.

Berman, J., and Damian J. Krysan. 2020. "Drug Resistance and Tolerance in Fungi." *Nature Reviews. Microbiology* 18 (6): 319–31.

Braun, B. R., Marco van Het Hoog, Christophe d'Enfert, Mikhail Martchenko, Jan Dungan, Alan Kuo, Diane O. Inglis, et al. 2005. "A Human-Curated Annotation of the *Candida albicans* Genome." *PLoS Genetics* 1 (1): 36–57.

Brown, A. J. P., Gordon D. Brown, Mihai G. Netea, and Neil A. R. Gow. 2014. "Metabolism Impacts upon *Candida* Immunogenicity and Pathogenicity at Multiple Levels." *Trends in Microbiology* 22 (11): 614–22.

Butler, G., Matthew D. Rasmussen, Michael F. Lin, Manuel A. S. Santos, Sharadha Sakthikumar, Carol A. Munro, Esther Rheinbay, et al. 2009. "Evolution of Pathogenicity and Sexual Reproduction in Eight *Candida* Genomes." *Nature* 459 (7247): 657–62.

Calderone, R. A., and Cornelius J. Clancy. 2011. *Candida and Candidiasis*. American Society for Microbiology Press.

Casalinuovo, I. A., P. Di Francesco, and E. Garaci. 2004. "Fluconazole Resistance in *Candida albicans*: A Review of Mechanisms." *European Review for Medical and Pharmacological Sciences* 8 (2): 69–77.

Chang, Y. C., Ami Khanal Lamichhane, and Kyung J. Kwon-Chung. 2018. "Cryptococcus Neoformans, Unlike *Candida albicans*, Forms Aneuploid Clones Directly from Uninucleated Cells under Fluconazole Stress." *mBio* 9 (6). https://doi.org/10.1128/mBio.01290-18.

Chevin, L. 2010. "On Measuring Selection in Experimental Evolution." *Biology Letters* 7 (2): 210–13.

Coste, A., Anna Selmecki, Anja Forche, Dorothée Diogo, Marie-Elisabeth Bougnoux, Christophe d'Enfert, Judith Berman, and Dominique Sanglard. 2007. "Genotypic Evolution of Azole Resistance Mechanisms in Sequential *Candida albicans* Isolates." *Eukaryotic Cell* 6 (10): 1889–1904.

Cottier, F., and Rebecca A. Hall. 2019. "Face/Off: The Interchangeable Side of *Candida albicans*." *Frontiers in Cellular and Infection Microbiology* 9:471.

Cowen, L. E., and Susan Lindquist. 2005. "Hsp90 Potentiates the Rapid Evolution of New Traits: Drug Resistance in Diverse Fungi." *Science* 309 (5744): 2185–89.

Cowen, L. E., D. Sanglard, D. Calabrese, C. Sirjusingh, J. B. Anderson, and L. M. Kohn. 2000. "Evolution of Drug Resistance in Experimental Populations of *Candida albicans*." *Journal of Bacteriology* 182 (6): 1515–22.

Crow, J. F. 2017. *An Introduction to Population Genetics Theory*. Scientific Publishers.

Darwin, Charles. 1859. "On the Origins of Species by Means of Natural Selection." *London: Murray* 247:1859.

Delarze, E., Ludivine Brandt, Emilie Trachsel, Marion Patxot, Claire Pralong, Fabio Maranzano, Murielle Chauvel, et al. 2020. “Identification and Characterization of Mediators of Fluconazole Tolerance in *Candida albicans*.” *Frontiers in Microbiology* 11 (November):591140.

DeLuna, A., Kalin Vetsigian, Noam Shoresh, Matthew Hegreness, Maritrini Colón-González, Sharon Chao, and Roy Kishony. 2008. “Exposing the Fitness Contribution of Duplicated Genes.” *Nature Genetics* 40 (5): 676–81.

Dimas M., Afonso, and Erida Gjini. 2020. “Modeling Competitive Mixtures With the Lotka-Volterra Framework for More Complex Fitness Assessment Between Strains.” *Frontiers in Microbiology* 11 (September):572487.

Diogo, D., Christiane Bouchier, Christophe d’Enfert, and Marie-Elisabeth Bougnoux. 2009. “Loss of Heterozygosity in Commensal Isolates of the Asexual Diploid Yeast *Candida albicans*.” *Fungal Genetics and Biology: FG & B* 46 (2): 159–68.

Draskau, M. K., and Terje Svingen. 2022. “Azole Fungicides and Their Endocrine Disrupting Properties: Perspectives on Sex Hormone-Dependent Reproductive Development.” *Frontiers in Toxicology* 4 (April):883254.

Druseikis, M., Austin Mottola, and Judith Berman. 2023. “The Metabolism of Susceptibility: Clearing the FoG Between Tolerance and Resistance in *Candida albicans*.” *Current Clinical Microbiology Reports* 10 (2): 36–46.

Ehrlén, J. 2003. “Fitness Components versus Total Demographic Effects: Evaluating Herbivore Impacts on a Perennial Herb.” *The American Naturalist* 162 (6): 796–810.

Ene, I. V., Sascha Brunke, Alistair J. P. Brown, and Bernhard Hube. 2014. “Metabolism in Fungal Pathogenesis.” *Cold Spring Harbor Perspectives in Medicine* 4 (12): a019695.

Ene, I. V., Rhys A. Farrer, Matthew P. Hirakawa, Kennedy Agwamba, Christina A. Cuomo, and Richard J. Bennett. 2018. “Global Analysis of Mutations Driving Microevolution of a Heterozygous Diploid Fungal Pathogen.” *Proceedings of the National Academy of Sciences of the United States of America* 115 (37): E8688–97.

Escobar D. G., Rodrigo, Lina Carvalho, Thomas Bocklitz, Juergen Popp, and José Luis Oliveira. 2022. “Software Tools and Platforms in Digital Pathology: A Review for Clinicians and Computer Scientists.” *Journal of Pathology Informatics* 13 (January):100103.

Fallarero, A. 2017. “Practical Tips for Cellular Quantification and Imaging Using Thermo Scientific Varioskan LUX Multimode Reader and Invitrogen EVOS FL Auto Cell Imaging System.” *BioTechniques* 62 (3): 135–37.

Fidel, P. L. 1999. "*Candida albicans*: From Commensal to Pathogen." In *Medical Importance of the Normal Microflora*, edited by Gerald W. Tannock, 441–76. Boston, MA: Springer US.

Fijarczyk, A., Mathieu Hénault, Souhir Marsit, Guillaume Charron, and Christian R. Landry. 2021. "Heterogeneous Mutation Rates and Spectra in Yeast Hybrids." *Genome Biology and Evolution* 13 (12). https://doi.org/10.1093/gbe/evab282.

Fisher, M. C., Ana Alastruey-Izquierdo, Judith Berman, Tihana Bicanic, Elaine M. Bignell, Paul Bowyer, Michael Bromley, et al. 2022. "Tackling the Emerging Threat of Antifungal Resistance to Human Health." *Nature Reviews. Microbiology* 20 (9): 557–71.

Fitzpatrick, D. A., Mary E. Logue, Jason E. Stajich, and Geraldine Butler. 2006. "A Fungal Phylogeny Based on 42 Complete Genomes Derived from Supertree and Combined Gene Analysis." *BMC Evolutionary Biology* 6 (November):99.

Forche, A., D. Abbey, T. Pisithkul, M. A. Weinzierl, T. Ringstrom, D. Bruck, K. Petersen, and J. Berman. 2011. "Stress Alters Rates and Types of Loss of Heterozygosity in *Candida albicans*." *mBio* 2 (4). https://doi.org/10.1128/mBio.00129-11.

Forche, A., Kevin Alby, Dana Schaefer, Alexander D. Johnson, Judith Berman, and Richard J. Bennett. 2008. "The Parasexual Cycle in *Candida albicans* Provides an Alternative Pathway to Meiosis for the Formation of Recombinant Strains." *PLoS Biology* 6 (5): e110.

Forche, A., P. T. Magee, Anna Selmecki, Judith Berman, and Georgiana May. 2009. "Evolution in *Candida albicans* Populations during a Single Passage through a Mouse Host." *Genetics* 182 (3): 799–811.

Ford, C. B., Jason M. Funt, Darren Abbey, Luca Issi, Candace Guiducci, Diego A. Martinez, Toni Delorey, et al. 2015. "The Evolution of Drug Resistance in Clinical Isolates of *Candida albicans*." *eLife* 4 (February):e00662.

Franz, R., S. L. Kelly, D. C. Lamb, D. E. Kelly, M. Ruhnke, and J. Morschhäuser. 1998. "Multiple Molecular Mechanisms Contribute to a Stepwise Development of Fluconazole Resistance in Clinical *Candida albicans* Strains." *Antimicrobial Agents and Chemotherapy* 42 (12): 3065–72.

Gallet, R., Tim F. Cooper, Santiago F. Elena, and Thomas Lenormand. 2012. "Measuring Selection Coefficients Below 10−3: Method, Questions, and Prospects." *Genetics* 190 (1): 175–86.

Gerstein, A. 2016. "diskImageR: A Pipeline to Analyze Resistance and Tolerance from Drug Disk Diffusion Assays." *R Package Version*.

Gerstein, A. C., L. A. Cleathero, M. A. Mandegar, and S. P. Otto. 2011. "Haploids Adapt Faster

than Diploids across a Range of Environments." *Journal of Evolutionary Biology* 24 (3): 531–40.

Gerstein, A. C., and Judith Berman. 2020. "*Candida albicans* Genetic Background Influences Mean and Heterogeneity of Drug Responses and Genome Stability during Evolution in Fluconazole." *mSphere* 5 (3). https://doi.org/10.1128/mSphere.00480-20.

Gerstein, A. C., and Nathaniel P. Sharp. 2021. "The Population Genetics of Ploidy Change in Unicellular Fungi." *FEMS Microbiology Reviews* 45 (5). https://doi.org/10.1093/femsre/fuab006.

Goa, K. L., and Lee B. Barradell. 1995. "Fluconazole." *Drugs* 50 (4): 658–90.

Haase, S. B., and Steven I. Reed. 2002. "Improved Flow Cytometric Analysis of the Budding Yeast Cell Cycle." *Cell Cycle* 1 (2): 132–36.

Hall, B. G., Hande Acar, Anna Nandipati, and Miriam Barlow. 2014. "Growth Rates Made Easy." *Molecular Biology and Evolution* 31 (1): 232–38.

Harrison, B. D., Jordan Hashemi, Maayan Bibi, Rebecca Pulver, Danny Bavli, Yaakov Nahmias, Melanie Wellington, Guillermo Sapiro, and Judith Berman. 2014. "A Tetraploid Intermediate Precedes Aneuploid Formation in Yeasts Exposed to Fluconazole." *PLoS Biology* 12 (3): e1001815.

Hickman, M. A., Guisheng Zeng, Anja Forche, Matthew P. Hirakawa, Darren Abbey, Benjamin D. Harrison, Yan-Ming Wang, et al. 2013. "The 'Obligate Diploid' *Candida albicans* Forms Mating-Competent Haploids." *Nature* 494 (7435): 55–59.

Hirakawa, M. P., Diego A. Martinez, Sharadha Sakthikumar, Matthew Z. Anderson, Aaron Berlin, Sharvari Gujja, Qiandong Zeng, et al. 2015. "Genetic and Phenotypic Intra-Species Variation in *Candida albicans*." *Genome Research* 25 (3): 413–25.

Jones, T., Nancy A. Federspiel, Hiroji Chibana, Jan Dungan, Sue Kalman, B. B. Magee, George Newport, et al. 2004. "The Diploid Genome Sequence of *Candida albicans*." *Proceedings of the National Academy of Sciences of the United States of America* 101 (19): 7329–34.

Kainz, K., Maria A. Bauer, Frank Madeo, and Didac Carmona-Gutierrez. 2020. "Fungal Infections in Humans: The Silent Crisis." *Microbial Cell Factories* 7 (6): 143–45.

Kao, K, C., and Gavin Sherlock. 2008. "Molecular Characterization of Clonal Interference during Adaptive Evolution in Asexual Populations of *Saccharomyces cerevisiae*." *Nature Genetics* 40 (12): 1499–1504.

Kaushik, P., Pranab Kumar Pati, M. L. Khan, and P. K. Khare. 2022. "Plant Functional Traits Best Explain Invasive Species' Performance within a Dynamic Ecosystem - A Review."

Trees, Forests and People 8 (100260): 100260.

Keightley, P. D., Rob W. Ness, Daniel L. Halligan, and Penelope R. Haddrill. 2014. "Estimation of the Spontaneous Mutation Rate per Nucleotide Site in a *Drosophila melanogaster* Full-Sib Family." *Genetics* 196 (1): 313–20.

Kibota, T. T., and Michael Lynch. 1996. "Estimate of the Genomic Mutation Rate Deleterious to Overall Fitness in *E. Coli*." *Nature* 381 (6584): 694–96.

Kidd, S. E., Alireza Abdolrasouli, and Ferry Hagen. 2023. "Fungal Nomenclature: Managing Change Is the Name of the Game." *Open Forum Infectious Diseases* 10 (1): ofac559.

Kimura, M. 1979. "The Neutral Theory of Molecular Evolution." *Scientific American* 241 (5): 98–100, 102, 108 passim.

Korona, R. 1999. "Unpredictable Fitness Transitions Between Haploid and Diploid Strains of the Genetically Loaded Yeast *Saccharomyces cerevisiae*." *Genetics* 151 (1): 77–85.

Kumamoto, C. A. 2011. "Inflammation and Gastrointestinal *Candida* Colonization." *Current Opinion in Microbiology* 14 (4): 386–91.

Lakhani, P., Akash Patil, and Soumyajit Majumdar. 2019. "Challenges in the Polyene- and Azole-Based Pharmacotherapy of Ocular Fungal Infections." *Journal of Ocular Pharmacology and Therapeutics: The Official Journal of the Association for Ocular Pharmacology and Therapeutics* 35 (1): 6–22.

Lenski, R. E. 2023. "Revisiting the Design of the Long-Term Evolution Experiment with *Escherichia coli*." *Journal of Molecular Evolution* 91 (3): 241–53.

Lenski, R. E., Michael R. Rose, Suzanne C. Simpson, and Scott C. Tadler. 1991. "Long-Term Experimental Evolution in *Escherichia coli*. I. Adaptation and Divergence During 2,000 Generations." *The American Naturalist* 138 (6): 1315–41.

Levinson, T., Alon Dahan, Anna Novikov, Yael Paran, Judith Berman, and Ronen Ben-Ami. 2021. "Impact of Tolerance to Fluconazole on Treatment Response in *Candida Albicans* Bloodstream Infection." *Mycoses* 64 (1): 78–85.

Liang, S., and Richard J. Bennett. 2019. "The Impact of Gene Dosage and Heterozygosity on The Diploid Pathobiont *Candida albicans*." *Journal of Fungi (Basel, Switzerland)* 6 (1). https://doi.org/10.3390/jof6010010.

Li, L., Teng Zhang, Jianrong Xu, Jing Wu, Yida Wang, Xiran Qiu, Yu Zhang, et al. 2019. "The Synergism of the Small Molecule ENOblock and Fluconazole Against Fluconazole-Resistant *Candida albicans*." *Frontiers in Microbiology* 10 (September):2071.

Limon, J. J., Joseph H. Skalski, and David M. Underhill. 2017. "Commensal Fungi in Health and Disease." *Cell Host & Microbe* 22 (2): 156–65.

Liu, H. 2002. “Co-Regulation of Pathogenesis with Dimorphism and Phenotypic Switching in *Candida albicans*, a Commensal and a Pathogen.” *International Journal of Medical Microbiology: IJMM* 292 (5-6): 299–311.

Liu, H, and Jianzhi Zhang. 2021. “The Rate and Molecular Spectrum of Mutation Are Selectively Maintained in Yeast.” *Nature Communications* 12 (1): 4044.

Li, Y., Sandeep Venkataram, Atish Agarwala, Barbara Dunn, Dmitri A. Petrov, Gavin Sherlock, and Daniel S. Fisher. 2018. “Hidden Complexity of Yeast Adaptation under Simple Evolutionary Conditions.” *Current Biology: CB* 28 (4): 515–25.e6.

Lu, H., Manjari Shrivastava, Malcolm Whiteway, and Yuanying Jiang. 2021. “*Candida Albicans* Targets That Potentially Synergize with Fluconazole.” *Critical Reviews in Microbiology* 47 (3): 323–37.

Lynch, M., Way Sung, Krystalynne Morris, Nicole Coffey, Christian R. Landry, Erik B. Dopman, W. Joseph Dickinson, et al. 2008. “A Genome-Wide View of the Spectrum of Spontaneous Mutations in Yeast.” *Proceedings of the National Academy of Sciences of the United States of America* 105 (27): 9272–77.

Massey, S. E., Gabriela Moura, Pedro Beltrão, Ricardo Almeida, James R. Garey, Mick F. Tuite, and Manuel A. S. Santos. 2003. “Comparative Evolutionary Genomics Unveils the Molecular Mechanism of Reassignment of the CTG Codon in *Candida* Spp.” *Genome Research* 13 (4): 544–57.

Mba, I. E., and Emeka Innocent Nweze. 2020. “Mechanism of Candida Pathogenesis: Revisiting the Vital Drivers.” *European Journal of Clinical Microbiology & Infectious Diseases: Official Publication of the European Society of Clinical Microbiology* 39 (10): 1797–1819.

Miller, T. E. X., and Aldo Compagnoni. 2022. “Two-Sex Demography, Sexual Niche Differentiation, and the Geographic Range Limits of Texas Bluegrass (Poa Arachnifera).” *The American Naturalist* 200 (1): 17–31.

Mixão, V. and Toni Gabaldón. 2020. “Genomic Evidence for a Hybrid Origin of the Yeast Opportunistic Pathogen *Candida albicans*.” *BMC Biology* 18 (1): 48.

Morio, F., Cedric Loge, Bernard Besse, Christophe Hennequin, and Patrice Le Pape. 2010. “Screening for Amino Acid Substitutions in the *Candida albicans* Erg11 Protein of Azole-Susceptible and Azole-Resistant Clinical Isolates: New Substitutions and a Review of the Literature.” *Diagnostic Microbiology and Infectious Disease* 66 (4): 373–84.

Muzzey, D., Katja Schwartz, Jonathan S. Weissman, and Gavin Sherlock. 2013. “Assembly of a Phased Diploid *Candida albicans* genome Facilitates Allele-Specific Measurements and

Provides a Simple Model for Repeat and Indel Structure." *Genome Biology* 14 (9): R97.

Negri, M., Mariana Henriques, Terezinha I. E. Svidzinski, Claudete Rodrigues Paula, and Rosário Oliveira. 2009. "Correlation between Etest, Disk Diffusion, and Microdilution Methods for Antifungal Susceptibility Testing of *Candida* Species from Infection and Colonization." *Journal of Clinical Laboratory Analysis* 23 (5): 324–30.

Nicholls, S., Donna M. MacCallum, Florian A. R. Kaffarnik, Laura Selway, Scott C. Peck, and Alistair J. P. Brown. 2011. "Activation of the Heat Shock Transcription Factor Hsf1 Is Essential for the Full Virulence of the Fungal Pathogen *Candida albicans*." *Fungal Genetics and Biology: FG & B* 48 (3): 297–305.

Niemiec, M. J., Mario Kapitan, Melanie Polke, and I. Jacobsen. 2021. "Commensal to Pathogen Transition of *Candida albicans*." *Encyclopedia of Mycology*. https://doi.org/10.1016/B978-0-12-809633-8.12077-1.

Nishant, K. T., Wu Wei, Eugenio Mancera, Juan Lucas Argueso, Andreas Schlattl, Nicolas Delhomme, Xin Ma, et al. 2010. "The Baker's Yeast Diploid Genome Is Remarkably Stable in Vegetative Growth and Meiosis." *PLoS Genetics* 6 (9): e1001109.

Nobile, C. J., and Aaron P. Mitchell. 2009. "Large-Scale Gene Disruption Using the UAU1 Cassette." *Methods in Molecular Biology* 499:175–94.

Odds, F. C., Alistair J. P. Brown, and Neil A. R. Gow. 2003. "Antifungal Agents: Mechanisms of Action." *Trends in Microbiology* 11 (6): 272–79.

Ohta, T.. 1992. "The Nearly Neutral Theory of Molecular Evolution." *Annual Review of Ecology and Systematics* 23:263–86.

Oladele, R. O., Iorhen E. Akase, Ahmed H. Fahal, Nelesh P. Govender, Martin Hoenigl, Jean Pierre Gangneux, Tom M. Chiller, David W. Denning, Oliver A. Cornely, and Arunaloke Chakrabarti. 2020. "Bridging the Knowledge Gap on Mycoses in Africa: Setting up a Pan-African Mycology Working Group." *Mycoses* 63 (3): 244–49.

Olaiya, A. F., and S. J. Sogin. 1979. "Ploidy Determination of *Candida albicans*." *Journal of Bacteriology* 140 (3): 1043–49.

Orr, H. A. 2009. "Fitness and Its Role in Evolutionary Genetics." *Nature Reviews. Genetics* 10 (8): 531–39.

Pappas, P. G., Michail S. Lionakis, Maiken Cavling Arendrup, Luis Ostrosky-Zeichner, and Bart Jan Kullberg. 2018. "Invasive Candidiasis." *Nature Reviews. Disease Primers* 4 (May):18026.

Pellon, A., Neelu Begum, Shervin Dokht Sadeghi Nasab, Azadeh Harzandi, Saeed Shoaie, and David L. Moyes. 2022. "Role of Cellular Metabolism during *Candida*-Host Interactions."

Pathogens 11 (2). https://doi.org/10.3390/pathogens11020184.

Perea S., López-Ribot José L., Kirkpatrick William R., McAtee Robert K., Santillán Rebecca A., Martínez Marcos, Calabrese David, Sanglard Dominique, and Patterson Thomas F. 2001. "Prevalence of Molecular Mechanisms of Resistance to Azole Antifungal Agents in *Candida albicans* Strains Displaying High-Level Fluconazole Resistance Isolated from Human Immunodeficiency Virus-Infected Patients." *Antimicrobial Agents and Chemotherapy* 45 (10): 2676–84.

Pfaller, M. A., Daniel J. Diekema, John D. Turnidge, Mariana Castanheira, and Ronald N. Jones. 2019. "Twenty Years of the SENTRY Antifungal Surveillance Program: Results for *Candida* Species From 1997–2016." *Open Forum Infectious Diseases* 6 (Supplement_1): S79–94.

Pinto, J., Nik Tavakolian, Chun-Biu Li, and Rike Stelkens. 2024. "The Relationship between Cell Density and Cell Count Differs among *Saccharomyces* Yeast Species." *microPublication Biology* 2024 (May). https://doi.org/10.17912/micropub.biology.001215.

Ram, Y., Eynat Dellus-Gur, Maayan Bibi, Kedar Karkare, Uri Obolski, Marcus W. Feldman, Tim F. Cooper, Judith Berman, and Lilach Hadany. 2019. "Predicting Microbial Growth in a Mixed Culture from Growth Curve Data." *Proceedings of the National Academy of Sciences* 116 (29): 14698–707.

Richardson, K., K. Cooper, M. S. Marriott, M. H. Tarbit, P. F. Troke, and P. J. Whittle. 1990. "Discovery of Fluconazole, a Novel Antifungal Agent." *Reviews of Infectious Diseases* 12 Suppl 3:S267–71.

Riggsby, W. S., L. J. Torres-Bauza, J. W. Wills, and T. M. Townes. 1982. "DNA Content, Kinetic Complexity, and the Ploidy Question in *Candida albicans*." *Molecular and Cellular Biology* 2 (7): 853–62.

Ropars, J., Corinne Maufrais, Dorothée Diogo, Marina Marcet-Houben, Aurélie Perin, Natacha Sertour, Kevin Mosca, et al. 2018. "Gene Flow Contributes to Diversification of the Major Fungal Pathogen *Candida albicans*." *Nature Communications* 9 (1): 2253.

Rosenberg, A., Iuliana V. Ene, Maayan Bibi, Shiri Zakin, Ella Shtifman Segal, Naomi Ziv, Alon M. Dahan, Arnaldo Lopes Colombo, Richard J. Bennett, and Judith Berman. 2018. "Antifungal Tolerance Is a Subpopulation Effect Distinct from Resistance and Is Associated with Persistent Candidemia." *Nature Communications* 9 (1): 2470.

Rosenberg, S. M. 2011. "Stress-Induced Loss of Heterozygosity in *Candida*: A Possible Missing Link in the Ability to Evolve." *mBio*. Am Soc Microbiol.

https://doi.org/10.1128/mBio.00200-11.

Salama, O. E., and Aleeza C. Gerstein. 2022. “Differential Response of *Candida* Species Morphologies and Isolates to Fluconazole and Boric Acid.” *Antimicrobial Agents and Chemotherapy* 66 (5): e0240621.

Samuel, P. O., Great Iruoghene Edo, Gift Onyinyechi Oloni, Ufuoma Ugbune, Gracious Okeoghene Ezekiel, Arthur Efeoghene Athan Essaghah, and Joy Johnson Agbo. 2023. “Effects of Chemical Contaminants on the Ecology and Evolution of Organisms a Review.” *Chemistry and Ecology* 39 (10): 1071–1107.

San Juan Galán, J., Vanessa Poliquin, and Aleeza Cara Gerstein. 2023. “Insights and Advances in Recurrent Vulvovaginal Candidiasis.” *PLoS Pathogens* 19 (11): e1011684.

Santos, M. A., and M. F. Tuite. 1995. “The CUG Codon Is Decoded in Vivo as Serine and Not Leucine in *Candida albicans*.” *Nucleic Acids Research* 23 (9): 1481–86.

Schneider, C. A., Wayne S. Rasband, and Kevin W. Eliceiri. 2012. “NIH Image to ImageJ: 25 Years of Image Analysis.” *Nature Methods* 9 (7): 671–75.

Selmecki, A., Sven Bergmann, and Judith Berman. 2005. “Comparative Genome Hybridization Reveals Widespread Aneuploidy in *Candida albicans* Laboratory Strains.” *Molecular Microbiology* 55 (5): 1553–65.

Selmecki, A., Anja Forche, and Judith Berman. 2006. “Aneuploidy and Isochromosome Formation in Drug-Resistant *Candida albicans*.” *Science* 313 (5785): 367–70.

Sharp, N. P., Linnea Sandell, Christopher G. James, and Sarah P. Otto. 2018. “The Genome-Wide Rate and Spectrum of Spontaneous Mutations Differ between Haploid and Diploid Yeast.” *Proceedings of the National Academy of Sciences of the United States of America* 115 (22): E5046–55.

Sheehan, D. J., Steven D. Brown, Michael A. Pfaller, David W. Warnock, John H. Rex, Vishnu Chaturvedi, Ana Espinel-Ingroff, et al. 2004. “Method for Antifungal Disk Diffusion Susceptibility Testing of Yeasts; Approved Guideline.” *Pennsylvania, USA: National Committee for Clinical Laboratory Standards M27-A2*.

Silva, S., Melyssa Negri, Mariana Henriques, Rosário Oliveira, David W. Williams, and Joana Azeredo. 2012. “*Candida glabrata, Candida parapsilosis and Candida tropicalis:* Biology, Epidemiology, Pathogenicity and Antifungal Resistance.” *FEMS Microbiology Reviews* 36 (2): 288–305.

Soll, D. R. 2002. “*Candida* Commensalism and Virulence: The Evolution of Phenotypic Plasticity.” *Acta Tropica* 81 (2): 101–10.

Stritt, M., Anna K. Stalder, and Enrico Vezzali. 2020. “Orbit Image Analysis: An Open-Source

Whole Slide Image Analysis Tool." *PLoS Computational Biology* 16 (2): e1007313.

Suh, S., Meredith Blackwell, Cletus P. Kurtzman, and Marc-André Lachance. 2006. "Phylogenetics of Saccharomycetales, the Ascomycete Yeasts." *Mycologia* 98 (6): 1006–17.

Szymański, M., Sandra Chmielewska, Urszula Czyżewska, Marta Malinowska, and Adam Tylicki. 2022. "Echinocandins - Structure, Mechanism of Action and Use in Antifungal Therapy." *Journal of Enzyme Inhibition and Medicinal Chemistry* 37 (1): 876–94.

Talapko, J., Martina Juzbašić, Tatjana Matijević, Emina Pustijanac, Sanja Bekić, Ivan Kotris, and Ivana Škrlec. 2021. "*Candida albicans* -The Virulence Factors and Clinical Manifestations of Infection." *Journal of Fungi (Basel, Switzerland)* 7 (2). https://doi.org/10.3390/jof7020079.

Travisano, M., and R. E. Lenski. 1996. "Long-Term Experimental Evolution in *Candida albicans* IV. Targets of Selection and the Specificity of Adaptation." *Genetics* 143 (1): 15–26.

Trindade, S., Lilia Perfeito, and Isabel Gordo. 2010. "Rate and Effects of Spontaneous Mutations That Affect Fitness in Mutator *Escherichia coli*." *Philosophical Transactions of the Royal Society of London. Series B, Biological Sciences* 365 (1544): 1177–86.

Vylkova, S., Aaron J. Carman, Heather A. Danhof, John R. Collette, Huaijin Zhou, and Michael C. Lorenz. 2011. "The Fungal Pathogen *Candida albicans* Autoinduces Hyphal Morphogenesis by Raising Extracellular pH." *mBio* 2 (3): e00055–11.

Wahl, L. M., and Deepa Agashe. 2022. "Selection Bias in Mutation Accumulation." *Evolution; International Journal of Organic Evolution* 76 (3): 528–40.

Wahl, L. M., and Anna Dai Zhu. 2015. "Survival Probability of Beneficial Mutations in Bacterial Batch Culture." *Genetics* 200 (1): 309–20.

White, T. C. 1997. "Increased mRNA Levels of ERG16, CDR, and MDR1 Correlate with Increases in Azole Resistance in *Candida albicans* Isolates from a Patient Infected with Human Immunodeficiency Virus." *Antimicrobial Agents and Chemotherapy* 41 (7): 1482–87.

White, T. C., K. A. Marr, and R. A. Bowden. 1998. "Clinical, Cellular, and Molecular Factors That Contribute to Antifungal Drug Resistance." *Clinical Microbiology Reviews* 11 (2): 382–402.

Wickham, H., Mara Averick, Jennifer Bryan, Winston Chang, Lucy McGowan, Romain François, Garrett Grolemund, et al. 2019. "Welcome to the Tidyverse." *Journal of Open Source Software* 4 (43): 1686.

Wiser, M. J., and Richard E. Lenski. 2015. “A Comparison of Methods to Measure Fitness in *Escherichia coli*.” *PloS One* 10 (5): e0126210.

Wiser, M. J., Noah Ribeck, and Richard E. Lenski. 2013. “Long-Term Dynamics of Adaptation in Asexual Populations.” *Science* 342 (6164): 1364–67.

Yang, F., Eduardo F. C. Scopel, Hao Li, Liu-Liu Sun, Nora Kawar, Yong-Bing Cao, Yuan-Ying Jiang, and Judith Berman. 2023. “Antifungal Tolerance and Resistance Emerge at Distinct Drug Concentrations and Rely upon Different Aneuploid Chromosomes.” *mBio* 14 (2): e0022723.

Yang, Z., Qiao Wang, Ke Ma, Ping Shi, Wenbin Liu, and Zhiwei Huang. 2018. “Fluconazole Inhibits Cellular Ergosterol Synthesis to Confer Synergism with Berberine against Yeast Cells.” *Journal of Global Antimicrobial Resistance* 13 (June):125–30.

Zeyl, C., and J. A. DeVisser. 2001. “Estimates of the Rate and Distribution of Fitness Effects of Spontaneous Mutation in *Saccharomyces cerevisiae*.” *Genetics* 157 (1): 53–61.

SUPPLEMENTARY MATERIAL FOR CHAPTER 3

Supplementary Table 1: Tukey test results followed by ANOVA test tests to examine the influence of fluconazole on competitive fitness

Fluconazole concentration (µg /mL)	***p adj***	***diff***
0.25 – 0	$p < 0.001$	1.147
1 – 0	$p < 0.001$	1.805
4 – 0	$p < 0.001$	2.451
8 – 0	$p < 0.001$	2.409
16 – 0	$p < 0.001$	3.157
1 – 0.25	$p < 0.001$	0.657
4 – 0.25	$p < 0.001$	1.304
8 – 0.25	$p < 0.001$	1.262
16 – 0.25	$p < 0.001$	2.009
4 – 1	$p < 0.001$	0.646
8 – 1	$p < 0.001$	0.604
16 – 1	$p < 0.001$	1.351
8 – 4	$P = 0.999$	-0.041
16 – 4	$p < 0.001$	0.705
16 - 8	$p < 0.001$	0.747

Supplementary Table 2: Tukey test results followed by ANOVA test tests to examine the influence of fluconazole on tolerance

Fluconazole concentration (µg /mL)	***p adj***	***diff***
0.25 – 0	$p = 0.999$	0.007
1 – 0	$p < 0.001$	0.241
4 – 0	$p < 0.001$	0.399
8 – 0	$p < 0.001$	0.402
16 – 0	$p < 0.001$	0.292
16 – 0	$p < 0.001$	0.320
1 – 0.25	$p < 0.001$	0.234
4 – 0.25	$p < 0.001$	0.392
8 – 0.25	$p < 0.001$	0.395
16 – 0.25	$p < 0.001$	0.285
16 – 0.25	$p < 0.001$	0.312
4 – 1	$p = 0.493$	0.158
8 – 1	$p = 0.068$	0.160
16 – 1	$p < 0.001$	0.0512
16 – 1	$p < 0.001$	0.078
8 – 4	$P = 0.949$	0.002
16 – 4	$p = 0.003$	- 0.107
16 – 4	$p = 0.002$	- 0.079
16 – 8	$p = 0.063$	- 0.109
16 – 8	$p = 0.050$	- 0.082
16 – 16	$p = 0.999$	0.027